



## EDITORIAL BOARD

E.O. Paton Electric Welding Institute, Kyiv, Ukraine:

**S.I. Kuchuk-Yatsenko** (*Editor-in-Chief*),

**V.M. Lipodaev** (*Deputy Editor-in-Chief*),

**O.M. Berdnikova, Yu.S. Borisov,**

**V.V. Knysh, V.M. Korzhyk, I.V. Krivtsun,**

**Yu.M. Lankin, L.M. Lobanov, S.Yu. Maksimov,**

**M.O. Pashchin, V.D. Poznyakov,**

**I.O. Ryabtsev, K.A. Yushchenko;**

**V.V. Dmitrik, NTUU**

«Kharkiv Polytechnic Institute», Kharkiv, Ukraine;

**E.P. Chvertko, V.V. Kvasnitsky, NTUU**

«Igor Sikorsky Kyiv Polytechnic Institute»,

Kyiv, Ukraine;

**M.M. Student, Karpenko Physico-Mechanical**

Institute, Lviv, Ukraine;

**M. Zinigrad, Ariel University, Israel;**

**Ya. Pilarczyk, Welding Institute, Gliwice, Poland;**

**U. Reisgen, Welding and Joining Institute,**

Aachen, Germany

### Founders

E.O. Paton Electric Welding Institute

International Association «Welding»

### Publisher

International Association «Welding»

### Translators

A.O. Fomin, I.M. Kutianova

*Editor*

N.G. Khomenko

*Electron galley*

D.I. Sereda, T.Yu. Snegiryova

### Address

E.O. Paton Electric Welding Institute,

International Association «Welding»

11 Kazymyr Malevych Str. (former Bozhenko),

03150, Kyiv, Ukraine

Tel./Fax: (38044) 200 82 77

E-mail: journal@paton.kiev.ua

www://patonpublishinghouse.com/eng/journals/tpwj

State Registration Certificate

KV 4790 of 09.01.2001

ISSN 0957-798X

DOI: <http://dx.doi.org/10.37434/tpwj>

### Subscriptions

12 issues per year, back issues available.

\$384, subscriptions for the printed (hard copy) version,  
air postage and packaging included.

\$312, subscriptions for the electronic version  
(sending issues of Journal in pdf format  
or providing access to IP addresses).

Institutions with current subscriptions on printed version  
can purchase online access to the electronic versions  
of any back issues that they have not subscribed to.

Issues of the Journal (more than two years old)  
are available at a substantially reduced price.

All rights reserved.

This publication and each of the articles contained  
herein are protected by copyright.

Permission to reproduce material contained in this  
journal must be obtained in writing from the Publisher.

## CONTENTS

### SCIENTIFIC AND TECHNICAL

- Berdnikova O.M.* Physico-mechanical properties of welded joints of high-strength steel with the yield strength of 690–1300 MPa ..... 2
- Zavdoveev A.V., Poznyakov V.D., Gaivoronskyi O.A., Denysenko A.M. and Baudin T.* Optimization by calculation method of pulsed-arc welding modes using high alloy welding material ..... 9
- Marchenko A.E., Glot I.O. and Skorina N.V.* Influence of liquid glass characteristics on quality of coating formation of welding electrodes ..... 14
- Falchenko Iu.V., Petrushynets L.V., Fedorchuk V.Ye. and Polovetskyi Ye.V.* Investigation of heat treatment impact on the strength of Al–Ti bimetal honeycomb core ..... 20

### INDUSTRIAL

- Labur T.M., Yavorska M.R. and Koval V.A.* Weld formation in consumable electrode welding of butt joints of AMg5M aluminium alloy in site with a forming backing element and without it ..... 25
- Nedosieka S.A., Nedosieka A.Ya., Yaremenko M.A., Boichuk O.I. and Ovsienko M.A.* Method of acoustic emission at evaluation of the state of welds and their service properties. Part 2. Practical application ..... 31
- Panteleimonov E.O.* Portable module for heat treatment of welded joints of railway rails ..... 43

### INFORMATION

- «Paton» Industrial Park ..... 47
- A New Stage in Development of Paton Trade Mark ..... 49
- In Memory of S.I. Kuchuk-Yatsenko ..... 51

# PHYSICO-MECHANICAL PROPERTIES OF WELDED JOINTS OF HIGH-STRENGTH STEEL WITH THE YIELD STRENGTH OF 690–1300 MPa

**O.M. Berdnikova**

E.O. Paton Electric Welding Institute of the NAS of Ukraine

11 Kazymyr Malevych Str., 03150, Kyiv, Ukraine. E-mail: [office@paton.kiev.ua](mailto:office@paton.kiev.ua)

The work is devoted to determination of regularities of influence of features of structural-phase composition (grain, subgrain, dislocation structures, etc.) of metal of welded joints of high-strength steels of different strength class on their mechanical characteristics and crack resistance by determining structural criteria providing the necessary set of these properties. The structure and properties of welded joints of high-strength steels with the yield strength from 690 to 1300 MPa was investigated depending on the rates of cooling and welding, welds alloying, heat treatment conditions and welding methods (mechanized arc, laser, hybrid laser-arc welding): structural low-carbon steels of bainitic-ferritic and bainitic-martensitic type; high-carbon ferritic-pearlitic type; alloy medium-carbon steels of martensitic-bainitic type of a special purpose. The correlation between structural parameters and such a set of properties as strength, fracture toughness, level of localized deformation and local inner stresses in the metal of welded joints was established. It was shown that in compliance with certain ratios of structural-phase components, the characteristics of dislocation and subgrain structure are decisive for providing strength and crack resistance of welded joint metal of high-strength steels. The indices of the level of localized deformation in the metal of welded joints of high-strength steels were obtained and it was found how structural components affect crack resistance of the metal. In order to provide the service reliability of structures in the creation of science-intensive and promising technologies for welding of high-strength steels on the basis of material experimental and theoretical studies, structural criteria were determined to provide the required set of mechanical properties and crack resistance of the mentioned joints. 12 Ref., 4 Figures.

*Keywords:* high-strength steels, welded joints, structural-phase composition, substructure, dislocation density, mechanical properties, local inner stresses, localized deformation, crack resistance

In different branches of modern industry, including construction, agricultural, transport, machine-building and defense, for the manufacture of welded metal structures, low-carbon, alloy medium- and high-carbon high-strength steels are widely used. At present, the equipment and structures for critical purpose require the use of high-strength steels in a quite wide range of mechanical properties and, accordingly, of different structural and phase composition. Thus, in the construction and transport industries of agricultural purpose, structural low-carbon steels with a yield strength of 350–740 MPa are used. These are steels with ferritic-pearlitic, bainitic-ferritic and bainitic-martensitic structure. The ultimate strength of such steels reaches 490–940 MPa. For high-carbon ferritic-pearlitic steels used in railway transport, this value amounts to 910–1130 MPa and for medium-carbon alloy steels of martensitic-bainitic type of a special purpose, the ultimate strength reaches 1500–1700 MPa. The use of high-strength steels allows not only reducing the weight of structures, but also improving their technical characteristics by providing the necessary set of mechanical properties: high values of static and

dynamic strength, fracture toughness and resistance to brittle fracture. Taking into account the fact that many structures made of high-strength steels are structures of a long-term use, it is particularly important to carry out studies of the influence of structural factors on the mechanical properties and crack resistance of the joints of these steels. Most often in the manufacture of the mentioned metal structures, mechanized or automatic welding in shielding gases are used [1–3]. At the same time, such modes of welding are performed, which, on the one hand, would allow providing a high efficiency, and on the other hand, providing a necessary set of mechanical properties and crack resistance of welded joints. Recently, such advanced technologies as laser and hybrid laser-arc welding have been introduced [4], which makes it possible to produce welded joints with much smaller sizes of joints and heat-affected zone and to improve the quality of welded joints and process efficiency as compared to arc welding.

The processes of structure formation in the metal of welded joints of high-strength steels are studied in detail at the PWI of the NASU in the Department of Physico-Chemical Research of Materials, which for many years was headed by Dr. of Tech. Sci., Academician of the NAS of Ukraine G.M. Grigorenko. A

significant contribution to the determination of structural and phase changes that occur under the influence of welding modes was made by Dr. of Tech. Sci., Prof. L.I. Markashova. Her scientific activity is devoted to comprehensive studies of the structural-phase state of the metal of welded joints of steels, alloys, dissimilar metals and metals with nonmetallic materials, etc. (more than 300 scientific papers).

The main technological works on producing welded joints of high-strength steels with a yield strength ranging from 690 to 1300 MPa was performed in the Department of Welding of Alloy Steels under the supervision of Dr. of Tech. Sci. V. D. Poznyakov, Corresponding Member of the NAS of Ukraine.

The experimental works on the development of new technologies for laser and hybrid laser-arc welding of structural steels were carried out in the Department of Specialized High-Voltage Equipment and Laser Welding under the supervision of Cand. of Tech. Sci. V.D. Shelyagin.

Producing reliable and high-quality welded joints of high-strength steels is an urgent problem, in solving of which it is the most important to conduct a detailed study of the influence of a structural-phase composition and specific parameters of the structure formed in the weld metal and the heat-affected zone (HAZ) on strength and crack resistance of these joints [5–11]. Taken into account that individual areas of the HAZ of welded joints have small sizes, it is not always possible to determine their mechanical properties in the traditional way (mechanical testing of specimens). For this purpose, analytical methods can be used that are based on the results of experimental studies of the structure.

The aim of the work was to determine the regularities of influence of features of structural-phase composition of metal of high-strength steel welded joints of different strength class on their mechanical characteristics and crack resistance by determining structural criteria that provide the necessary set of these properties [12].

The work was performed on welded joints of high-strength steels using different technological parameters of welding modes (cooling and welding speeds, heat treatment conditions, weld alloying). The following three groups of high-strength steels of different purpose and strength class were selected:

1. Structural steels of bainitic-ferritic and bainitic-martensitic type (alform 620M; 17Kh2M; 14Kh-GN2MDAFB; N-A-XTRA-700) with  $\sigma_{0.2} = 690\text{--}740$  MPa and  $\sigma_t = 760\text{--}940$  MPa.

2. High-carbon steels of ferritic-pearlitic type (wheel steel of grade 2; 65G) with  $\sigma_{0.2} = 785\text{--}980$  MPa and  $\sigma_t = 910\text{--}1110$  MPa. Studies of wheel steels were

aimed at determination of regularities of influence of different technological factors, inherent in the process of restoration of railway wheels by surfacing (surfacing modes, preheating temperature of joints, systems of deposited metal alloying, etc.), on the phase-structural state and parameters of the structure of different areas of welded joints.

3. Alloy medium-carbon steels of a special purpose of martensitic-bainitic type (armor — steel of type 30Kh2N2MF and MiiLux Protection 500) with  $\sigma_{0.2} = 1300\text{--}1500$  MPa and  $\sigma_t = 1500\text{--}1700$  MPa. The main problems during manufacture of critical welded assemblies and bodies in welding of special-purpose wheeled armored vehicles from heat-hardened high-strength steels is that as a result of welding such steels may soften and in the welded joints cracks may form. To a large extent, the properties of such joints depend on the type of structures which are formed in the HAZ metal during welding. This is significantly influenced by welding modes and cooling conditions of the metal. This study is devoted namely to the issue of a structure formation in the metal of welded joints of such steels.

The investigations were carried out on model specimens-simulators of selected steels produced by thermal welding cycles in the range of cooling temperatures of 600–500 °C at a rate of  $w_{6/5} = 2.5\text{--}28$  °C/s and the joints produced by arc mechanized welding in a mixture of shielding gases (82 % Ar + 18 % CO<sub>2</sub>) when using welding wires of the following grades: Sv-10KhN2GSMFTYu, Sv-08G2S, Sv-08Kh20N9G7T, DMO-1G (for structural steels); Sv-08G2S; PP-AN180MN (10KhN2GSMFTYu); Sv-08KhM; Sv-08KhMF (for wheel steels); Sv-10GSMT, Sv-08Kh20N9G7T (for steels of special purpose). Welded joints of steels 14KhGN2MDAFB (Sv-10KhN2GSMFTYu) and N-A-XTRA-700 (Union NiMoCr) were produced by arc welding methods at a cooling rate  $w_{6/5} = 10\text{--}38$  °C/s and welding speed  $v_w = 18\text{--}50$  m/h (14KhGN2MDAFB); laser welding at  $w_{6/5} = 28\text{--}103$  °C/s ( $v_w = 18\text{--}50$  m/h, without welding wire); hybrid laser-arc welding at  $w_{6/5} = 58\text{--}63$  °C/s ( $v_w = 72\text{--}110$  m/h). The mentioned modes of hybrid laser-arc welding provide cooling of HAZ metal in the temperature range of 600–500 °C in a very narrow range, but differ significantly in the parameter  $v_w$ .

An approach based on a set of methods of physical materials science was proposed. The microstructure of the weld and HAZ metal were studied by the methods of a light microscopy using Versamet-2 and Neophot-32 microscopes. The microhardness of the metal was measured in a microhardness tester M-400 of LECO Company at a load of 0.1 kg. To reveal grain and dislocation structure, chemical, electrolytic

etching methods and the methods of local thinning of specimens were used. During studies, the structures of ferrite, austenite, pearlite, martensite, upper and lower bainite and their parameters like size of packages and grains, as well as the corresponding values of microhardness were investigated. The nature of distribution of chemical elements, as well as fractographic examinations of fracture surface of welded joints were made using analytical scanning electron microscopy (SEM, scanning electron microscope SEM-515 of Philips, Netherlands). SEM examinations studied the nature of metal fracture in fracture zones depending on the load and test temperature, volume fraction of fracture type, size of microelements of fracture surface – facets of brittle or quasi-brittle chip, tough pits, secondary microcracks. Peculiarities of the substructure and distribution of dislocation density in welded joints were studied on thin foils by transmission electron microscopy (TEM) in a microscope JEM-200CX, JEOL Company (Japan) at an accelerating voltage of 200 kV.

Based on experimental investigations at all structural levels of welded joints of high-strength steels, analytical evaluations of strength, fracture toughness, local inner stresses and localized deformation for each class of steels were performed. The structural factors were determined that guarantee the required level of mechanical properties and crack resistance of welded joints. The analytical evaluation of strength was performed taking into account the contribution of each of the structural parameters: sizes of packages, subgrains, lath structure, dislocation density, sizes of carbide phases and intercarbide distances, volume fraction of structures formed in the metal of the welds of high-strength steels. Applying the methods of mathematical processing, taking into account the complex of all structural components and their parameters, the experimental-computational approach of analytical evaluation of strength, fracture toughness, level of local inner stresses and a localized deformation formed in the structure of welded joints of high-strength steels under the influence of thermal welding cycles was improved. The differential contribution to the strength of the structural components of different types of structural hardening was determined: lattice friction, solid-soluble, grain, subgrain, dislocation and dispersion hardening.

The studies of welded joints of structural low-carbon steels showed that under the influence of thermal cycles of arc welding at an increase in cooling rate from  $w_{6/5} = 2.5$  to  $28$  °C/s the nature of transformation of a supercooled austenite in the intermediate region changes, which leads to a change in the phase composition of the metal of welded joints, volume fractions

of structural components, increase in microhardness, general refinement of grain and package structure, substructure, increase in a scalar intragranular density of dislocations. It was determined that at equal conditions of ratios of structural-phase components and parameters of grain (or package) structure, characteristics of dislocation and subgrain structures are decisive for providing strength and crack resistance of metal of welded joints of high-strength steels with a yield strength from 600 to 1300 MPa [12].

In the metal of the heat-affected-zone of welded joints of low- and high-carbon steels with ferritic-bainitic and ferritic-pearlitic structure of the base metal, uniform distribution of dislocation density ( $(2-4) \cdot 10^{10} \text{ cm}^{-2} \leq \rho \leq (7-8) \cdot 10^{10} \text{ cm}^{-2}$ ) during the formation of fine-grained bainitic-ferritic or bainitic-martensitic structures, dispersion of the substructure (to  $0.2-1.4 \text{ }\mu\text{m}$ ) and the presence of 50–80 % of lower bainite provides a high level of strength properties and crack resistance of these joints. In arc welding, this is realized at cooling rates  $w_{6/5} = 20-28$  °C/s (for structural ferritic-bainitic and bainitic-martensitic steels) and  $w_{6/5} = 5-10$  °C/s (for wheel high-carbon ferritic-pearlitic steels) [12].

While studying welded joints of alloy medium-carbon steels of a special purpose, it was found that the gradientless density distribution of dislocations ( $(7-8) \cdot 10^{10} \text{ cm}^{-2} \leq \rho \leq 10^{11} \text{ cm}^{-2}$ ) at the formation of the refined structure of tempering martensite with a substructure of  $0.4-0.8 \text{ }\mu\text{m}$  and a small fraction (5–20 %) of the component of lower bainite, provides high operation properties of the produced joints [12]. Such structural state is provided in cases when during welding the metal of a HAZ cools down at rates  $w_{6/5} = 3.8-5$  °C/c. The compliance with this fact guarantees the maximum level of fracture toughness and crack resistance of welded joints. It is shown that the highest index of fracture toughness  $K_{1C} = 110 \text{ MPa}\cdot\text{m}^{1/2}$  was obtained at  $w_{6/5} = 3.8-5.0$  °C/s due to the formation mainly of the structure of tempered martensite with a small fraction of lower bainite (up to 12 %). As the cooling rate increases to  $w_{6/5} = 12.5$  and  $21$  °C/s, the value of  $K_{1C}$  decreases to 85 and 70  $\text{MPa}\cdot\text{m}^{1/2}$ , respectively. Such a decrease in  $K_{1C}$  is associated with a decrease in the fraction of lower bainite, an increase in the fraction of martensite component in the presence of hardening martensite.

In welded joints of medium-carbon alloy steels of special purpose with different systems of alloying of welds, exclusively martensitic structure at the presence of hardening martensite ( $M_{\text{hard}}$ ) at a nonuniform distribution of density of dislocations and its maximum indices ( $\rho = (1-1.6) \cdot 10^{11} \text{ cm}^{-2}$ ), formed during welding wires of ferritic-pearlitic type (Sv-10GSMT)

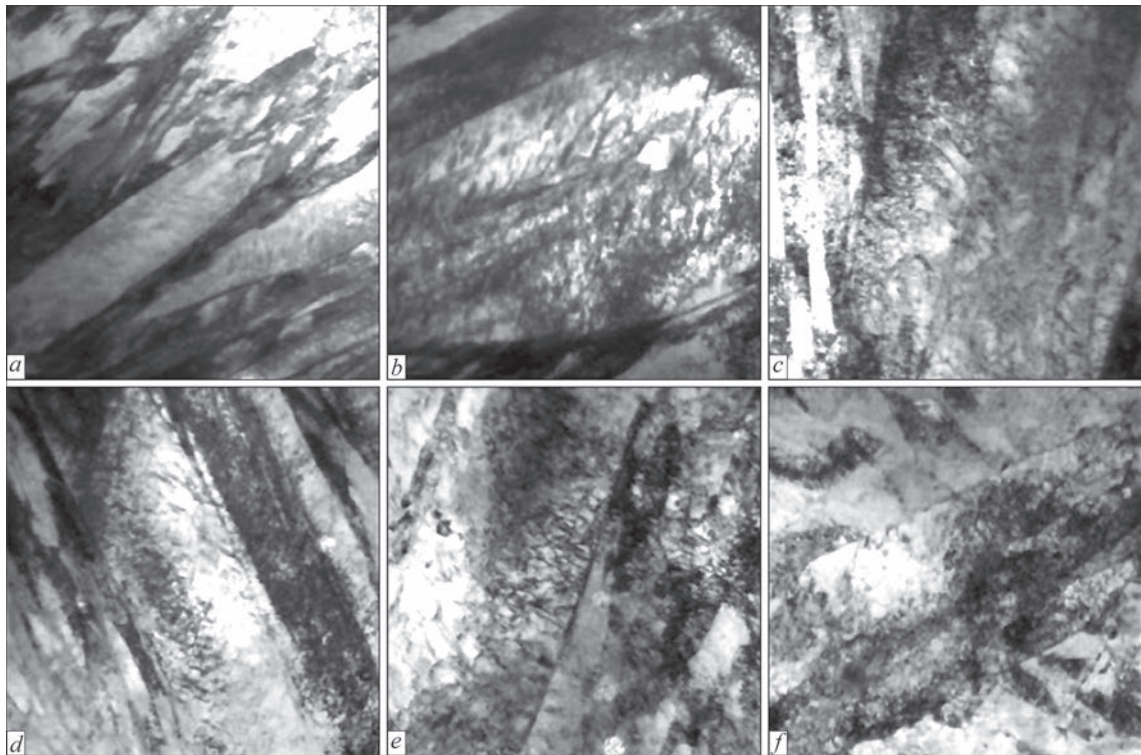


**Figure 1.** Thin structure of  $M_{hard}$  (*a, b*),  $M_{temp}$  (*c-e*) and  $B_1$  (*f*) in HAZ metal of welded joints of steel of type 30Kh2N2MF when using different wires: Sv-10GSMT (*a-c*); Sv-08Kh20N9G7T (*d-f*) after welding (*a* —  $\times 22000$ ; *b, d* —  $\times 35000$ ) and LTT (*c* —  $\times 35000$ ; *e* —  $\times 52000$ ; *f* —  $\times 35000$ )

(Figure 1, *a-c*). In the case of austenitic welding material (Sv-08Kh20N9G7T) in welds and HAZ metal, the density of dislocations decreases significantly ( $\rho = (8-9) \cdot 10^{10} \text{ cm}^{-2}$ ) at its uniform distribution. When using Sv-08Kh20N9G7T, the metal of the near-weld

HAZ area has mainly the structure of tempered martensite ( $M_{temp}$ , Figure 1, *d, e*) with a small share of lower bainite ( $B_1$ , Figure 1, *f*). In both cases of welded joints, low-temperature tempering (LTT) leads to a decrease in *HV*, uniform redistribution of dislocations

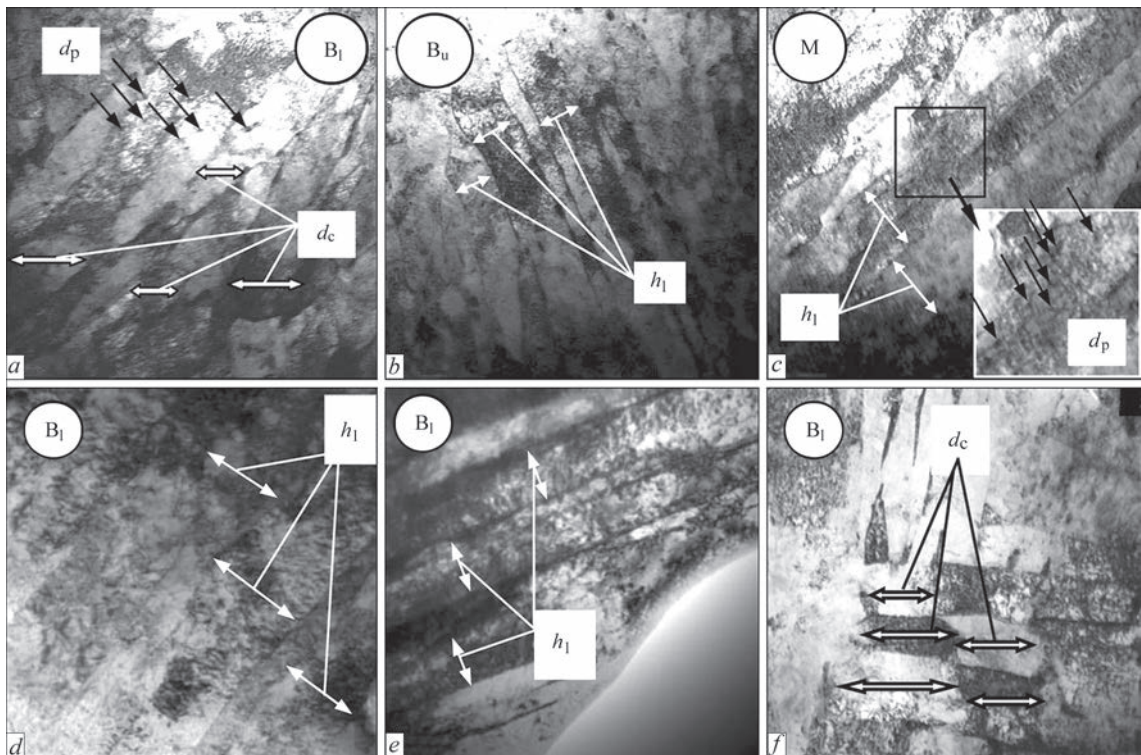


**Figure 2.** Thin structure of HAZ metal of welded joints of steels N-A-XTRA-70 (*a-c*) and 14KhGN2MDAFB (*d-f*) in hybrid laser-arc welding ( $w_{6/5} = 58 \text{ }^\circ\text{C/s}$ ;  $v_w = 72 \text{ m/h}$ ): *a, d, e, f* —  $B_1$ ; *b* —  $B_u$ ; *c* —  $M_{temp}$ ,  $\times 25000$

and a decrease in their density. To a greater extent, such structural changes are characteristic of the joints produced using Sv-10GSMT.

In the metal of structural low-carbon steels with a yield strength of more than 600 MPa (14KhGN-2MDAFB; N-A-XTRA-70) at high cooling rates in the modes of laser and hybrid laser-arc welding processes, in lower bainite and tempered martensite in the welds and HAZ metal nanostructures are formed [9, 12]. A typical feature of the structure formed during high-speed laser and hybrid welding of high-strength steels during dispersion of laths width ( $h_1$ , Figure 2, *a-e*)  $B_1$  and upper bainite ( $B_u$ ) is the presence of a fragmented substructure of  $B_1$  of the size of 80–300 nm and clear boundaries (Figure 2, *a, f*). In this case, both the structure of  $B_1$  and  $M_{temp}$  are char-

acterized by the presence of nanoparticles of carbide phases. The size of nanoparticles of carbide phases ( $d_p$ ), uniformly distributed throughout the volume of the structure, is 10–30 nm (Figure 2, *a, c*). The formation of the nanostructured state in lower bainite and tempered martensite will increase the strength, fracture toughness and crack resistance of structural steel joints.

With a respective change in the modes of arc, laser and hybrid laser-arc welding of structural steels, the ratio of the components of lower and upper bainite, martensite, their parameters, volume fraction, as well as density and distribution of dislocations change also. Under the modes with a high input energy, the structures of upper bainite are mainly formed at a general increase in the size of grain and subgrain structures

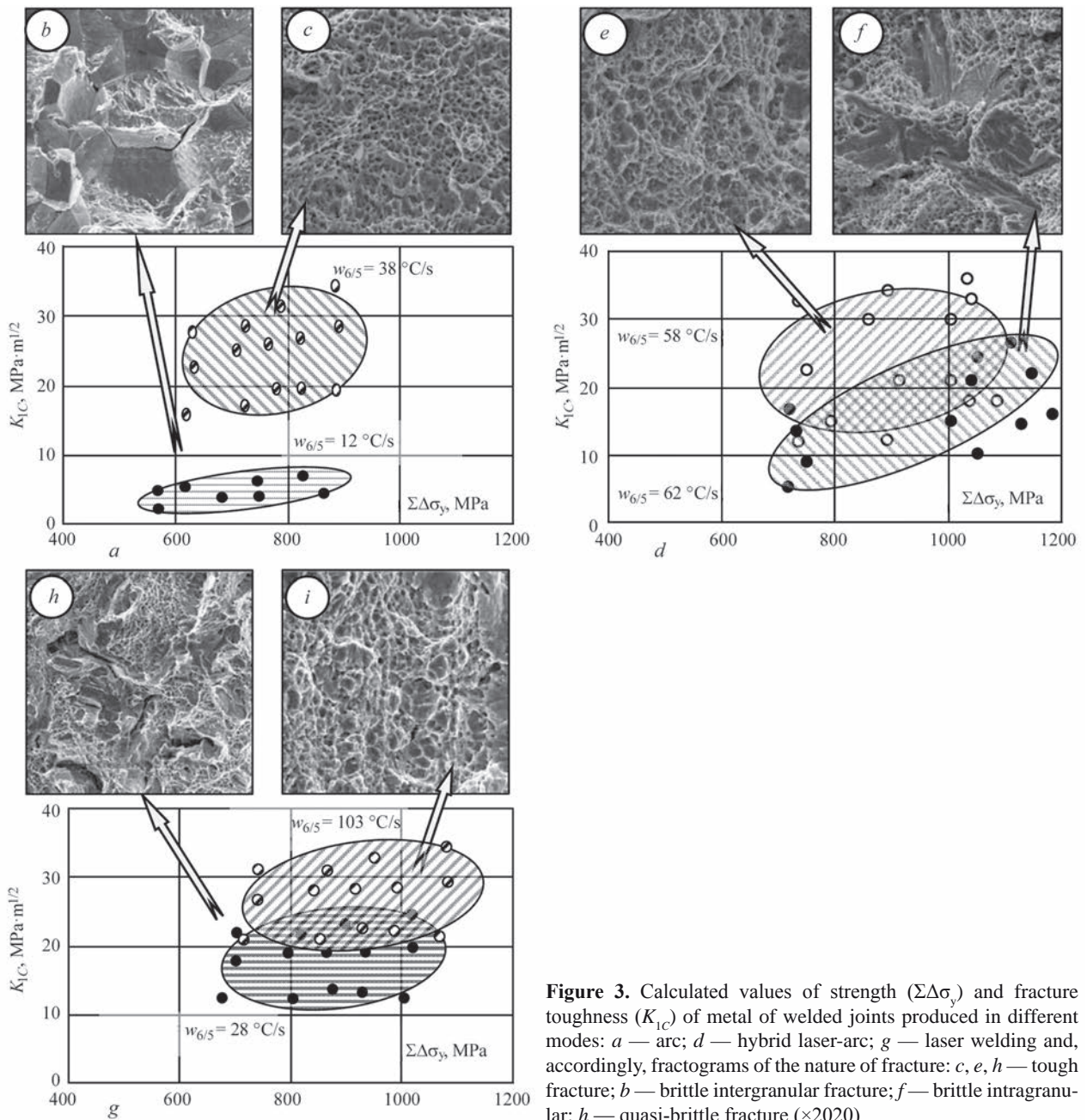


**Figure 3.** Calculated values of strength ( $\Sigma\Delta\sigma_y$ ) and fracture toughness ( $K_{1C}$ ) of metal of welded joints produced in different modes: *a* — arc; *d* — hybrid laser-arc; *g* — laser welding and, accordingly, fractograms of the nature of fracture: *c, e, h* — tough fracture; *b* — brittle intergranular fracture; *f* — brittle intragranular; *h* — quasi-brittle fracture ( $\times 2020$ )

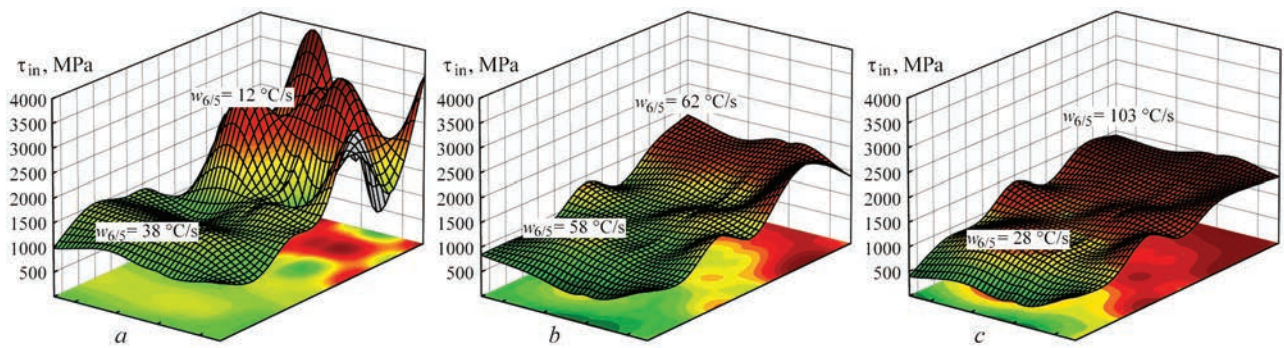


**Figure 4.** Distribution of local inner stresses  $\tau_{in}$  in the structure of welded joints in arc (a), hybrid laser-arc (b) and laser welding (c): maximum values of  $\tau_{in}$  at  $w_{6/5} = 12; 62; 103$  °C/s; minimum  $\tau_{in}$  at  $w_{6/5} = 38; 58; 28$  °C/s

with a nonuniform distribution of dislocation density (from  $\rho = (4-6) \cdot 10^{10}$  cm<sup>-2</sup> to  $\rho = (1-2) \cdot 10^{11}$  cm<sup>-2</sup>). A decrease in input energy contributes to the predominant formation of the structures of lower bainite at a significant grain and subgrain refinement with a uniform distribution of dislocation density ( $\rho = (6-8) \cdot 10^{10}$  cm<sup>-2</sup>). Such structural changes provide a set of properties of strength and fracture toughness (Figure 3).

Evaluations of the level of local inner stresses ( $\tau_{in}$ ), presented in the diagrams of Figure 4, show the following. Extended zones with the maximum values of  $\tau_{in}$  (1900–3700 MPa) are formed in the conditions of arc welding at the modes with the minimum cooling rate along the intergranular boundaries of  $B_u$  in the places of extended dislocation clusters ( $\rho = 2 \cdot 10^{11}$  cm<sup>-2</sup>), Figure 4, a. This leads to the initiation of microcracks in these areas and, accordingly, to a reduction in the crack resistance of welded joints. A decrease in the values of  $\tau_{in}$  is characteristic of welded joints produced in hybrid welding ( $\tau_{in} = 1470-1867$ , Figure 4, b) and especially in laser welding ( $\tau_{in} = 1470-1663$  MPa, Figure 4, c) which is contributed by the formation of fine-grained structures of  $B_l$  in combination with a uniform distribution of dislocation density in the welding zone.

As a result, it was found that the optimal properties of strength, ductility and crack resistance of welded joints of high-strength structural steels are provided in the conditions of arc welding at a cooling rate  $w_{6/5} = 38$  °C/s, in laser welding at  $w_{6/5} = 103$  °C/s, and in hybrid laser-arc welding at  $w_{6/5} = 58$  °C/s, which is predetermined by the formation of the most dispersed structures: lower bainite, fine-grained tempered martensite in the absence of extended dislocation clusters — concentrators of local inner stresses.

Establishing the regularities of influence of the structural-phase composition of the metal of welded joints of high-strength steels with a yield strength from 600 to 1300 MPa, produced in different ways and using different welding modes on their physical

and mechanical properties, allowed determining the conditions under which in the welds and HAZ metal the structures will form that will provide them with the necessary set of mechanical properties and a high crack resistance. TEM examinations established the relationship between the parameters of the formed substructure directly with the dislocation structure, namely with the level of a localized deformation ( $\varepsilon_l$ ) with the fields of  $\tau_{in}$ , which grow with an increase in  $\rho$  [12]. Such evaluations were made taking into account the average distance of dislocation displacement ( $S$ , which according to TEM examinations corresponds to the parameters of the substructure) in the process of thermodeformation effect for welded joints of all investigated high-strength steels.

Thus, for lower bainite  $\varepsilon_l \leq 20$  % at  $\rho = (4-8) \cdot 10$  cm<sup>-2</sup> and with the sizes of its substructure being 0.1–0.8  $\mu$ m. In the structure of upper bainite the formation of the zones of a localized deformation in the range of 10 %  $\leq \varepsilon_l \leq 70$  % at  $\rho = (8 \cdot 10-1.4 \cdot 10^{11})$  cm<sup>-2</sup> is typical. The values of the level of deformations in martensitic structures also differ. In tempered martensite it is  $\varepsilon_l \leq 50$  % and in hardened one it is 40 %  $\leq \varepsilon_l \leq 140$  %. It was found that the formation of zones of a localized deformation significantly reduces the crack resistance of metal in the range of 50–140 % at  $\rho = (1.1-2.0) \cdot 10^{11}$  cm<sup>-2</sup> in the structural components of upper bainite and hardening martensite.

Such structures as lower bainite and tempered martensite provide a high set of mechanical properties of the metal of welded joints of high-strength steels. These structures are characterized by the absence of extended concentrators of crack formation due to the absence of dislocation clusters – zones of deformation localization, which significantly affect the level of local inner stresses.

TEM examinations allowed establishing the relationship between the parameters of the substructure formed directly with a dislocation structure, namely the level of a localized deformation and inner stress fields, which grow with an increase in dislocation

density. It is shown that one of the factors influencing the level of a localized deformation, in addition to the value of dislocation density, is also the substructure of the metal, which causes redistribution of dislocations.

### Conclusions

Regularities of influence of technological parameters (cooling rate and welding speed, weld alloying, heat treatment conditions) on structural-phase composition, parameters of grain, subgrain, dislocation structures of welds and heat-affected-zone metal of low-carbon (structural) welded joints of medium-carbon alloy (of special purpose) and high-carbon (wheel) steels and the relationship of the structure with mechanical properties of these joints, level of local inner stresses and a localized deformation formed in different structural components (lower and upper bainite, hardened and tempered martensite, etc.) were determined.

The improvement of experimental-analytical procedure of evaluating the complex of physical and mechanical properties according to specific structural parameters of all elements of the structure was carried out, mathematical data processing was introduced. The correlation between structural parameters and values of strength, fracture toughness, local inner stresses in the metal of welded joints of high-strength steels was established, which allowed classifying the conditions of crack formation relative to the complex of structural components taking into account the density of dislocations and features of the substructure.

It is shown how the microstructure affects the physical and mechanical properties of welded joints of high-strength steels of a wide strength range. The generalization of structural conditions for providing a high level of the complex of mechanical properties and crack resistance of welded joints of high-strength steels made it possible to propose structural criteria and indicate methods to apply them in technologies and promising methods of welding. Based on the structural criteria for the phase composition, dispersion of grain and subgrain structure with a gradientless distribution of dislocation density, scientific

ically substantiated recommendations for producing high-quality welded joints of high-strength steels for different purposes and a wide range of strength were developed.

1. Paton, B.E. (2008) *Selected proceedings*. Kiev, PWI [in Russian].
2. (2018) *Science of materials, achievements, prospects*. Ed. by L.M. Lobanov. Kyiv, Akadempriodyka, Vol. 2 [in Ukrainian].
3. Poznyakov, V.D. (2017) Welding technologies for production and repair of metal structures from high-strength steels. *Bulletin of the National Academy of Sciences of Ukraine*, **1**, 65–73.
4. (2018) *Physical processes in welding and processing of materials. Theoretical investigation, mathematical modeling, computational experiment*: Coll. of articles and reports. Ed. by I.V. Krivtsun. Kiev, IAW. ISBN 978-617-7015-74-0 [in Russian].
5. Madej, K., Świderegoł, S., Jakubiec, P. (2015) Analysis of Cracks in Welded joints of pipes with eyes made of S890QL1 steel. *Biuletyn Instytutu Spawalnictwa*, **6**, 11–22. DOI: <https://doi.org/10.17729/ebis.2015.6/2>
6. Laukhin, D., Pozniakov, V., Beketov, O. et al. (2020) Analysis of the effects of welding conditions on the formation of the structure of welded joints of low-carbon low-alloy steels. *Engineering Materials*, **844**, 146–154.
7. Ostash, O.P., Kulyk, V.V., Poznyakov, V.D. et al. (2019) Influence of the modes of heat treatment on the strength and cyclic crack-growth resistance of 65G steel. *Mater Sci.*, **54**(6), 776–782.
8. Kostin, V.A., Grigorenko, G.M., Poznyakov, V.D. et al. (2020) Structural transformations of the metal of heat-affected zone of welded joints of high-strength armor steels. *Ibid.*, **55**(6), 863–869. DOI: <https://doi.org/10.1007/s11003-020-00380-7>
9. Markashova, L., Berdnikova, O., Alekseienco, T. et al. (2019) *Nanostructures in welded joints and their interconnection with operation properties. Advances in thin films, nanostructured materials, and coatings*. Ed. by A.D. Pogrebnyak, V. Novosad. Singapore, Springer, 119–128. DOI: [https://doi.org/10.1007/978-981-13-6133-3\\_12](https://doi.org/10.1007/978-981-13-6133-3_12)
10. Vimalraj, C., Kah, P., Layus, P. et al. (2019) High-strength steel S960QC welded with rare earth nanoparticle coated filler wire. *The Int. J. of Advanced Manufacturing Technology*, **102**, 105–119.
11. Francois Njock Bayock, Kah, P., Layus, P., Karkhin, V. (2019) Numerical and experimental investigation of the heat input effect on the mechanical properties and microstructure of dissimilar weld joints of 690 MPa QT and TMCP Steel. *Metals*, **9**(3), 355, 1–19. DOI: <https://doi.org/10.3390/met9030355>
12. Berdnikova, O.M. (2020) *Structural criteria of strength and crack resistance of high-strength steel welded joints*: Syn. of Thesis for Dr. of Tech. Sci. Degree. Kyiv, PWI [in Ukrainian].

Received 23.02.2021

### BOOKS IN ELECTRONIC FORMAT

**Paton E.O.: Photo Album.** — Kyiv: «Gorobets», 2020. — 116 p., il.

The photo album was published on the occasion of the 150th anniversary of the birth of academician E.O. Paton (1870–1953) and contains a photo chronicle of his activities in the field of welding and bridge construction.

**Paton B.E.: Photo Album.** — Kyiv: «DIA», 2019. — 196 p., il.

The photo album was published on the occasion of the 100th anniversary of the birth of academician B.E. Paton (1918–2020) and contains a photo chronicle of his multifaceted activities in the field of welding, metallurgy and materials science.

Order: Tel./Fax: (38044) 200-82-77; E-mail: [journal@paton.kiev.ua](mailto:journal@paton.kiev.ua)

# OPTIMIZATION BY CALCULATION METHOD OF PULSED-ARC WELDING MODES USING HIGH ALLOY WELDING MATERIAL

A.V. Zavdoveev<sup>1</sup>, V.D. Poznyakov<sup>1</sup>, O.A. Gaivoronskyi<sup>1</sup>, A.M. Denysenko<sup>1</sup> and T. Baudin<sup>2</sup>

<sup>1</sup>E.O. Paton Electric Welding Institute of the NAS of Ukraine

11 Kazymyr Malevych Str., 03150, Kyiv, Ukraine. E-mail: [office@paton.kiev.ua](mailto:office@paton.kiev.ua)

<sup>2</sup>Université Paris-Saclay, CNRS, Institut de Chimie Moléculaire et des matériaux Tériaux d'Orsay  
91405 Orsay, France. E-mail: [thierry.baudin@u-psud.fr](mailto:thierry.baudin@u-psud.fr)

The use of modern pulsed-arc welding technologies allows a significant improvement of the quality of welded joints. However, a large number of possible welding modes hinder the development and implementation of pulse technologies in modern production. This is associated with the fact that in pulsed-arc welding at least four independently variable parameters exist, which in totality requires a large number of experiments to determine their impact. To optimize the number of experiments in this study, the experimental calculation Taguchi algorithm for the process of pulsating arc welding using a high alloy welding material was implemented. The quantitative contribution of each variable welding parameter in the formation of the penetration depth is shown. The optimal welding modes were proposed, providing a set penetration depth. 15 Ref., 6 Tables, 4 Figures.

*Keywords:* pulsating arc welding, penetration depth, Taguchi algorithm, high alloy welding material

Pulsed-arc welding (PAW) is qualitatively different from traditional welding in shielding gases [1–4]. This is predetermined by expanded capabilities of PAW in affecting the processes of melting and transfer of the electrode metal, formation of the structure in the weld and HAZ metal of welded joint, regulating the weld shape, penetration depth, etc. Today, this method of welding is increasingly used in world practice in the manufacture of critical welded structures from high-strength steels [4–7].

At present, the leading companies developed many inverter welding current sources based on pulse technologies for MIG/MAG welding. Thus, the Swedish Company Esab developed the power source Aristo 500, the American Company Hobart — Ultra-Arc 350, the German Company EWM — Phoenix 501 pulse. Due to a wide range of tasks that can be solved in PAW, they are in demand in the domestic production of critical

metal structures. However, it should be noted that these sources have built-in programs with a wide range of modes, from which it is difficult to choose the optimal one for a specified variant of welding.

In PAW, there are four variable mode parameters: base current ( $I_b$ ), pulse current ( $IP$ ), frequency ( $f$ ), and duty cycle ( $C$ ). Therefore, while choosing a mode, it is necessary to conduct a large number of experiments. Also, a well-known experimental calculation Taguchi method exists [8], which allows evaluating the influence of each of the parameters of a mode on welded joint formation.

The aim of the work was to make the selection of PAW modes using the Taguchi method, which provide a set penetration depth of the V-shaped groove without a gap of a butt joint of high-strength alloy steel with a reverse weld formation with the use of a high-alloy welding material.

**Table 1.** Selected parameters for PAW

Parameter	Note	Level					
		Value			Coding		
		Minimum	Mean	Maximum	Minimum	Mean	Maximum
Pulse current, A	A	160	200	240	1	2	3
Pause current, A	B	80	120	140	1	2	3
Frequency, Hz	C	0.5	1	5	1	2	3
Duty cycle, %	D	40	60	80	1	2	3

A.V. Zavdoveev — <https://orcid.org/0000-0003-2811-0765>, V.D. Poznyakov — <https://orcid.org/0000-0001-8581-3526>,  
O.A. Gaivoronskyi — <https://orcid.org/0000-0002-5922-5541>, Baudin T. — <https://orcid.org/0000-0002-6765-360X>

© A.V. Zavdoveev, V.D. Poznyakov, O.A. Gaivoronskyi, A.M. Denysenko and T. Baudin, 2021

**Table 2.** Performance of tests on the base of designing plan

Number	Pulse current, A		Pause current, A		Frequency, Hz		Duty cycle, %	
	Value	Code	Value	Code	Value	Code	Value	Code
1	160	1	80	1	0.5	1	40	1
2	160	1	120	2	1	2	60	2
3	160	1	140	3	5	3	80	3
4	200	2	80	1	1	2	80	3
5	200	2	120	2	5	3	40	1
6	200	2	140	3	0.5	1	60	2
7	240	3	80	1	5	3	60	2
8	240	3	120	2	0.5	1	80	3
9	240	3	140	3	1	2	40	1

**Experimental procedure.** When performing the investigations, the parameters of PAW by pulsating arc were selected, which are given in Table 1.

In the mentioned experiment there are four independently controlled process parameters and three experimental levels. In full, for four factors and three levels it would be necessary to conduct a  $3^4 = 81$  experiment. The method proposed by Taguchi uses orthogonal arrays (OAs) for determination of the minimum number of experiments in real time to evaluate all designing factors. In such an experimental scheme, each factor is evaluated individually and one does not affect the other. The conditions that emerged in this study, i.e. four parameters together with their three levels, are suitable for the selection of the L9 matrix as an experimental project. Table 2 presents nine experimental tests in real time, which were compiled as specified in the scheme L9 ( $3^4$ ) according to the Taguchi method [8, 9]. In this case, the experiments should be carried out in random order to bypass noise sources.

*Calculation of signal-to-noise ratio.* When conducting experiments, different process parameters are used, which give different values of «response». As a «response», penetration depth (PD) was chosen. In the course of experimental tests, it was necessary to evaluate the influence of each selected factor with the help of the received «responses», which may not be unique and have both desirable and undesirable characteristics. According to the Taguchi method, the signal/noise ratio ( $S/N$ ) is a deviation of the qualitative characteristic from the desired value. During calcu-

lation of the  $S/N$  ratio, one should choose among the three available operating values — a higher, a lower and a nominal one (HB, LB and NB).

The calculation of the  $S/N$  ratio was performed according to the equation (1). The generalized calculated  $S/N$  ratios for all experiments are presented in Table 3.

$$\frac{S}{N} = -10 \log \left( \frac{\sum_1^n \frac{1}{Y^2}}{n} \right). \quad (1)$$

The next step in the analysis consists in dividing the influence of each individual parameter on all three considered levels and ranking them in the order of their influence on the response parameter. This is possible because the selected experimental scheme corresponds to the orthogonal L9 matrix [10].

The average efficiency of the factor is calculated by dividing the sum of the test results including the factor by a number of the tests performed at the same level (equation (2)):

$$\text{for example, } \langle S/N \rangle_{A1} = (S/N_1 + S/N_2 + S/N_3) / 3. \quad (2)$$

*Contribution of individual factors to the penetration depth.* Rated control of the final answer requires knowledge of the degree of contribution of individual process parameters, and they can be evaluated using a statistical method, namely ANOVA [11]. In the ANOVA methodology,  $SS$ ,  $SS'$ ,  $D$ ,  $V$  and  $P$  are typical symbols of the parameters, used in the abovementioned analysis to represent the factors, sum and adjusted

**Table 3.** Results of measuring penetration depth and signal-to-noise ratio

Number	Parameters				Response		Q/V, kJ/mm
	Pulse current, A	Pause current, A	Frequency, Hz	Duty cycle, %	PD	S/N	
1	160	80	0.5	40	0.88	-1.128	0.42
2	160	120	1	60	2.159	6.673	0.55
3	160	140	5	80	2.47	7.851	0.61
4	200	80	1	80	3.37	10.55	0.68
5	200	120	5	40	3.31	10.4	0.62
6	200	140	0.5	60	2.091	6.374	0.72
7	240	80	5	60	2.926	9.322	0.67
8	240	120	0.5	80	3.597	11.12	0.93
9	240	140	1	40	3.349	10.5	0.75

sum of squares, degree of freedom, dispersion and a percentage contribution of each factor, respectively [12, 13]. A brief explanation of the abovementioned factors is presented below.

The total sum of  $SS_T$  squares can be calculated from the  $S/N$  ratio from the equation (3), which uses the terms «total number of experiments ( $m = 9$ )» and « $i$ -th current signal-to-noise ratio  $\eta_i$ »:

$$SS_T = \sum_{i=1}^9 S / N_i^2 - \frac{1}{9} \left( \sum_{i=1}^9 S / N_i \right)^2. \quad (3)$$

The sum of squares of factors, denoted as  $SS_p$  is calculated by the equation (4), which has the following conditions: factor « $p$ », number of its level as « $j$ », repetition of each level for the tested factor  $p$ , as « $t$ » ( $= 3$ ), summation of the signal-to-noise ( $S/N$ ) ratio, that connects this coefficient  $p$  and its level  $j$  as  $S/Npj = (S/N_1 + S/N_2 + S/N_3)$  for the level  $A_j = 1$ ,  $(S/N_2 + S/N_3 + S/N_4)$  for the level  $A_j = 2$ ,  $(S/N_7 + S/N_8 + S/N_9)$  for the level  $A_j = 3$

$$SS_p = \sum_{j=1}^3 \frac{(\sum S / Npj)^2}{3} - \frac{1}{9} \left( \sum_{i=1}^9 S / N_i \right)^2. \quad (4)$$

The degree of freedom (DOF) is one of the elements that should be taken into account when calculating ANOVA [11].  $D_p$  and  $V_p$  are the notations used to represent the degree of freedom and the dispersion of the factor  $p$ .  $V_p$  is determined as a percentage with the use of  $SS_p$  from  $D_p$  in accordance with the equation (5).

$$V_p (\%) = \frac{SS_p}{D_p} \cdot 100. \quad (5)$$

The summation of DOF, accompanied near the tests and the mean value, is called the total DOF. The degree of freedom for the mean value is always equal to 1. Therefore, the total degree of freedom for this experimental study is 8, which is equal to the number of tests (9 tests) – 1, and the degree of freedom for the parameters is 2, which is obtained by subtracting 1 from the number of parameter levels (3 levels).

The difference between  $SS_p$  (sum of squares of factors) and the product of the dispersion of errors and DOF of each test factor is called the adjusted sum of squares and is denoted as  $SS'_p$  which is calculated by the equation (6).

$$SS'_p = SS_p - D_p V_e. \quad (6)$$

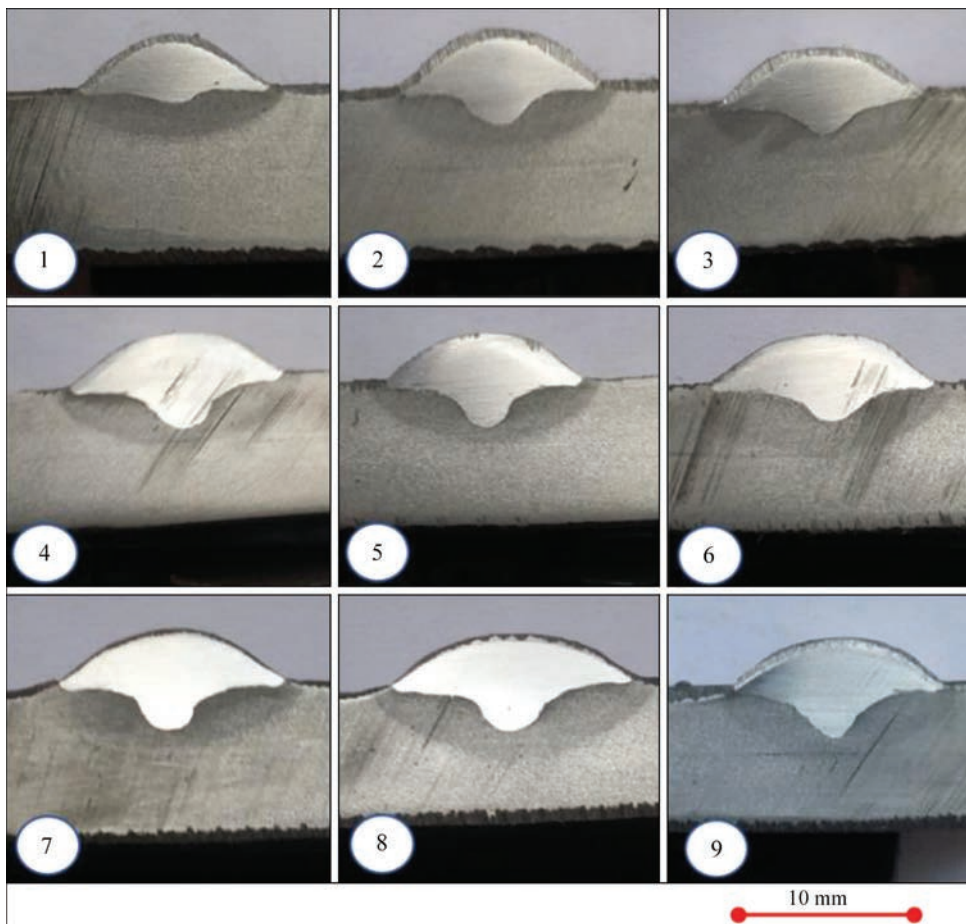


Figure 1. Photo of macrosections of experimental deposits

**Table 4.** Calculation of *S/N* values according to the algorithm of Taguchi

Parameter	Note	Level 1	Level 2	Level 3	$\Delta = \text{max} - \text{min}$	Rank
Pulse current, A	A	4.465	9.107	10.31	5.85	1
Pause current, A	B	6.249	9.395	8.241	3.15	4
Frequency, Hz	C	5.454	9.24	9.189	3.79	2
Duty cycle, %	D	6.588	7.456	9.84	3.25	3

The percentage ratio of the tested factors between their corrected sum and the total sum of squares is called their percentage contribution and is denoted as  $P_p$ . The equation (7) is used to determine  $P_p$ :

$$P_p (\%) = \frac{SS'_p}{SS_T} \cdot 100. \tag{7}$$

**Results and discussion.** Macrosections of the deposits produced in accordance with the program (Table 2) are shown in Figure 1, where the number corresponds to the surfacing mode. The results of the calculation of the penetration depth for the mentioned specimens are given in Table 3.

Using the Taguchi algorithm, taking into account the corresponding values of the signal-to-noise ratio, the mean values for each level and welding parameter are calculated, which are given in Table 4.

As is seen from the calculations, pulse current for penetration depth parameter is ranked by the number «1», which indicates that it has the greatest influence on penetration depth than on pause current, frequency and duty cycle.

The ANOVA results provide information on the quantitative contribution of each parameter.

*Compliance test for checking repeatability.* After selecting the optimal level of designing process parameters, this is a mandatory step to determine and check the improvement of quality characteristics with the use of the optimal level of designing parameters. According to [11–15], the predicted signal-to-noise ratio for the optimal level of the design process parameters can be calculated as

$$\hat{\eta} = \eta_m + \sum_{i=1}^n (\bar{\eta}_i - \eta_m). \tag{8}$$

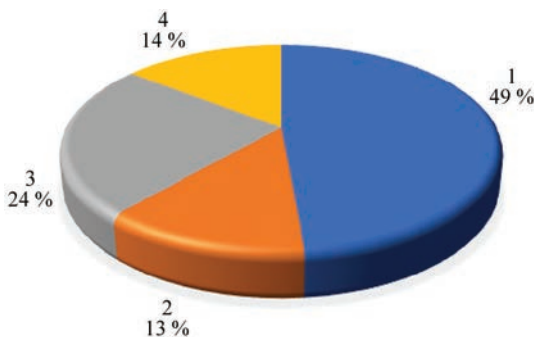


**Figure 2.** Results of calculations by ANOVA method: 1 — pulse current; 2 — pause current; 3 — frequency; 4 — duty cycle

In the abovementioned equation,  $\eta_m$ ,  $\eta_i$  and  $n$  represent the mean *S/N* ratio (Table 4) and the total number of important projects of experimental parameters affecting the quality. The predicted *S/N* ratio can be found using the optimal parameters of the pulsating arc welding process (Tables 5, 6).

The results of checking the predicted welding modes in order to obtain the maximum and minimum penetration depth during pulsating arc welding are shown in Figure 3. As is seen, the experimental-calculation algorithm of Taguchi makes it possible to predict the response of the studied parameter, namely penetration depth with a high accuracy.

The results of the studies were used while selecting the optimal PAW mode for the root layer of the V-shaped joint of high-strength steel, the groove of which was made without a gap and had a 4 mm blunting (Figure 4). At the same time, it was possible to obtain the proper quality of the welded joint, namely to provide penetration of the groove root with the reverse weld formation already in the course of the first experiment.

It should be noted that the Taguchi method can also be used when selecting PAW modes for multilayer joints in order to obtain the optimal HAZ dimensions. This is a very important factor that significantly affects the technological and operational properties

**Table 5.** Results of evaluating the predicted number and confirming the results for the optimal state of the PA-GMAW process (PD is the maximum)

Parameters	A	B	C	D	S/N	
					Prediction	Experiment
Optimal coded value	3	2	2	3	14.9	12.04
Optimal value	240	120	1	80		
Deviation = 19 %.						

**Table 6.** Results of evaluating the predicted number and confirming the results for the optimal state of the PA-GMAW process (PD is the minimum)

Parameters	A	B	C	D	S/N	
					Prediction	Experiment
Optimal coded value	2	1	2	1	-1.13	-1.21
Optimal value	200	80	1	40		
Deviation = 7 %						

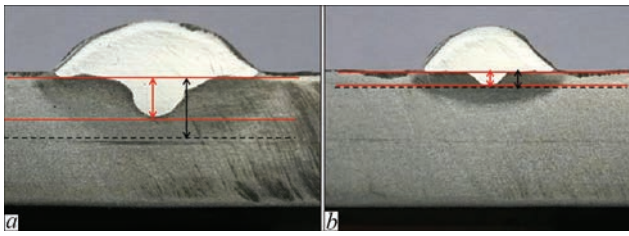


**Figure 3.** Macrosections of deposits produced according to the calculated modes, with maximum (a) and minimum (b) PD (dotted line shows calculated value of penetration and solid line shows experimental one)

of welded joints of critical metal structures made of high-strength alloy heat-hardened steels. The studies in this direction are performed and the results will be presented in future publications.

### Conclusions

1. A study of the influence of pulsed-arc welding modes (welding current, pause current, frequency, duty cycle) on penetration depth using a high-alloy welding wire by means of the experimental calculation Taguchi method was carried out. The possibility of controlling the parameters of pulsating arc welding in order to obtain the required penetration depth in a wide range was shown.

2. It was found that pulse current has a predominant influence on penetration depth. The influence of frequency, duty cycle and pause current is the next in importance. The quantitative analysis revealed that the influence of these parameters is distributed as follows: pulse current — 49 %, pause current — 13 %, frequency — 24 %, duty cycle — 14 %.

3. The carried out studies allowed proposing the optimal modes of pulsed-arc welding, which provide the set values of penetration depth, namely the minimum and the maximum one. The verification experiment showed that within the limits of insignificant deviations the predicted values of penetration depth correlate with the experimental ones.

4. Experimental calculation Taguchi method is a powerful and promising tool that can be used while selecting the optimal modes and in the development of pulsed-arc welding technologies.

1. Poznyakov, V.D., Zhdovoev, A.V., Gajvoronsky, O.A. et al. (2018) Effect of pulsed-arc welding modes on the change of weld metal and HAZ parameters of welded joints produced with Sv-08kh20N9G7T wire. *The Paton Welding J.*, **9**, 7–12. DOI: <https://doi.org/10.15407/tpwj2018.09.02>
2. Palani, P.K., Murugan, N. (2006) Selection of parameters of pulsed current gas metal arc welding. *J. Mater. Process. Technol.*, **172**, 1–10.

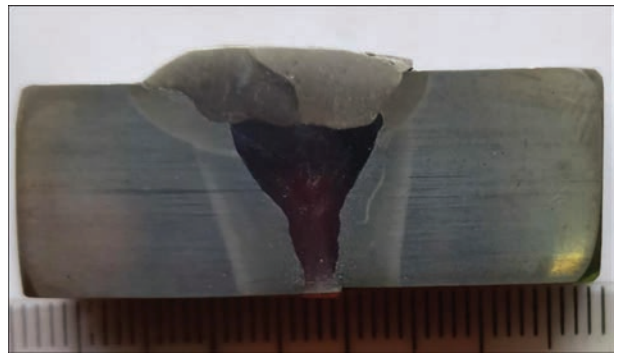


**Figure 4.** Butt joint of high-strength steel (V-shaped, without a gap, 4 mm blunting)

3. Tong, H., Ueyama, T. (2001) Quality and productivity improvement in aluminium alloy thin sheet welding using alternating current pulsed metal inert gas welding system. *Sci. Technol. Weld. Join.*, **6**(4), 203–208.
4. Rajasekaran, S. (1999) Weld bead characteristics in pulsed GMA welding of Al–Mg alloys. *Weld. J.*, **78**(12), 397–407.
5. Zhdovoev, A., Rogante, M., Poznyakov, V. et al. (2020) Development of the PC-GMAW welding technology for TMCP steel in accordance with welding thermal cycle, welding technique, structure and properties of welded joints. *Reports in Mechanical Engineering*, **1**(1), 26–33.
6. Murray, P.E. (2002) Selecting parameters for GMAW using dimensional analysis. *Weld. J.*, **81**(7), 125–131.
7. Essers, W.G., Van Gompal. (1984) Arc control with pulsed GMA welding. *Ibid.*, **64**(6), 26–32.
8. Ross, P.J. (1988) *Taguchi techniques for quality engineering: Loss function, orthogonal experiments, parameter and tolerance design*. New York, McGraw-Hill, 1988 Aug.
9. Phadke, M.S. (1995) *Quality engineering using robust design*. Prentice Hall PTR, 1995 Dec. 1.
10. Ma, Y, Hu, H, Northwood, D, Nie, X. (2007) Optimization of the electrolytic plasma oxidation processes for corrosion protection of magnesium alloy AM50 using the Taguchi method. *J. Mater. Process. Technol.*, Feb. **182**(2), 58–64.
11. Wang, Y, Northwood, D.O. (2008) Optimization of the poly-pyrrole-coating parameters for proton exchange membrane fuel cell bipolar plates using the Taguchi method. *J. Power Sources*, Oct. 15, **185**(1), 226–32.
12. Magudeeswaran, G, Balasubramanian, V, Reddy, G.M. (2008) Effect of welding processes and consumables on high cycle fatigue life of high strength, quenched and tempered steel joints. *Materials & Design.*, Oct. 1, **29**(9), 1821–7.
13. Yousefieh, M, Shamanian, M, Saatchi, A. (2011) Optimization of the pulsed current gas tungsten arc welding (PCGTAW) parameters for corrosion resistance of super duplex stainless steel (UNS S32760) welds using the Taguchi method. *J. Alloys Compd.*, Jan. 21, **509**(3), 782–8.
14. Do Kim, K, Han, D.N, Kim, H.T. (2004) Optimization of experimental conditions based on the Taguchi robust design for the formation of nano-sized silver particles by chemical reduction method. *Chem Eng J.*, Nov. 15, **104**, 55–61.
15. Yang WP, Tarng YS. (1998) Design optimization of cutting parameters for turning operations based on the Taguchi method. *J. Mater. Process. Technol.*, Dec. 1, **84**, 122–129.

Received 24.02.2021

# INFLUENCE OF LIQUID GLASS CHARACTERISTICS ON QUALITY OF COATING FORMATION OF WELDING ELECTRODES

**A.E. Marchenko<sup>1</sup>, I.O. Glot<sup>2</sup> and N.V. Skorina<sup>1</sup>**

<sup>1</sup>E.O. Paton Electric Welding Institute of the NAS of Ukraine

11 Kazymyr Malevych Str., 03150, Kyiv, Ukraine. E-mail: [office@paton.kiev.ua](mailto:office@paton.kiev.ua)

<sup>2</sup>Institute of Continuous Media Mechanics of the Ural Branch of the RAS

1 Academician Korolyov Str., 614018, Perm, RF

The viscosity of 6 % dispersions of Na-CMC in liquid Na- and K-glasses depending on temperature, as well as viscosity of pure liquid Na, K- and NaK-glasses depending on excess pressure and temperature was studied. Each of them represents a consistent medium of real electrode coating mixtures. With the use of the obtained results by mathematical methods, the functioning of the model of a joint effect of excess pressure and dissipative heating on viscosity, velocity profile and stability of pressure flow of electrode coating mixtures in the step channel under the conditions of coating formation by extrusion deposition on steel bars was verified. Although two competing sources of change in shear viscosity of the coating mass (temperature and pressure) are available, the calculations did not reveal situations with unstable (pulsating) flow modes through a suddenly narrowing channel, which could cause instability of the coating mixture flow and, therefore, electrode coatings with a thickness variation. At least, they were not revealed in the studied range of capillary sizes  $L/R_k < 10$  and pressures, at which the electrodes are actually pressed. 10 Ref., 1 Table, 8 Figures.

*Keywords:* arc welding, coated electrodes, production technology, coating thickness variation, rheology, visco-elasticity of coatings

Variable coating thickness is the most dangerous defect of coated electrodes in fusion arc welding. It deteriorates technological characteristics of welding process, weld quality and reduces the operational reliability of products manufactured by welding.

Variable coating thickness occurs while manufacturing electrodes by extrusion deposition of a paste coating transformed into a high-gradient nonisothermal pressure flow in the forming head of the electrode extrusion press on steel rods with a layer of a circumferential cross-section. The speed of process is up to 800 electrodes with a rod diameter from 2 to 6 mm per minute, each from 250 to 450 mm length. The forming pressure on the mass  $P$  is up to 80 MPa. As a result of dissipative heating, the surface of the coating sheath at the outlet from the die can reach 90–100 °C.

Due to the reasons that have not yet been fully clarified, the pressure flow of the coating suddenly transfers to the mode of elastic turbulence. Interacting in this state with the elastic metal core located inside the flow, the coating covers it with a nonuniform layer. In this case, the channel between the core and the calibration bushing is overcome by the filling mixture and the energy consumption is as lower, as the more it differs from the symmetrical circumferential config-

uration, although the total cross-sectional area of the channel remains unchanged.

The rheological characteristics of electrode coating masses, as well as other extrusion-formed paste materials, in the state of pressure flow are determined by the gradients of the rate of shear  $\gamma$ , longitudinal  $\varepsilon$ , and circulating (rotational) deformation  $\omega$ .

The natural convergent zone directly adjacent to the flat inlet of the calibration channel in the head of the electrode extrusion press or capillary viscosimeter is formed by a mutual competition between the shear and longitudinal deformation [1]. It acquires a narrowing profile that minimizes the energy consumption for overcoming resistance to shear (with viscosity  $\eta$ ) and longitudinal flow (with viscosity  $\lambda$ ) by the flow.

The value of the effective shear viscosity in this state depends, first of all, on the degree of destruction of its coagulation structure. The higher the stress or shear rate, the more the structure is destroyed and the lower the viscosity of the coating. The effect of temperature and excess pressure in the channel is taken into account by adjusting the activation energy of viscous flow  $\alpha$ , and, accordingly, the piezoelectric effects and the coefficient  $\beta$ . The combined effect of temperature  $T$  and excess pressure  $P$  on the effective

shear viscosity of non-Newtonian polymeric fluids is calculated according to the formula [2]:

$$\eta = \eta_0 e^{-\alpha \Delta T} \eta_0 e^{-\beta \Delta P} \quad (1)$$

From the formula (1) it follows that the value of viscosity decreases with an increase in temperature, and grows with an increase in pressure.

According to our data, the viscosity of liquid glass suspensions of CMC and liquid glasses, on the base of which they are composed, decreases with an increase both in temperature and pressure. And the latter, according to our data, is increased at least within the limits not exceeding the values at which the electrodes are crimped. At higher pressures, the viscosity of liquid glasses like in many other liquids increases [3].

It is known that an effective viscosity of the vast majority of suspensions is unambiguously proportional to the viscosity of the dispersed medium, and their activation energies and baric viscosity coefficients are the same, even when the viscosity of the former ones exceeds the viscosity of the latter by hundreds and thousands of times [4]. In this regard, we used liquid glasses and their 6 % Na-CMC dispersions as rheological models of electrode coating mixtures in evaluation of the effect of heating and excess pressure on them.

In the present article, the results of our investigations on the joint role of effective, temperature and baric viscosity as a possible source of rheological instability of coating mixtures under the conditions of a shear deformation are presented.

**Effect of temperature, stress and strain rate on shear viscosity of liquid glass suspensions of Na-CMC.** In Figure 1 the viscosity polytherms of liquid glass suspensions of Na-CMC are compared, which are produced using a rotary viscometer Reotest II.

It is seen that  $\eta$  of liquid-glass dispersions of CMC in the temperature range to which the coating mixture

spontaneously heats up during the process of deposition on the electrode rods, represents an exponential function of temperature  $\eta(T) = \eta_0 e^{\alpha (\dot{\gamma}, \tau) / RT}$  and simultaneously the velocity  $\dot{\gamma}$  and the shearing stress  $\tau$ . Figure 1, a, b, the values of  $\dot{\gamma}$  (curves 1 and 2) amount to 1 and 100 s<sup>-1</sup>, respectively.

At the «c» position, they are denoted by nominal values of  $\dot{\gamma}$  in the range from 0.8 to 175 s<sup>-1</sup> and located along the viscosity polytherms. As we see, as the temperature increases, the viscosity of the suspensions really decreases, and its extent is as greater, the higher  $\dot{\gamma}$  and  $\tau$ , as well as the more sensitive the structure of the test material to thermal and mechanical fracture. In the flow modes  $\dot{\gamma} = \text{const}$  and  $\tau = \text{const}$ , potassium modifications of glasses and suspensions of Na-CMC based on them are characterized by a higher activation energy than sodium ones, which, according to [5], can be represented as

$$\alpha_\tau > \dot{\gamma} \frac{\alpha_\tau}{\alpha_{\dot{\gamma}}} = 1 - \dot{\gamma} \left( \frac{\eta}{\tau} \right)_T; \quad (2)$$

$$\alpha_\tau = \frac{d \ln \eta}{d(T^{-1})} \text{ at } \tau = \text{const}; \quad (3)$$

$$\alpha_{\dot{\gamma}} = \frac{d \ln \eta}{d(T^{-1})} \text{ at } \dot{\gamma} = \text{const}.$$

**Effect of excess pressure on viscosity of liquid glass.** The effect of excess pressure on the viscosity of liquid Na-, K-, and combined NaK-liquid glasses is shown in Figure 2.

As follows from the abovementioned data, the nature of the baric changes in the viscosity of liquid glasses can, in principle, be represented by the power function  $\eta(P) = \eta_0 (1 - P)^2$ . Depending on the composition and concentration of the liquid glass, its di-

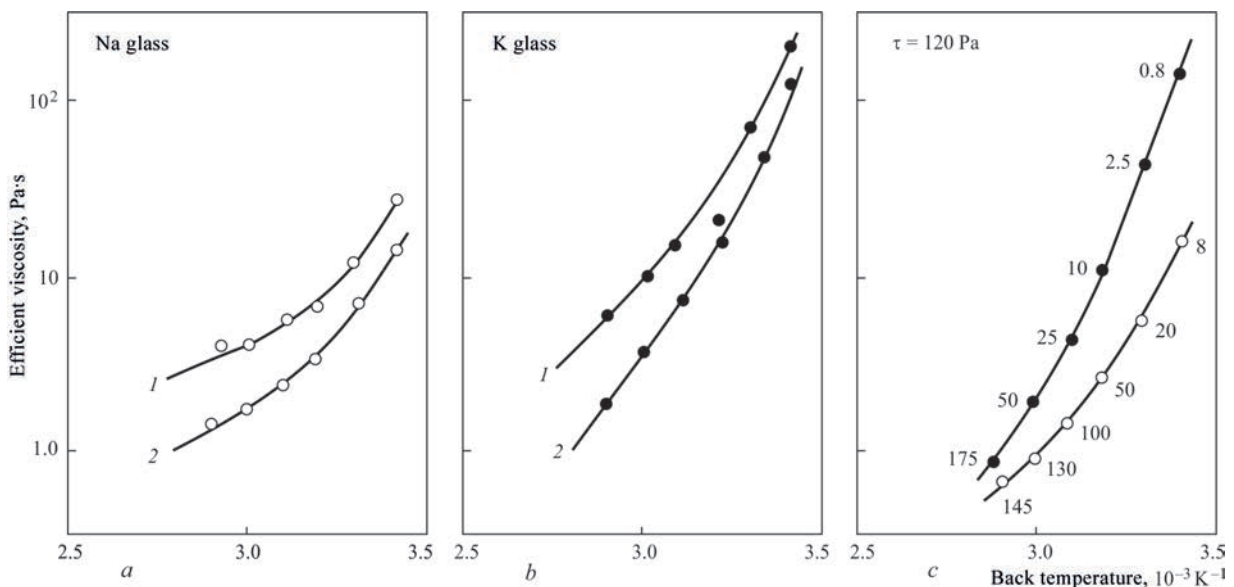


**Figure 1.** Viscosity polytherms of 6 % dispersions of CMC of grade 72/470 in liquid Na- and K-glass with M = 2.9. Flow mode:  $\dot{\gamma} = \text{const}$  (a, b) and  $\tau = \text{const}$  (c). See the rest of the symbols in the text

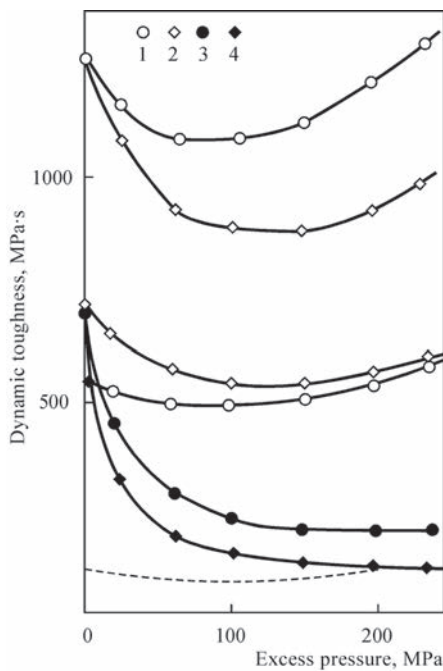


**Figure 2.** Effect of excess pressure on viscosity of Na (1), NaK (2) and K (3) liquid glasses with a modulus of 2.9, as well as NaK (4) liquid glass with  $M = 3.4$ ; initial viscosity of glasses is 500, 700 and 1250 mPa·s [3]

agram takes the form of either a complete parabola or its left or right branch within the pressure range we use. In low-viscosity liquid glasses, the parabola degenerates into a straight line.

In liquid glasses, which to a greater or lesser extent reacted to the increase in pressure, the diagrams  $\eta(P)$  have an extreme rather than a monotonically incrementing form, as in the case of polymeric objects. The greatest decrease in viscosity is mostly observed in the values of pressures, which are usually not recommended to be exceeded while crimping electrodes.

The parabolic form  $\eta = f(P)$  was revealed in liquid 2.9NaK- and 2.9Na-glasses with a viscosity of 1250 mPa·s. At the first glass the minimum of viscosity and the left asymmetry of the parabola are more brightly expressed, at the second one — the left asymmetry of the parabola at a smaller minimum of viscosity.

As the viscosity of the compared glasses decreases to 570–500 mPa·s, the extremity of the  $\eta = f(P)$  curves decreased significantly, but the shape of asymmetry remained the same. When the viscosity of the glasses is reduced to 100 mPa·s, the extremity and asymmetry of curves are completely degenerated (in Figure 2 they are presented by a dotted line).

From the technological point of view, the most favourable form of the curves is  $\eta = f(P)$ , which was revealed in potassium and sodium-potassium liquid glasses with values of modulus of 3.0 and 3.3, respectively, because from the technological point of view they do not have a dangerous ascending parabolic branch.

Since the baric viscosity of liquid glasses was measured in our experiments with a Heppler viscosimeter, the obtained results cannot be graded by

$\tau$  and  $\dot{\gamma}$ . Taking into account that the course of the baric dependence  $\eta(P)$  in principle coincides with the temperature change in the viscosity  $\eta(T)$ , the baric viscosity coefficients by analogy with the activation ones can be represented as [5]:

$$\beta_{\dot{\gamma}} = \frac{1}{\eta} \left( \frac{\eta}{P} \right)_{\dot{\gamma}, T} = \frac{1}{\tau} \left( \frac{\tau}{P} \right)_{\dot{\gamma}, T}, \quad (4)$$

and their correlation in the form

$$\beta_{\tau} = \frac{\tau}{\dot{\gamma}} \frac{\gamma}{\tau} \beta_{\dot{\gamma}} = \frac{d \ln \dot{\gamma}}{d \ln \tau} \beta_{\dot{\gamma}} \quad (5)$$

Moreover  $\beta_{\tau} \geq \beta_{\dot{\gamma}}$ , as far as  $\frac{d \ln \dot{\gamma}}{d \ln \tau} \geq 1$ .

The higher the temperature, velocity and shear stresses, the lower the values of the piezoelectric coefficients [5].

Let us note that to identify the conditions, under which the values of viscosity  $P_0$  and other rheological characteristics are obtained, along with the consistent variables  $\tau$  and  $\dot{\gamma}$ , the mode symbols of the pressure-flow characteristics  $Q$  and  $P$  are used.

The decrease in viscosity under the influence of excess pressure and temperature is most likely caused by the destruction of relatively weak structural bonds in the liquid glass. Moreover, these are those bonds that are formed by the structural elements of silicon-oxygen anions (SOA), and not the solvent.

Indeed, to the effect of pressure the viscosity of potassium and high-modulus potassium-sodium liquid glasses is mostly subjected. According to the concepts of the polyelectrolytic nature of aqueous solutions of alkaline silicates, the structure of namely such liquid glasses, as a rule, is formed by weak, chaotic and synergistic bonds.

The structures themselves belong to the cluster type, which determines their low resistance to mechanical, activation and baric destruction [6, 7].

In terms of effect on the structure of objects, the comparable types of influence can be considered almost equal to each other. This agrees with the results of an experimental evaluation of the effect of pressure and temperature on viscosity, which are shown in Figures 3 and 4.

On the other hand, this is agreed with the strength of the structural bonds of  $Q^n$ , which were revealed in the structure of SOA of liquid K-, as well as high-modulus NaK-glasses by the method of MRS spectroscopy. The total fraction of elastic bonds ( $Q^2 + Q^3$ ) prevails in the structure of SOA of potassium  $M = 3.65$  (76.5 %) and combined NaK  $M = 3.15$  liquid glasses (78.5 %). The minimum fraction of the hardest siloxane bonds  $Q^4$  is revealed in the SOA structure of combined liquid NaK (11.5 %), the intermediate fraction is in LiNa (22.5 %), and the maximum is in LiK modifications (27.0 %), containing about 30 mol.% of the accompanying component. As a rule, the same glasses also showed the highest synergistic growth in viscosity [8].

**Combined effect of pressure and temperature on pressure flow of electrode coating mixtures in a suddenly narrowing channel.** The combined effect on the nature of flow of the coating mixture of two factors — excess pressure and temperature, was investigated using mathematical modeling. The flow and heat transfer of a viscous fluid in a cylindrical channel with a sudden narrowing were analyzed. The system of equations of movement and heat balance was solved numerically applying the finite difference method [9]. To evaluate the technological properties of the coating mixture, the following ratio was used

$$\eta(T, P) = \eta_0 \varphi(T) \psi(P), \quad (6)$$

where  $\eta_0$  is the viscosity at a room temperature and atmospheric pressure.

The temperature decrease in viscosity was considered as the coefficient

$$\varphi(T) = A \exp(B/T), \quad (7)$$

and the baric changes were considered by the power law (by the square trinomial):

$$\psi(P) = \left[ 1 - 5.7 \left( \frac{P}{10^9} \right) + \left( \frac{P}{10^9} \right)^2 \right], \quad (8)$$

where  $A$  is a pre-exponential factor;  $B$  is the activation energy of viscous flow.

The accepted rheological correlation (6) allows obtaining pressure drops in the channel from 20 MPa at a flow rate of 1 l/min to 170 MPa at a flow rate of 10 l/min.

The flow region was modeled by coupling a cylindrical tank (supply cylinder) and the capillary with a ratio of diameters  $D_R/d_k > 5$ , at which the steric effect is absent, i.e. the nature of the flow in the capillary is independent of the flow in the tank. The dimension of the used computational grid (15×15 in the tank and 8×6 in the capillary) was chosen for the reasons of combining an acceptable accuracy and economy of calculations. The consumption of the coating mixture was taken equal to 10 l/min: in this case, the real conditions of the flow are simulated, under which in the capillary a section of both decreasing and increasing viscosity of liquid glass is realized [3]. A series of numerical experiments demonstrated the role of each of the mentioned factors (temperature and pressure drop) in the formation of a flow in the capillary. The calculations show that the main part of the pressure drop in the channel with a sudden narrowing is formed in the capillary.

The dependence of viscosity on temperature increases the nonuniformity of viscosity and temperature fields both in the radial and also in the longitudinal section of the capillary. The pattern for distribution of viscosity in the capillary at a fixed flow rate is shown in Figure 5. Heating of the near-wall layer due to the dissipative factor is accompanied by the outflow of material from the central zone. However, neither the change

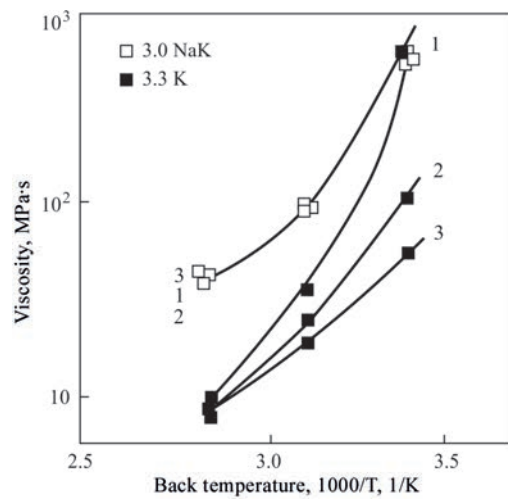


**Figure 3.** Combined effect of temperature and pressure on viscosity of K ( $M = 3.3$ ) and NaK ( $M = 3.0$ ) liquid glass with a viscosity of 700 mPa·s: 1, 2, 3 — atmospheric and excess pressure of 10 and 20 MPa [3]

in the velocity field, nor the temperature significantly (not more than 0.5 %) affects the radial pressure distribution. Dissipative heating of the material grows with an increase in the flow rate (Figure 6). However, in this case, the heated layer does not propagate into the flow core. The revealed regularities are agreed with the experimentally observed «plug» flow mode through the calibrating bushing. However, in real conditions, the recorded viscous heating temperature in the near-wall layer is twice higher than its calculated value.

A different pattern is observed when modeling a flow, the viscosity of which depends only on the increase in pressure. In this case, as follows from the calculations, the viscosity changes only along the capillary, while along its cross-section it remains unchanged.

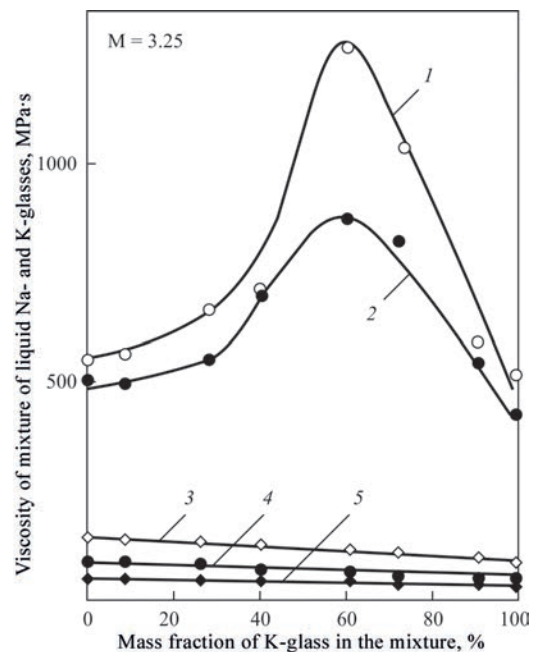


**Figure 4.** Dependence of viscosity of binary liquid Na- and K-glasses immediately after mixing (1) and after thermostating at a temperature of 20 (2), 40 (3), 60 (4) and 80 °C (5)

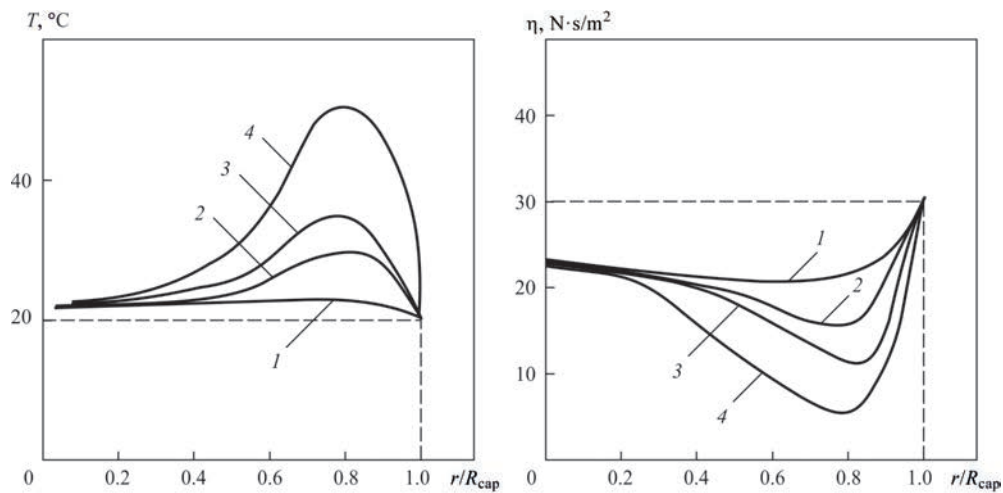


**Figure 5.** Temperature (a) and viscosity (b) field in the capillary. Distance from the capillary inlet  $l/L_{cap}$ : 0 (1), 2 (2), 4 (3) and 15 (4).  $Q = 1.67 \cdot 10^{-4} \text{ m}^3 \cdot \text{s}^{-1}$

In Figure 7 the pressure distribution along the channel for the extruded mass with Newtonian properties (1), mass with baric (2) and thermosensitive viscosity (3) are compared.

Here the curves 1 and 2 refer to the Newtonian and baric viscosity, respectively. It is seen that, in general, the pressure drop for a liquid with a baric viscosity is lower than that for a Newtonian one. Depending on the flow rate, this deviation of the liquid from the Newtonian behaviour is described by an extreme law, and the maximum decrease in pressure falls on the flow rate approximately equal to  $8.0 \cdot 10^{-5} \text{ m}^3 \cdot \text{s}^{-1}$ .

Thus, the responsibility for reducing the pressure drop in a suddenly narrowing channel mainly falls on dissipative heating. The dependence of viscosity on pressure causes an additional (much smaller) decrease in pressure at a set flow rate (Figure 8).

Despite the presence of two competing sources of decrease in the viscosity of the extruded material in the form of temperature and pressure, at least in the range  $L/R_k < 10$ , the calculations did not reveal situ-

ations in which unstable (pulsating) flow conditions would arise through a suddenly narrowing channel, capable of provoking a variable coating thickness during crimping of electrodes. At higher values of  $L/R_k$ , such situations can become quite expected as a result of antibiotic changes, on the one hand, in the effective and temperature viscosity, and on the other, in the baric viscosity of the coating mixture.

It was experimentally found that the viscous heating of the mass in the capillary is influenced by the type of coating mixture, chemical composition, viscosity of liquid glass, proportion of alkaline hydrosilicate introduced by the glass into coating mixture, and the grain size composition of the filler. To a certain extent, this may be a consequence of the combined effect of the material composition of the coating and the characteristics of liquid glass on thermophysical characteristics of the coating masses. As follows from the data given in Table, with almost the same thermal conductivity  $\nu$ , the thermal diffusivity  $\nu$  of the UONI 13/55 coating is lower, and the volumetric heat capacity  $\rho \cdot c$  is higher than that of the ANO-4 coating mixture [10].

It is also important that the UONI 13/55 coating mixture, especially made on high-modulus low-vis-

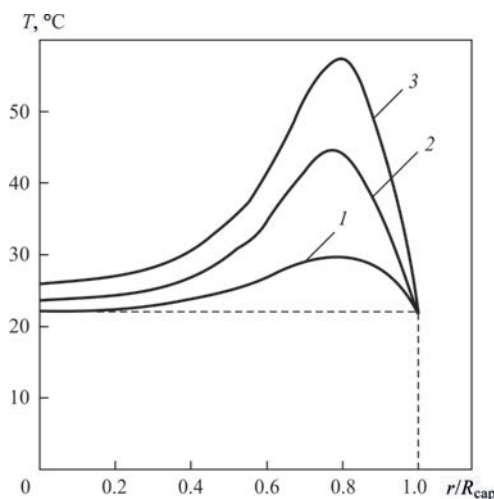


**Figure 6.** Temperature of coating mixture at the outlet from the capillary at a flow rate per second: 1 —  $1.7 \cdot 10^{-5}$ ; 2 —  $5.0 \cdot 10^{-5}$ ; 3 —  $1.7 \cdot 10^{-4} \text{ m}^3 \cdot \text{s}^{-1}$ ;  $\eta = \eta_0 A_{exp}(B/T)$

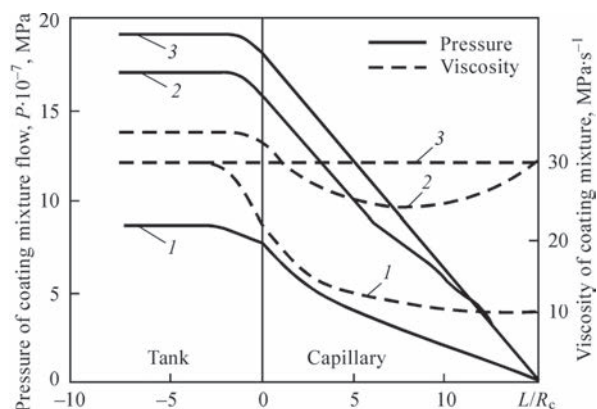


**Figure 7.** Distribution of pressure and viscosity of the extruded mass along the length of the capillary: 1 — Newtonian; 2 — baric; 3 — heat-sensitive coating mixture properties

Comparison of thermophysical characteristics of coating mixtures for ANO-4 and UONI 13/55 electrodes (humidity is 11.5 wt.%, room temperature) [10]

Type of electrodes	Liquid glass			$\lambda$ , W/m·K	$\alpha \cdot 10^7$ , m <sup>2</sup> /s	$\rho \cdot c \cdot 10^{-6}$ , J/m <sup>3</sup> ·K
	Modulus	Viscosity, mPa·s	wt.%			
UONI 13/55	2.9	700	29.0	$\frac{1.30-1.35}{1.30}$	$\frac{4.60-5.30}{5.0}$	$\frac{2.50-2.80}{2.60}$
	3.2	50	19.5	$\frac{1.25-1.40}{1.35}$	$\frac{2.50-3.75}{3.20}$	$\frac{3.65-5.55}{4.20}$
ANO-4	2.9	700	29.0	$\frac{0.95-1.15}{1.05}$	$\frac{5.70-10.0}{7.80}$	$\frac{0.95-1.80}{1.30}$
	3.2	50	18.5	$\frac{1.20-1.25}{1.18}$	$\frac{4.65-11.5}{7.5}$	$\frac{1.05-2.35}{1.70}$

Note. In the numerator the minimum and maximum values and in the denominator the average of the three definitions are given.

cosity liquid glass, has a high structuredness. Some part of the energy is spent on the destruction of its coagulation structure, as a result of which its viscous heating is weakened. The restoration of the structure occurs outside the capillary and cannot affect the heat balance in the capillary.

### Conclusions

1. According to the results of the carried out rheological studies of liquid glass dispersions of Na-CMC and pure Na- and K- and NaK liquid glasses, which represent a consistent medium of real coating masses, the change in their structural, activation and baric viscosity depending on strain rate, temperature and excess pressure was modeled applying the mathematical methods. The values of the latter were varied within the limits characteristic of real conditions for crimping electrodes.

2. Despite the presence of two competing sources of change in the shear viscosity of the coating mixture (temperature and pressure), the calculations did not reveal the situations with unstable (pulsating) flow modes through a suddenly narrowing channel, at least they were not revealed in the studied range  $L/R_k < 10$  and pressures at which the electrodes are actually crimped. At higher values of  $L/R_k$  and pressures, such situations are quite possible as a result of the antibate change in the temperature and baric viscosity of some types of liquid glasses and coating mixture made on them: the first stops a decrease, and the second one after reaching a minimum, begins to increase at  $L/R_k > 10$  and  $P > 100$  MPa.

3. From the technological point of view, potassium and NaK liquid glasses, especially their high-modulus modifications, deserve preference. They provide consistency of coating mixtures, little prone to the appearance of instabilities in the state of the pressure flow, since they do not reveal a dangerous ascending branch of the parabolic dependence of viscosity on excessive pressure.

1. Cogswell, F.N. (1972) Converging flow of polymer melts in extrusion dies. *Polym. Eng. and Sci.*, 12(2), 64–73.

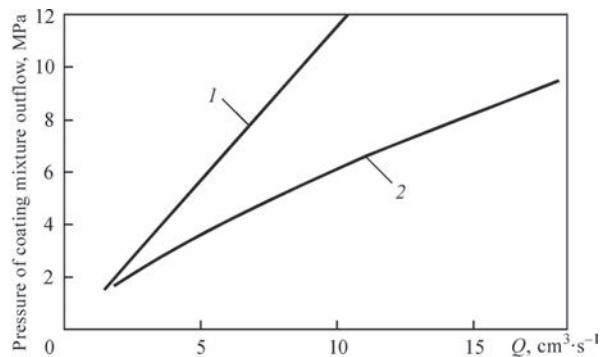


Figure 8. Flow-pressure characteristic of the Newtonian (1) and temperature-sensitive (2) coating mass:  $\eta = \eta_0 = \text{const}$ ; 2 —  $\eta = \eta_0 A \exp(B/T)$ ;  $\eta_0 = 30$  n·s/m<sup>2</sup>;  $A = 0.52$ ;  $B = 65$

2. Kamal, M.R., Nuyn, H. (1980) Capillary viscometry a complete analysis including pressure and viscous heating effect. *Ibid.*, 20(2), 109–119.
3. Marchenko, A.E., Skorina, N.V., Sidlin, Z.A., Kostyuchenko, V.P. (1992) Examination of viscosity of liquid glasses under pressure of electrode crimping. In: *Proc. of Sci.-Tech. Seminar dedicated to the 100<sup>th</sup> Anniversary of the Birth of K.V. Petran on New Welding and Surfacing Materials and their Application in Industry (St.-Petersburg, 19–20 May, 1992)*. St.-Petersburg, 43–49 [in Russian].
4. Khodakov, G.S. (2003) Rheology of suspensions. Theory of phase flow and its experimental substantiation. *Ros. Khim. Zhurnal*, XLVII, 2, 33–44 [in Russian].
5. Vinogradov, G.V., Malkin, A.Ya. (1977) *Rheology of polymers*. Moscow, Khimiya [in Russian].
6. Ayler R.K. (1982) *Chemistry of silica*. In: 2 Pts, Pt 1. Ed. by V.P. Pryanishnikov. Moscow, Mir [in Russian].
7. Korneev, V.I., Danilov, V.V. (1996) *Liquid and soluble glass*. St.-Petersburg, Strojizdat [in Russian].
8. Marchenko, A.E., Skorina, N.V., Kiselev, M.O., Trachevsky, V.V. (2017) Nuclear magnetic spectroscopy study of the structure of liquid glasses for welding electrodes. *The Paton Welding J.*, 1, 41–45.
9. Yankov, V.I., Glot, I.O., Trufanova, N.M., Shakirov, N.V. (2010) *Flow of polymers in die holes. Theory, calculation, practice*. Moscow, Izhevsk, ICI [in Russian].
10. Marchenko, A.E. (2015) On thermal environment created by viscous heating of electrode paste in the zone of formation of pressure flow. Welding materials — 2015 (Petran lectures). In: *Proc. of Int. Sci.-Tech. Conf. (St.-Petersburg, 15–17 October, 2015)*. St.-Petersburg, 65–68.

Received 22.03.2021

# INVESTIGATION OF HEAT TREATMENT IMPACT ON THE STRENGTH OF Al–Ti BIMETAL HONEYCOMB CORE

Iu.V. Falchenko, L.V. Petrushynets, V.Ye. Fedorchuk and Ye.V. Polovetskyi

E.O. Paton Electric Welding Institute of the NAS of Ukraine

11 Kazymyr Malevych Str., 03150, Kyiv, Ukraine. E-mail: office@paton.kiev.ua

The effect of heat treatment on the strength of aluminium-titanium bimetal honeycomb structures is considered. Aluminium-titanium bimetal was produced by vacuum diffusion welding of strips of AD1 aluminium and VT1-0 titanium low alloys. The possibility of spot welding of bimetal strips 12 mm wide for producing the honeycomb core was studied with different combinations of titanium and aluminium layers. It is shown that the optimal variant is welding the strips in Al/Ti + Al/Ti combination. Here, the average compressive strength of the honeycombs is equal to 41.1 MPa. Annealing of bimetal honeycombs was performed at temperatures of 600 °C and 700 °C. Annealing time at 600 °C was 60–1200 min, at 700 °C it was 10–30 min. It is found that annealing for 60 min at 600 °C leads to formation of individual sites of an intermetallic interlayer up to 1 µm thick in the butt joint between the aluminium and titanium layers that results in increase of compressive strength of the honeycomb samples by 11.7 %, compared to the initial condition. Further increase of annealing time leads to growth of the intermetallic interlayer in the butt joint and to lowering of the compressive strength of the honeycomb samples. It is shown that the honeycomb samples after annealing for 60–600 min at 600 °C at compression with the maximum deformation level of 50 % deform without fracture of the welding location or bimetal material walls. Increase of annealing time leads to embrittlement of both the welding locations, and the material as a whole. 9 Ref., 3 Tables, 7 Figures.

*Keywords:* aluminium, titanium, foil, bimetal joints, diffusion welding, annealing, intermetallic interlayer, compressive strength

Three-layer aluminium panels with honeycomb core have become widely accepted in aircraft- and ship-building, construction and other industries due to their unique properties, owing to the fact that these structures with their relatively small weight are characterized by high values of strength and rigidity. Moreover, they have good vibration and radiotechnical characteristics, sound and heat-insulating properties. Such structures can be used as load-bearing elements in the wing, fuselage, flooring, as well as thermal shielding elements [1, 2].

Improvement of service properties of honeycomb panels, as well as increase of resistance of three-layer panel core can be achieved through application of a stronger material, for instance, titanium. So, authors of work [3] proposed installing box-shaped profile elements from a titanium alloy between the skin sheets and transverse stiffeners from an aluminium alloy, which prevent buckling during welding. Box-shaped profile in such panels acts as the main load-carrying structural element, while aluminium alloy sheets are the skin. However, considering that the weight of titanium is almost two times greater than that of aluminium, its application will lead to an essential increase of the total weight of the structure, which is undesirable for the aerospace industry.

An optimal variant between minimum weight and maximum strength of the honeycomb structures, in

our opinion, is application of a honeycomb core, produced using bimetal materials. The possibility of producing Al–Ti bimetal by vacuum diffusion welding (VDW) was shown in work [4].

Investigations conducted in [5] lead to the assumption that application of layered composite materials (LCM), which could include foil-based bimetals, can greatly improve the properties of honeycomb structures. Considering the possibility of wide adjustment of LCM structure and composition at the stage of joint formation, investigations on producing such materials with a controlled content of the intermetallic phase in the butt joint are quite relevant.

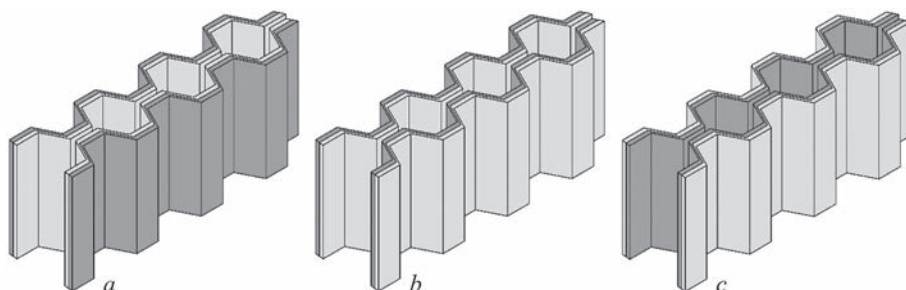
The good prospects for application of aluminium-titanium bimetal produced by vacuum diffusion welding, to make three-layer honeycomb panels, as well as the possibility of their operation at higher temperatures, will be determined by the strength and intensity of intermetallic phase growth in the bimetal during manufacture of honeycomb structures and their service.

The objective of this work was studying the heat treatment impact on the strength of Al–Ti honeycomb core.

**Investigation procedures, materials and sample preparation.** The honeycomb core was produced using Al–Ti bimetal blanks of 130×130×0.180 mm size, earlier made by VDW method. Used as initial materi-

**Table 1.** Chemical composition of AD1 and VT1-0 alloys [6], wt.%

Alloy	Al	Ti	Fe	Si	Mn	Cu	Mg	Zn	Amount of additives
AD1	Base	0.15	0.3	0.3	0.025	0.02	0.05	0.1	–
VT1-0	–	Base	0.025	0.10	–	–	–	–	0.30

**Figure 1.** Schematic image of possible variants of joining two corrugated Al–Ti bimetal strips: *a* — Ti/Al + Al/Ti; *b* — Al/Ti + Al/Ti; *c* — Al/Ti + Ti/Al

als were aluminium AD1 and titanium VT1-0 alloys, the composition of which is given in Table 1 [6]. Bi-metal sheets were used to make 12 mm wide strips, which, in their turn, were used to form the corrugated strips with 10 mm corrugation pitch.

Unlike the monolithic material, certain difficulties may arise in spot welding of bimetal strips, which are due not only to material heterogeneity by thickness, but also to different physico-mechanical properties of titanium and aluminium. Titanium has low electro- and thermal conductivity, and it is very active towards gases, contained in the atmosphere. Its welding is conducted at relatively small parameters of current, compression force and heating duration. Aluminium has a high heat conductivity, low electric resistance and refractory film on the surface. Therefore, before welding, the part surfaces should be thoroughly cleaned to remove the thick oxide film, in order to prevent lacks-of-penetration [7].

To obtain sound joints from corrugated strips and determine optimal configuration of the layers relative to each other, experiments with three variants of combination of bimetal samples (Figure 1) were conducted:

- Ti/Al + Al/Ti due to welding aluminium layer to aluminium layer;
- Al/Ti + Al/Ti due to welding aluminium layer to titanium layer;
- Al/Ti + Ti/Al due to welding titanium layer to titanium layer.

Spot welding was conducted at room temperature in air. Before welding the contact surfaces of corrugated strips were cleaned mechanically and degreased. Welding was conducted at constant values of voltage  $U_w = 3$  V and current  $I_w = 270$ – $300$  A, heating intensity was here determined by pulse duration  $t_w = 0.5$ – $5.0$  s and number  $N = 1$ – $20$ .

Investigations of the impact of heat treatment on formation of an interlayer of intermetallic between titanium and aluminium were conducted under normal conditions

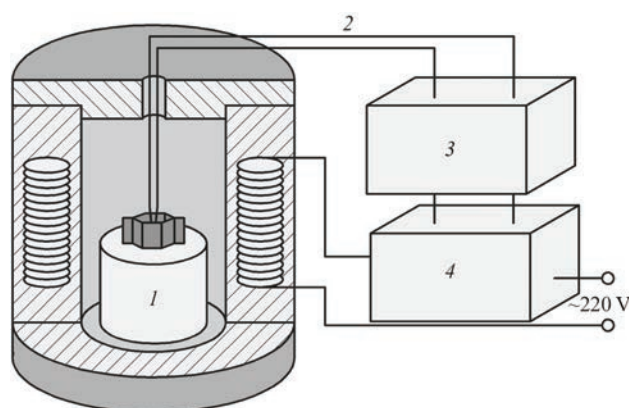
in a specially developed stand, which was made up of a muffle furnace and system of temperature control, which consisted of thermocontroller REX C-100, solid-state relay SSR-40 DA and chromel–alumel thermocouple (Figure 2). The sample was placed inside a furnace on a ceramic support. Heat treatment parameters were assigned in the following ranges: temperature  $T_{an} = 600$ – $700$  °C, soaking duration  $t_{an} = 10$ – $1200$  min.

Analysis of structural characteristics of foil and welded joints was performed on sections, using scanning electron microscope CAMSCAN 4, fitted with a system of energy dispersive analysis EDX INCA 200 for local chemical composition on flat samples.

Preparation of transverse microsections of welded joints was conducted by a standard procedure using grinding-polishing equipment of Struers Company.

Mechanical properties of the samples were determined at their compression testing that corresponds to the procedure given in works [1, 8].

Mechanical compression tests of the honeycomb structure were conducted using a digital pressure controller of XK3118T1 grade of KOLI Company, and

**Figure 2.** Scheme of a set-up for heat treatment of samples: *1* — ceramic support; *2* — thermocouple; *3* — thermocontroller REX C-100; *4* — solid-state relay SSR-40 DA

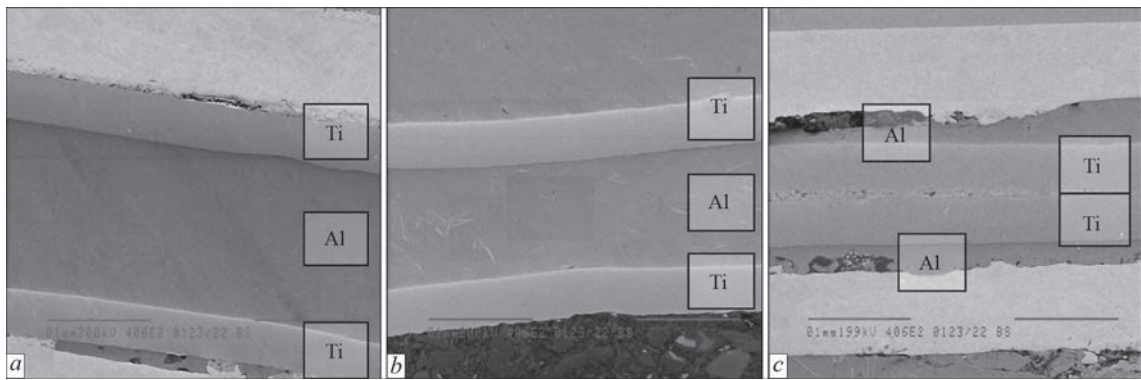


**Figure 3.** Microstructure of spot joints of Al-Ti bimetal foil: *a* — Ti/Al + Al/Ti; *b* — Ti/Al + Ti/Al; *c* — Al/Ti + Ti/Al



**Figure 4.** General view of samples of individual honeycombs before (*a*) and after mechanical compression tests (*b*)

pressure sensor of MNC-1 grade of CAS Company with working interval from 0 up to 1000 kg.

**Investigation results.** In order to produce a honeycomb structure of the core, a technology of welding bimetal profiled strips was developed. It was found that in order to obtain joints of bimetal samples in welding of an aluminium layer to aluminium layer (Ti/Al + Al/Ti), it is enough to use a welding cycle from 2 current pulses of duration  $t_w = 3$  s. In order to produce a core at contact of the aluminium and titanium layer (Ti/Al + TiAl), the number of pulses rises up to 4, while the duration remains constant,  $t_w = 3$  s. In order to produce a core at contact of the titanium layer with titanium layer (Al/Ti + Ti/Al), pulse duration rises up to  $t_w = 5$  s, while their number increases up to 20. Here, excess overheating of aluminium interlayer under the electrodes with its flowing out of the joint zone, is observed. The joint microstructure is given in Figure 3.

**Table 2.** Results of compression testing of bimetal samples of a honeycomb core

Combinations of bimetal strip surfaces	Sample testing	Compressive strength, MPa	Average value of compressive strength, MPa
Ti/Al + Al/Ti	Without fracture	42.1	44.5
		54.1	
		37.4	
Ti/Al + Ti/Al	Without fracture	40.3	41.1
		38.5	
		44.6	
Al/Ti + Ti/Al	With fracture	38.2	35.2
		32.2	
		35.1	

Analysis of the modes of welding the honeycomb cores suggests that the variant of welding the aluminium layer to aluminium layer is the least power- and labour-consuming. However, considering that at production of the honeycomb core there is a need for contact between the aluminium and titanium layers, the optimal variant is welding the aluminium layer to the titanium one.

Compression tests of individual honeycomb samples were conducted to assess their strength (Figure 4, *a*). Honeycomb upsetting was specified on the level of 50 % from the initial height. It was established that in the case of joining Ti/Al + Ti/Al and Ti/Al + Ti/Al metal layers (Figure 4, *b*), deformation of the honeycomb core walls takes place at compression without breaking of the spot welds, and in the case of joining Al/Ti + Ti/Al layers (Figure 4, *c*) delamination between the titanium layers is observed. The average strength of the

**Table 3.** Dependence of the intermetallic interlayer thickness and strength of Al-Ti bimetal on heat treatment mode

Sample	Sample heating temperature, $T_{an}$ , °C	Sample soaking duration, min	Average	
			Intermetallic interlayer thickness, $\mu\text{m}$	Compressive strength, MPa
1	—	—	—	41.1
2	600	60	—	45.9
3	600	150	2	39.9
4	600	300	4	35.6
5	600	600	10	32.4
6	600	1200	11	29.8
7	700	10	4	33.3
8	700	30	14	27.2

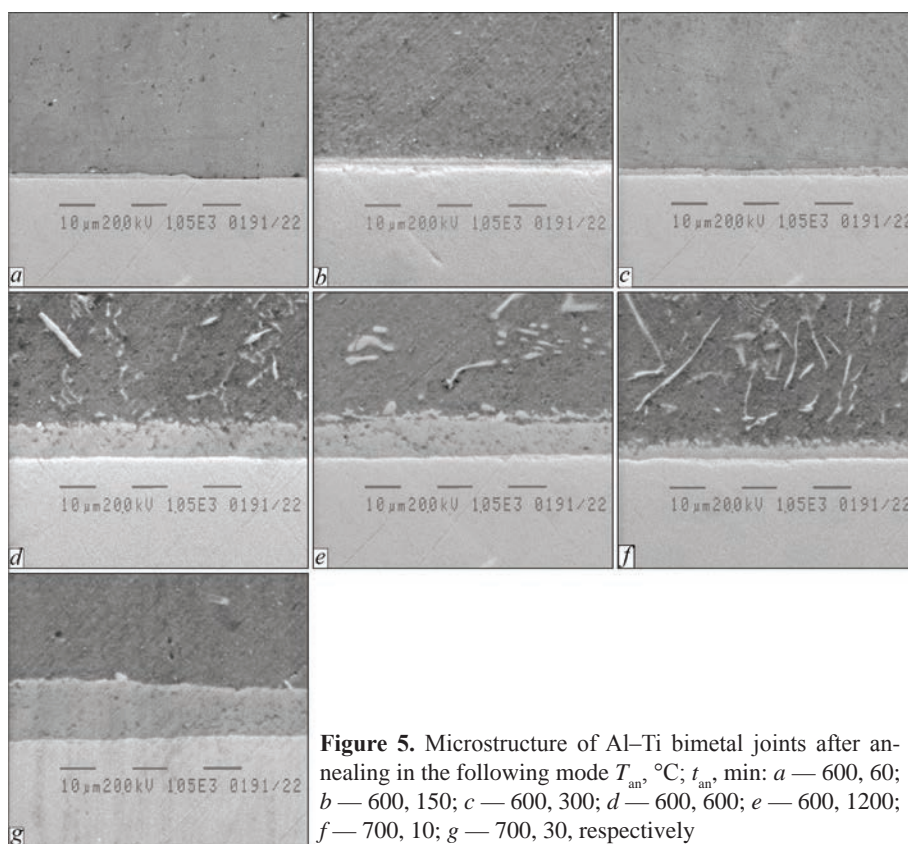


**Figure 5.** Microstructure of Al–Ti bimetal joints after annealing in the following mode  $T_{an}$ , °C;  $t_{an}$ , min: *a* — 600, 60; *b* — 600, 150; *c* — 600, 300; *d* — 600, 600; *e* — 600, 1200; *f* — 700, 10; *g* — 700, 30, respectively

joints, when joining Ti/Al + Al/Ti and Ti/Al + Ti/Al bimetal is close in its value, and is equal to 44.5 and 41.1 MPa, respectively. Combining Al/Ti + Ti/Al leads to decrease of the average strength value to 35.2 MPa and breaking of the joints (Table 2). A possible cause for drop in strength is oxidation of the surfaces of titanium during welding, and formation of a large number of defects in the butt joint (Figure 3, *c*).

In order to study the features of growth of the intermetallic interlayer between the titanium and aluminium layers during heat treatment, Al–Ti bimetal joints were heated up to temperatures of 600 and 700 °C. Analysis of the microstructure of Al–Ti bimetal showed that formation and growth of the intermetallic interlayer takes place during heating, while increase of its thickness depends primarily on the temperature and duration of heat treatment (Table 3).

In the structure of Al–Ti bimetal foil after diffusion welding the intermetallic interlayer is not identified [4]. Investigations of the impact of heat treatment showed that soaking at the temperature of 600 °C for 60 min does not lead to formation of a continuous intermetallic interlayer (Figure 5, *a*), but formation of individual intermetallic areas of up to 1 μm thickness is observed in the zone of aluminium-titanium joint. At increase of the annealing duration up to 150 min formation and growth of a continuous intermetallic interlayer of up to 2 μm thickness is observed on aluminium/titanium boundary (Figure 5, *b*). Further increase of annealing duration up to 300 min leads to growth of intermetallic interlayer thickness up to

4 μm that is two times greater than the previous result (Figure 5, *c*). Conducting heat treatment for 600 min leads to formation of an intermetallic interlayer about 10 μm thick (Figure 5, *d*). Increase of the time of soaking at 600 °C temperature up to 1200 min only slightly influences the thickness of the intermetallic interlayer. Average thickness of the intermetallic layer is equal to 11 μm (Figure 5, *e*).

Chemical analysis conducted using a scanning electron microscope showed that the intermetallic interlayers are of the following composition, wt.%: 55.58–58.93 Al and 41.07–44.42 Ti. According to Al–Ti binary diagram, this composition corresponds to an alloy based on a mixture of  $Al_2Ti$  and  $Al_3Ti$  intermetallics.

Dependence of intermetallic interlayer thickness on annealing duration at 600 °C is shown in Figure 6.

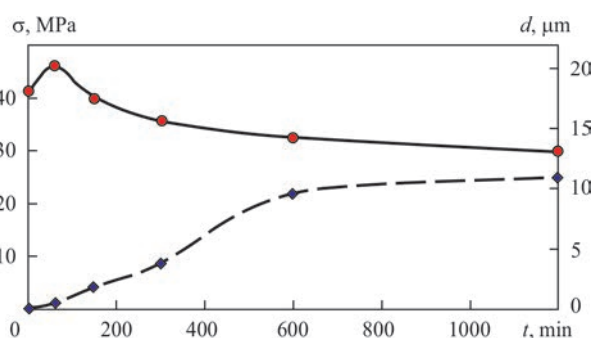


**Figure 6.** Dependence of compressive strength  $\sigma$  (1) and thickness  $d$  (2) of intermetallic interlayer on sample annealing duration at 600 °C temperature



**Figure 7.** General view of samples of individual honeycombs after annealing and mechanical compression testing,  $T_{\text{an}}$ , °C;  $t_{\text{an}}$ , min: a — 600, 150; b — 600, 600; c — 600, 1200

Increase of soaking temperature up to 700 °C leads to acceleration of the growth of intermetallic interlayers (Table 3, Figure 5, f, g).

Determination of the strength of samples after heat treatment was conducted on individual honeycombs (Figure 3, a). It was established that after annealing for 60 min at 600 °C 11.7 % increase of compressive strength of honeycomb samples takes place, compared to the initial condition (45.9 against 41.1 MPa) (Table 3, Figure 6). Such an increase of strength can be related to formation of individual centers of the intermetallic phase in the zone of titanium-aluminium joint. Sample annealing for 150 min, in keeping with the results of metallographic studies, leads to formation of a thin intermetallic layer (~ 2 µm) in the butt joint, the presence of which has a minor influence on the load-carrying capacity of the honeycomb, while the strength remains almost on the level of the initial values (39.9 MPa). Further increase of soaking time to 1200 min at 600 °C has a negative impact on strength, the values of which drop to 29.8 MPa. The cause for it is the nonuniformity of the growth and defectiveness of the intermetallic layer that can be associated with the change of its formation mechanism [9], as well as intensive recrystallization of aluminium.

Increase of heat treatment temperature to 700 °C leads to a considerable drop of strength as a result of degradation of the aluminium layer structure (Table 3).

Analysis of the honeycombs after conducting mechanical investigations shows that at compression of samples annealed at 600 °C for 300 min inclusive, deformation of the honeycomb core walls takes place with formation of individual cracks without destruction of the welded spots (Figure 7, a). Increase of the heat treatment duration up to 600 min leads to partial destruction of the honeycomb material and welded spots (Figure 7, b). After soaking at 600 °C for 1200 min the honeycomb material decomposes into individual elements (Figure 7, c).

Thus, obtained results of research conducted on samples consisting from an individual honeycomb, show that use of Al–Ti bimetal core, compared to aluminium one allows increasing its compressive strength four times from 9.8 up to 41.1 MPa, respectively.

## Conclusions

1. Studied was the possibility of spot welding of bi-metal strips for producing honeycomb core with different combinations of titanium and aluminium layers. It is shown that an optimal variant is welding strips, which corresponds to Al/Ti + Al/Ti joints, the average strength of which is equal to 41.1 MPa.

2. It is shown that annealing of the honeycomb core at the temperature of 600 °C for 60 min leads to formation of individual particles of the intermetallic phase of up to 1 µm size in the butt joint between aluminium and titanium layers that results in 11.7 % increase of compressive strength of the samples, compared to the initial condition.

3. Further increase of annealing time from 60 up to 1200 min leads to formation and growth of the intermetallic layer in the butt joint and lowering of the compressive strength of honeycomb samples.

4. It is shown that samples of the honeycomb core after annealing at 600 °C for 60–600 min at compression with maximum level of deformation of 50 %, deform without destruction of the welded spot and the bimetal material walls. Increase of annealing time leads to embrittlement of both the welded spots, and the honeycomb material as a whole.

5. Use of bimetal honeycomb core, compared to aluminium one, allows increasing its compressive strength from 9.8 up to 41.1 MPa.

1. Bitzer, T. (1997) *Honeycomb technology. materials, design, manufacturing, applications and testing*. Springer-Science+Business Media Dordrecht.
2. Panin, V.F., Gladkov, Yu.A. (1991) *Structures with filler: Refer. Book*. Moscow, Mashinostroenie [in Russian].
3. Bashurin, A.V., Mastikhin, E.Yu., Kolmykov, V.I. (2010) Diffusion welding of hollow bimetal panels. *Zagotov. Proizvodstvo v Mashinostroenii*, **1**, 13–15 [in Russian].
4. Falchenko, Ju.V., Petrushynets, L.V., Polovetskii, E.V. (2020) Peculiarities of producing Al–Ti bimetal sheet joints by the method of vacuum diffusion welding. *The Paton Welding J.*, **8**, 25–28. DOI: <https://doi.org/10.37434/tpwj2020.08.04>.
5. Wadsworth, J., Lesuer, D.R. (2000) Ancient and modern laminated composites – from the Great Pyramid of Gizeh to Y2K. *Materials Characterization*, **4–5**, 289–313. DOI: [https://doi.org/10.1016/S1044-5803\(00\)00077-2](https://doi.org/10.1016/S1044-5803(00)00077-2).
6. Karpachev, D.G., Doronkin, E.D., Tsukerman, S.A. et al. (2001) *Nonferrous metals and alloys: Refer. Book*. Nizhny Novgorod, Venta-2 [in Russian].
7. Vasiliev, K.V., Vill, V.I., Volchenko, V.N. et al. (1978) *Welding in mechanical engineering: Refer. Book*. In: 4 Vol., Vol. 1. Moscow, Mashinostroenie [in Russian].
8. Seemann, R. (2020) *A virtual testing approach for honeycomb sandwich panel joints in aircraft interior*. Springer Vieweg.
9. Falchenko, Ju.V., Petrushynets, L.V., Polovetskii, E.V. (2020) Peculiarities of producing layered metal composite materials on aluminium base. *The Paton Welding J.*, **4**, 9–18. DOI: <https://doi.org/10.37434/tpwj2020.04.02>.

Received 22.03.2021

# WELD FORMATION IN CONSUMABLE ELECTRODE WELDING OF BUTT JOINTS OF AMg5M ALUMINIUM ALLOY IN SITE WITH A FORMING BACKING ELEMENT AND WITHOUT IT

**T.M. Labur, M.R. Yavorska and V.A. Koval**

E.O. Paton Electric Welding Institute of the NAS of Ukraine

11 Kazymyr Malevych Str., 03150, Kyiv, Ukraine. E-mail: [office@paton.kiev.ua](mailto:office@paton.kiev.ua)

The paper presents the results of studying the features of weld formation at consumable electrode pulsed-arc welding of 4 mm AMg5M alloy in different positions at the speed of 23 m/h with forming backing element (FBE) and without it. It is shown that sound welds form irrespective of the angle of butt joint inclination relative to the horizontal plane. FBE presence increases the geometrical dimensions of welds made with consumable electrode by 4–12 % on average, depending on the position of butt joints. Obtained data clearly demonstrates the possibility of achieving the required quality of welds and high level of mechanical properties in consumable electrode welding of aluminium-magnesium alloys at different positions of the butt joints without FBE application. 6 Ref., 3 Tables, 4 Figures.

*Keywords:* aluminium alloy, argon-arc welding, consumable electrode, filler wire, butt joint positions, forming backing element, welded joints, welds, solidification, structure, mechanical properties

AMg5M aluminium alloy belongs to the class of deformed magnaliums of Al–Mg–Mn alloying system (4.8–5.2 Mg, 0.3–0.8 Mn) and is not heat-hardenable. Its strength is  $\sigma_t = 295\text{--}305$  MPa. It has high ductility ( $\delta = 20\%$ ) in a broad range of application temperatures, as well as considerable corrosion strength (after performing the annealing operation) and vibration resistance [1]. This alloy and its welded joints are applied for manufacturing parts and components of various-purpose structures, in particular, panels of shells and cases, bottoms, flanges, tube plates, etc.

Metal heating in welding leads to a change of the structure — increase of grain size, localizing and coagulation of phases along the grain boundaries, appearance of oxide inclusions that on the whole negatively affects the values of mechanical properties of welded joints [2, 3]. Therefore, relevant is the need to ensure the quality of welded structures from AMg5M aluminium alloy, sensitive to the heat treatment cycle of welding. The process, which takes place in site, requires searching for more perfect technologies of welding the butt joints, when it is not always possible to use the forming backing elements that promote sound formation of the weld root. The joints here are made in different positions, which differ from the generally accepted ones. In this connection, the objective of this work is studying the nature of weld formation on 4 mm AMg5M aluminium alloy at consumable

electrode pulsed-arc welding (CEPAW) and establishing its impact on mechanical properties of welded joints produced in different positions with application of forming backing element (FBE) and without it.

It should be noted that the main feature of CEPAW method is the possibility of transfer of electrode metal drop is a short time period of the order of several milliseconds. It is known that the weld pool mobility is associated with its fluidity and temperature, respectively [4]. It mainly depends on the average value of welding current, which is lower at CEPAW than in classical welding processes. That is, electrode metal transfer and kinetics of weld pool solidification are separated in time. During extended impact of the pulse, the welding current rises and corresponds to metal transfer mode. The drop formed at the electrode tip is detached due to considerable electromagnetic forces applied to it. During the period, when the welding current pulse is low, no electrode metal melting takes place, but just the arcing mode is supported. Reduction of average welding current, compared to DC welding conditions allows obtaining a smaller volume of the weld pool [2].

**Investigation procedure.** Before welding, AMg5M aluminium alloy plates of 350×100×4 mm size and 1.6 mm filler wire of SvAMg6 grade were traditionally cleaned in a solution of caustic soda with subsequent rinsing in cold water. Clarifying the plates and wire was performed in a solution of nitric acid,

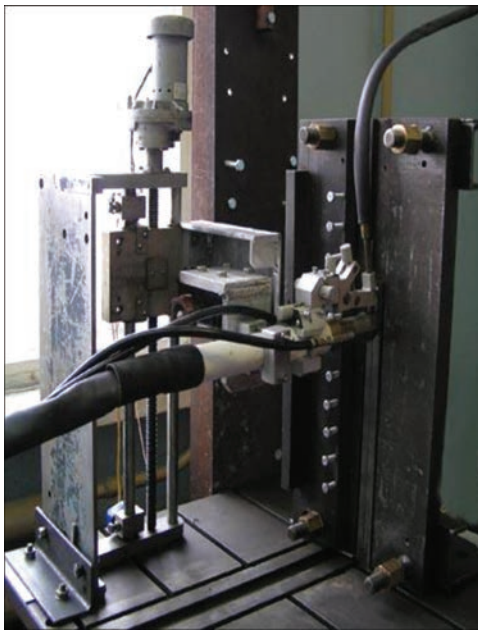


**Figure 1.** Appearance of PSO-600 unit for providing an adjustable angle of butt joint inclination from 0 up to 90° relative to the horizontal of the mobile platform in welding

with mandatory rinsing in water and final drying [5]. Ends of the butt joints were cleaned mechanically to the depth of not less than 0.1 mm. The scheduled operations were performed in keeping with the generally accepted procedure [6] and GOST-14806.

Welding of plates from AMg5M alloy was performed with consumable electrode by modulated pulse current at the speed of 23 m/h, using TPS 2700 power source of Fronius and PSO-600 unit to ensure an adjustable angle of inclination of the butt joints within 0 to 90° relative to the mobile platform horizontal (Figure 1). Welded joints were produced in one pass in process modes specified in Table 1. The arc length was equal to 3–5 mm, electrode extension was 8–10 mm, the flow rate of high-purity argon shielding gas of grade «A» (GOST 10157–76) was equal to 20 l/min, while the angle of the torch inclination relative to the vertical axis was 10–15°. The process of welding the butt joints was conducted with application of forming element (FBE) and without it, thus modeling different site conditions, applied in berth

welding. Figure 2 presents the appearance of AMg5M alloy welds, made in different positions at welding speed of 23 m/h without FBE and with it.

Visual control of the produced welds was conducted by their appearance, and radiography method (GOST 7512–89) was used to evaluate their quality. Analysis of the radiographs showed that the welds are tight and do not have coarse defects of the type of cracks, lacks-of-penetration or pores. Geometrical dimensions of the welds ( $B$  is weld width from the joint face side (technological reinforcement),  $b$  is the weld width from the reverse side of the joint (weld root),  $H$  is the height of technological reinforcement convexity,  $h$  is the height of weld root convexity;  $\delta$  is the blank thickness) were measured by electronic caliper APT – 34460-150 with 0.01 mm accuracy. By the data of Table 2, the width of the studied welds has close values, and the small difference observed in this case, can be due to impact of the gravitational component, that acts on the metal pool at different angles of its inclination relative to the horizontal surface.

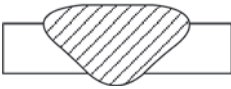
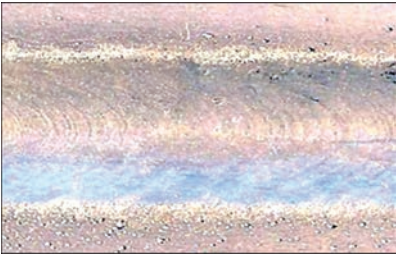
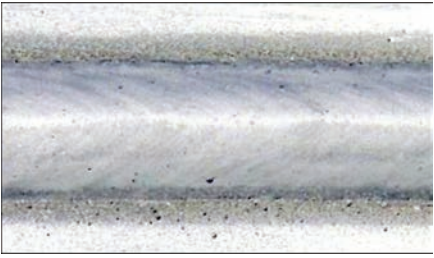
At FBE application in welding butt joints by modulated pulse current in the horizontal plane (angle of the butt joint inclination is 0°), the weld width is equal to 10.55 mm, and without the technological backing it is 10.20 mm. Welding of butt joints at up to 30° angle to the horizontal leads to widening of the welds up to 11.65 mm, and without backing — to its narrowing to 9.96 mm. In the case, when butt welding was performed at an angle of 60°, the width was 11.40 mm, and without FBE it was 9.74 mm. At welding of butt joints in the vertical position, i.e. at an angle of 90° to the horizontal, the weld width was 10.74 and 10.12 mm, respectively.

The values of weld root width here were as follows: at welding in the horizontal plane (0° angle) it was 4.58 mm without FBE and 5.9 mm with FBE. In the butt joint position at 30° angle relative to the horizontal, the root width was 5.24 and 4.84 mm, respectively. At butt joint location at 60° angle, the width of the weld root made without FBE was 6.96 mm, and that with FBE was 4.84 mm. Under the conditions of vertical welding of butt joints (90° relative to the horizontal) it was 6.62 and 5.21 mm, respectively.

**Table 1.** Modes of CEPAW of 4 mm AMg5M alloy at 23 m/h speed in different positions of butt joints relative to the horizontal plane

Angle of butt joint inclination to the horizontal plane in welding, deg	Without FBE application			With FBE application		
	$U_a$ , V	$I_w$ , A	$V_{w,f}$ , m/min	$U_a$ , V	$I_w$ , A	$V_{w,f}$ , m/min
0	18.9	100	6.9	19.0	112	7.5
30	19.0	100		18.9	111	
60	19.3	101		18.9	114	
90	19.1	103		19.11	115	

Note.  $U_a$  — arc voltage, V;  $I_w$  — welding current, A;  $V_{w,f}$  — welding wire feed rate, m/min

Angle of butt joint inclination to the horizontal plane, deg	Appearance of welds without FBE 	Appearance of welds with FBE 
0		
30		
60		
90		

**Figure 2.** Appearance of AMg5M alloy welds made by consumable electrode in different positions at welding speed of 23 m/h without FBE application and at its application

The metal hardness value which reflects its sensitivity to the thermal cycle of welding in joints of 4 mm AMg5M aluminium alloy, was measured by hardness meter by the generally accepted standard procedure (GOST 9012–59, Rockwell hardness). Dependence of the values of this characteristic on the angle of butt joint inclination is presented in Figure 3. As shown by analysis of hardness measurement results, application of SvAMg6 wire with higher magnesium content (6 %) provides increase of weld metal hardness, compared to base metal of AMg5M alloy. The values of the characteristic are almost not affected by the angle of butt joint location in welding. Hardness level coincides with the base metal in as-annealed condition and is equal to (*HRB* 72–73). In the weld central zone hardness is

higher by 3–4 units than that in the HAZ and base metal. This is attributable to positive influence of welding filler wire. Hardness of the metal of welds made in the horizontal position (0°) on a backing and without it is the same and is equal to 75 units. Hardness value of welds made in 30° position, is 75 units without FBE application and 77 units, when FBE is used. At butt joint location at 60° angle, hardness is equal to 77 units in both the cases. Butt welding in the vertical position (90°) without FBE ensures weld hardness on the level of 75 units, and with FBE — on the level of 76 units. Under the conditions of welding in the horizontal plane, HAZ extent is equal to 24 mm, including the weld, irrespective of FBE application. Change of the position from 0 to 90°, causes a reduction of the HAZ

**Table 2.** Geometrical parameters of welded joints of AMg5M alloy made by CEPAW in different positions at welding speed of 23 m/h without FBE and with FBE

Angle of butt joint inclination to the horizontal plane, deg	Geometrical parameters of the weld									
	Without FBE					With FBE				
	$B$ , mm	$b_{pen}$ , mm	$H_{rein}$ , mm	$h_{pen}$ , mm	$K$	$B$ , mm	$b_{pen}$ , mm	$H_{rein}$ , mm	$h_{pen}$ , mm	$K$
0	10.11–10.2	4.58–4.60	1.45–1.50	1.85–1.90	1.85	10.53–10.57	5.82–5.99	2.14–2.18	1.64–1.70	1.71
30	9.96–10.10	5.24–5.25	1.64–1.81	1.43–1.47	1.79	11.6–1.69	4.78–4.9	1.85–2.06	1.69–1.7	1.95
60	9.74	6.94–6.98	1.66–1.70	1.49–1.70	1.71	11.40–11.7	3.95–5.56	2.17–2.27	1.64–1.84	1.82
90	10.03–10.26	6.54–6.71	1.87–1.93	1.42–1.52	1.72	10.69–10.79	5.16–5.27	2.28–2.46	1.48–2.16	1.69

*Note.* 1.  $K$  is the weld form factor equal to the ratio of weld width ( $B$ , mm) to its thickness ( $H + \delta$ , mm):  $K = B/(H + \delta)$  2. Admissible  $K$  values are in the range from 0.5 to 4.0, values from 1.2 to 2.0 are regarded to be optimal.

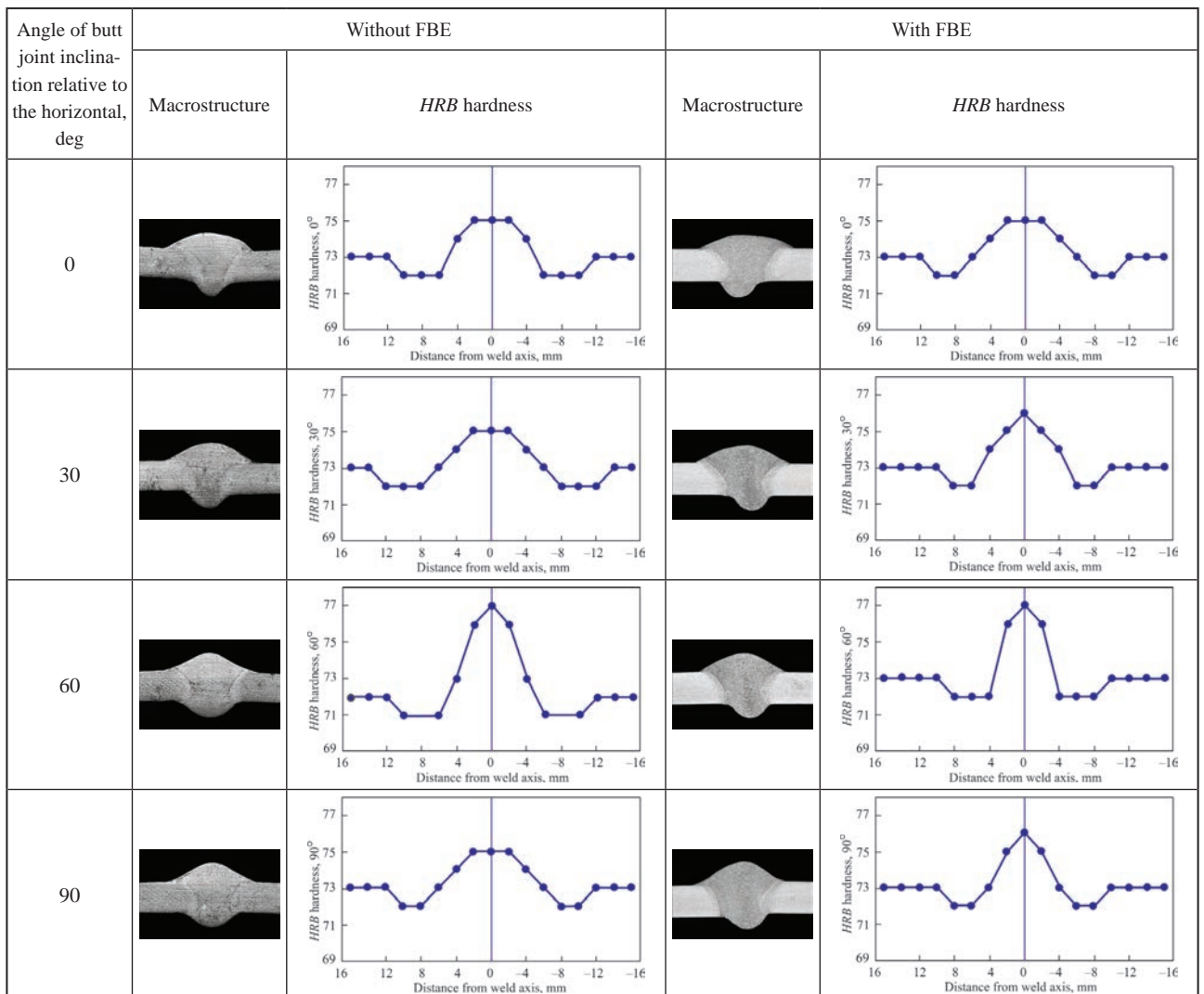


**Figure 3.** Macrostructure and hardness of welded joints of 4 mm AMg5M alloy made with consumable electrode in different positions at welding speed of 23 m/h without FBE application and with it

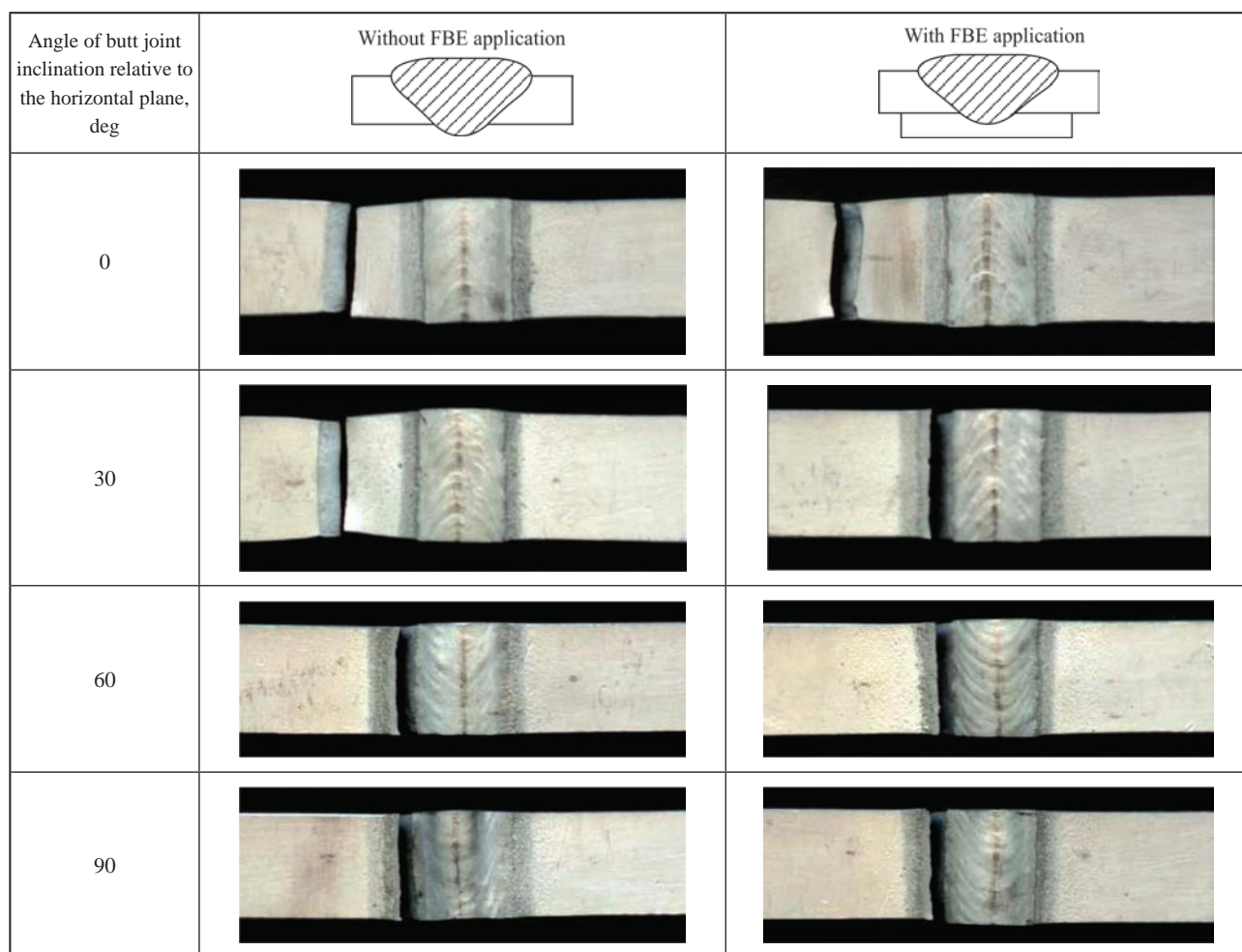


**Figure 4.** Fracture mode of welded joints of 4 mm AMg5M alloy produced by CEPAW in different positions with FBE and without it extent to 20 mm in butt joints made by the technology variant with FBE application. In the case of welding at an angle of 30° to the horizontal without backing application, HAZ size is 28 mm. At the change of welding position from 60 to 90°, when welding was performed without FBE application, the HAZ extent was reduced and was equal to 24 mm, including the weld.

Strength values ( $\sigma_T^{wj}$ ) of welded joints were established on standard samples with technological reinforcement on the weld face and with removed weld root. Weld metal strength ( $\sigma_T^w$ ) was determined on samples without reinforcement and weld root (GOST 6996–66). Welded joint samples failed in the base metal, as well as in the HAZ that was indicative of lowering of metal strength at heating (Figure 4). Proceeding from analysis results (Table 3), the strength of welds in the joints produced without FBE in the horizontal position, is equal to 280.0 MPa, and at BFE application, it is 299.3 MPa. The strength of joints made in the position at 30° angle, was 285.0 and 294.8 MPa, respectively. In the case, when welding is performed at 60° angle, the strength of the joints is equal to 291.3 and 279.8 MPa, and in the vertical position (90°) strength values are 282.0 MPa without FBE and 280.4 MPa with FBE. The strength coefficient of welded joints ( $K_T^{wj}$ ) produced in different positions in space, was equal to 0.89–0.95,

when welding was performed without FBE, and to 0.92–0.98 with FBE (Table 3).

Ductility value (bend angle  $\alpha$ ) of welded joints was assessed under the conditions of three-point bending with application of working load from weld root side. Technological reinforcement and weld root, respectively, were removed mechanically as required by GOST 6996–66. For comparison, the deformability characteristic was determined on base metal samples. Proceeding from analysis results (Table 3), the ductility values of the joints welded in the horizontal position, are as follows: without FBE — 85°, and with FBE — 129°. After welding the butt joints in 30° position without FBE application, the ductility value is equal to 105°, and at its application it is 127°. In the case, when welding is performed without FBE in butt joint position at 60° angle, the joint ductility is equal to 103°. Welding of butt joints with FBE application almost does not influence the ductility values (106°). In butt welding in the vertical position (at 90° angle), when FBE was not applied, the joint ductility was equal to 113°, and in the case of FBE application it was 98°. Compared to base metal ( $\alpha = 180^\circ$ ) the ductility values are lower in all the studied joints, but the following should be noted here. Welding of AMg5M alloy without FBE application leads to proportional increase of the ductility level with greater

**Table 3.** Influence of forming backing element and positions of butt joints of 4 mm AMg5M alloy on welded joint mechanical properties

Mechanical property values of welded joints	Without FBE application				With FBE application			
	Welding angle, deg							
	0	30	60	90	0	30	60	90
$\sigma_t^{wj}$ , MPa	<u>276.2–287</u> 280.0	<u>283.0–286.1</u> 285.0	<u>288.0–297.0</u> 291.3	<u>269–290</u> 282	<u>297.0–301.0</u> 299.3	<u>291.9–300.3</u> 294.8	<u>264.3–293.3</u> 279.8	<u>267.0–291.6</u> 280.4
$\sigma_t^w$ , MPa	<u>268.8–294.4</u> 282.7	<u>280.2–285.1</u> 282.1	<u>274.0–284.0</u> 280.2	<u>269–278</u> 272.8	<u>287.3–289.4</u> 288.0	<u>285.0–285.0</u> 285.0	<u>271.0–284.0</u> 278.6	<u>277.0–281.9</u> 278.8
$\alpha$ , deg	<u>78–89</u> 85	<u>107–110</u> 105	<u>93–116</u> 103	<u>106–126</u> 113	<u>128–130</u> 129	<u>125–130</u> 127	<u>104–108</u> 106	<u>97–98</u> 98
$K_t^{wj}$	0.92	0.93	0.95	0.92	0.98	0.97	0.92	0.92
$K_t^w$	0.93	0.92	0.92	0.89	0.94	0.93	0.91	0.91

Note. 1. Mechanical properties of AMg5M alloy:  $\sigma_t^w = 305$  MPa,  $\sigma_{0.2}^w = 180$  MPa,  $\delta = 20\%$ ,  $\alpha = 180^\circ$ . 2.  $K_t^{wj}$  — strength coefficient of welded joint,  $K_t^{wj} = \sigma_t^{wj} / \sigma_t^{b.m.}$ , strength coefficient of weld metal  $K_t^w = \sigma_t^w / \sigma_t^{b.m.}$ , respectively.

angle of the butt joint position: 85, 105, 103, 113°. If FBE is used in welding, then a reverse dependence is found – ductility value decreases: 129, 127, 106, 98°, respectively, while staying at a high enough level.

Investigations of the macrostructure of welds showed that they are tight, and characterized by presence of a granular structure. No coarse inadmissible porosity is observed in the structure of welds or fusion zone. The morphology of the cast metal of welds is the same, irrespective of the value of the angle of butt joint inclination in welding (see Figure 3). Temperature range of metal heating during welding of AMg5M alloy leads to characteristic formation of the following structural zones: weld, zone of weld metal fusion with the base metal and HAZ. The latter has an essential influence of the properties and fracture mode of welded joints.

## Conclusions

1. Additional data were obtained on the features of weld formation during consumable electrode pulsed-arc welding of 4 mm AMg5M in different positions at the speed of 23 m/h with application of forming backing elements (FBE) and without it. It is found that the process of consumable electrode welding without FBE, irrespective of the angle of butt joint inclination relative to the horizontal plane provides the required conditions for formation of sound welds of the alloy and does not have any significant influence on the level of joint strength. FBE presence leads to increase of the geometrical dimensions of welds made with consumable electrode, by 4–12 % on average, depending on butt joint position.

2. The found features of structure formation in welded joints of AMg5M alloy in different positions allow recommending the process of consumable electrode welding of various aluminium hull structures without

FBE for application in site. This is due to the fact that the welds have a macrostructure identical to that of welds produced with FBE application. In both the cases, the welds have no coarse inadmissible defects in the form of large pores, cracks, discontinuities, and oxide inclusions. Experimental results clearly demonstrate that FBE application in consumable electrode welding of aluminium-magnesium alloys in different positions of butt joints is not mandatory, in order to provide the due quality of the weld and high level of service properties. This CEPAW process can be recommended for working in site without FBE application, using optimal parameters of the welding modes at the respective angles of structural element inclination, without lowering the quality values of the welded joints.

1. Andreev, S.B., Golovachenko, V.S., Gobach, V.D., Russo, V.A. (2006) *Fundamentals of welding of ship structures*. St.-Petersburg, Sudostroenie [in Russian].
2. Kolpakov, I.N., Osokin, E.P., Pavlova, V.I., Ushkov, S.S. (2006) Structural aluminium materials in shipbuilding. TsNII Prometej. *TLS*, 1–2, 73–80 [in Russian].
3. Ishchenko, A.Ya., Labur, T.M., Bernadsky, V.N., Makovetskaya, O.K. (2006) *Aluminium and its alloys in modern welded structures*. Kiev, Ekotekhnologiya [in Russian].
4. Labur, T.M., Zhernosekov, A.M., Yavorskaya, M.R., Pashulya, M.P. (2013) Consumable electrode pulsed-arc welding of aluminium alloys with regulated pulse shape. *Svarochn. Proizvodstvo*, 11, 3–7 [in Russian].
5. DSTU EN ISO 10042:2015 ( EN ISO 10042:2005, TDT:I-SO10042:2005, IDT) *Welding. Arc-welded joints in aluminium and its alloys. Quality levels for imperfections* [in Ukrainian].
6. Labur, T.M., Gavrilyuk, Yu.M., Pashulya, M.P., Yavorskaya, M.R. (2014) Influence of welding technology on structure and physical-mechanical properties of joints of AMg5M aluminium alloy. In: *Proc. of 5<sup>th</sup> Int. Conf. on Fracture Mechanics of Materials and Strength of Structures (Ukraine, Lvov, 24–27.06.2014)*. PMI, 457–461 [in Russian].

Received 10.03.2021

# METHOD OF ACOUSTIC EMISSION AT EVALUATION OF THE STATE OF WELDS AND THEIR SERVICE PROPERTIES. Part 2. PRACTICAL APPLICATION

S.A. Nedosieka, A.Ya. Nedosieka, M.A. Yaremenko, O.I. Boichuk and M.A. Ovsienko

E.O. Paton Electric Welding Institute of the NAS of Ukraine

11 Kazymyr Malevych Str., 03150, Kyiv, Ukraine. E-mail: [inpat59@paton.kiev.ua](mailto:inpat59@paton.kiev.ua)

The majority of existing structures contain welded joints. Questions of monitoring service characteristics of welded joints, using acoustic emission method, are considered. Attention is given to a change in material properties of operating structures with welded elements after long-term service, taking into account the time and probable violation of service conditions. Examples of evaluation of the change in properties of welded structure materials by the data of acoustic emission, determination of their damage and residual service life, are given. 17 Ref., 5 Tables, 24 Figures.

*Keywords:* welds, service properties, acoustic emission (AE), AE activity, AE scanning, damage, destruction

Influence of the type of welded joint on acoustic emission (AE) and possibility of quantitative evaluation of such an influence by AE method was considered in part 1 of this paper [1].

High sensitivity of AE method to defect initiation and propagation in materials at very early stages of destruction allows controlling the service properties of welded joints both directly during welding, and at any stages of welded structure operation [2].

Part 2 deals with the questions of practical application of AE method for welding process control and evaluation of service properties of different types of welded joints in the case of some structures with prolonged operating period. Note that the load-carrying ability of the structure and its service life are largely formed at the fabrication stage. Correction of the above factors occurs during routine or unscheduled repairs. As the majority of metal structures are welded, their quality essentially depends on the state of welds,

in particular, those made during repair. Fracture in a gas pipe along the incomplete penetration line due to the arc shifting during welding, can be given as an example of poorly performed weld (Figure 1).

An important element, in terms of preventing the situations similar to those presented in Figure 1, is the possibility of controlling by AE method the weld quality directly during welding. Such experiments were conducted at PWI, and they showed that AE method allows rejecting the poor quality areas of welds on steel samples during welding.

In order to demonstrate the applicability of AE method to control defect initiation during welding of aluminium alloys we will perform studies of AMg5V alloy. A plate of 10 mm thickness was welded, weld dimensions were 600×12 mm. ADSV-2 unit was used for welding. Welding was performed by tungsten electrode with 2 mm filler wire from AMg6 alloy. Welding parameters were as follows: voltage  $U = 16$  V, cur-



**Figure 1.** Gas pipe after destruction (a) and enlarged image of an area, which shows the result of incomplete penetration of metal (c)

S.A. Nedosieka — <https://orcid.org/0000-0002-3239-381X>, A.Ya. Nedosieka — <https://orcid.org/0000-0001-9036-1413>,  
M.A. Yaremenko — <https://orcid.org/0000-0001-9973-4482>, O.I. Boichuk — <https://orcid.org/0000-0001-5800-1549>,  
M.A. Ovsienko — <https://orcid.org/0000-0002-2202-827X>

© S.A. Nedosieka, A.Ya. Nedosieka, M.A. Yaremenko, O.I. Boichuk and M.A. Ovsienko, 2021

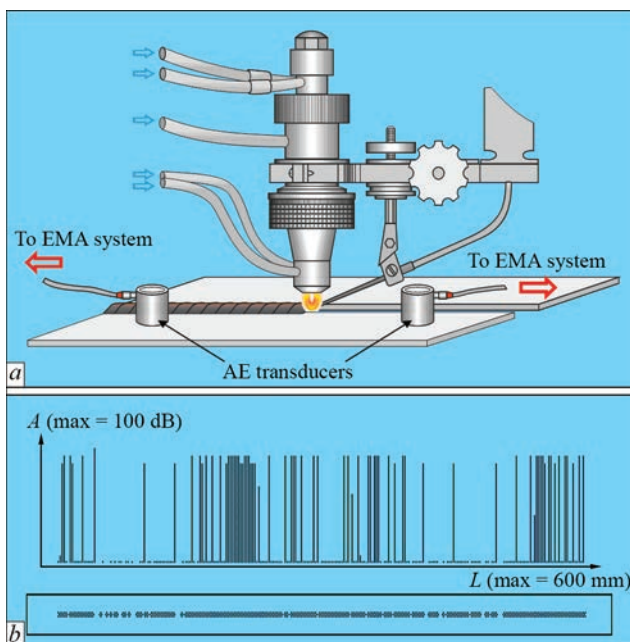


**Figure 2.** Investigation of AMg6 alloy: *a* — scheme of plate welding; *b* — histogram of amplitudes  $A$  of AE events along the weld, relative to coordinate  $L$  (top) and coordinate of these AE events (bottom)

rent  $I = 350$  A, arc movement speed 15 m/h. AE was recorded using EMA-1 system based «Defectophone» measuring device and two transducers of DAE-01 type, located at the ends of the welding zone, that allowed obtaining the coordinates and amplitudes of AE events arising during welding. The pattern of distribution of AE events and their amplitudes are given in Figure 2, *b*. By the data of investigations conducted after welding, weld quality was satisfactory, no defects inadmissible for service conditions were found. At the same time (Figure 2, *b*) a large number of AE events with high amplitudes were registered during testing. Accordingly, we can assume that AE system registered slight damage of the type of dislocation shifts, or similar ones. It means that coarser defects can also be registered, but filters have to be developed and applied for rejecting the obtained AE signals by certain criteria, extracting from them the events corre-

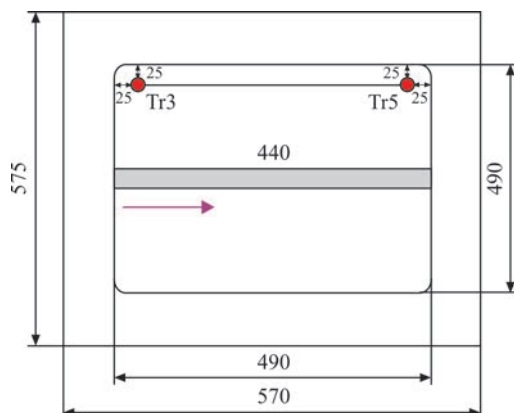


**Figure 3.** Typical scheme of steel plate welding testing

sponding to the presence of really dangerous defects. It requires additional studies.

In order to solve the set tasks for steels, welding of three samples from 09G2S material and of two samples from 13KhGMRB (material prone to defect formation) was conducted. Sample thickness was 20 mm. Locations of mounting AE transducers were determined and prepared beforehand, and their protection during welding was provided. Control was performed using EMA-2 system, and data was processed with EMA-3.92 software (SW) [3]. Before conducting AE testing, preliminary test sounding was performed to determine the initial data, required for EMA-2 system operation: fixed threshold — 10 mV; floating threshold —  $2\sigma$ ; measurement dead time — 10 ms; high-frequency filter cutoff frequency — 100 kHz. AE testing was conducted both during welding in order to evaluate AE levels, taking into account the impact of technological obstacles, evaluation of the impact of multipass and poor welding on the general AE pattern, and during the weld cooling.

During performance of AE testing, the discrete and continuous AE is registered. Discrete AE characterizes crack propagation, transition of structural material into the ductile state, opening of oxide films, etc. The mechanism of discrete AE generation is initiation of damage in the material structure and its discrete development. Continuous AE characterizes fluid or gas flowing out through discontinuities in the material or intensive displacement of dislocation groups. The mechanisms of continuous AE generation are processes of continuous local rebuilding of the material structure at their deformation or seepage and flowing out of fluids and gases through discontinuities and cracks.

Two transducers (channels Nos 3, 5 for 09G2S steel and Nos 1, 2 — for 13KhGMRB) were used to determine the coordinates of AE sources. Cluster location was used. The size of the cluster for recording the zones of higher AE activity during welding was determined as 10 % of that of the array base, which was 100–420 mm. Clustering of the registered events from acute discontinuity, such as a crack, is continuous, while the plastic deformation regions associated, for instance, with corrosion damage, form an area of the source with a high degree of indeterminateness in size. In most cases the growing crack is regarded as the most hazardous defect. The sources which are considered as low-active or low-intensive ones usually do not require further assessment.

The overall testing scheme is given in Figure 3 (other schemes differ only by the plate width and distance between AE transducers).

Let us focus on the most revealing research results. The main and most basic result is that a clear

**Table 1.** Parameters of welding 09G2S steel plates

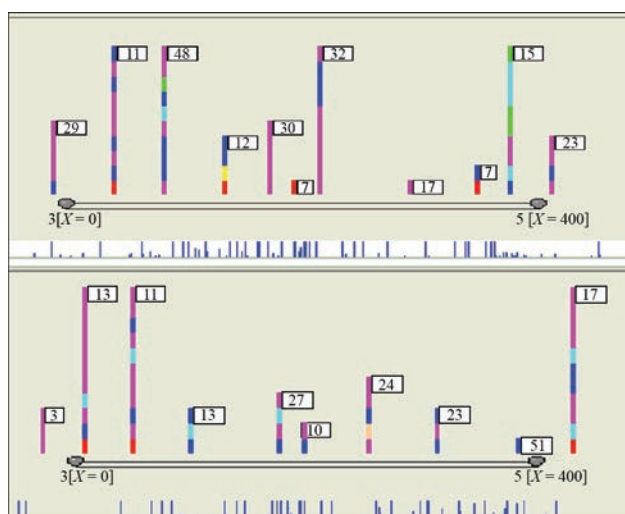
Pass number	Welding parameters		
	$I$ , A	$U$ , V	$V_w$ , m/h
1	220-230	36-37	16-17
2	250	35-36	20
3	250	35	20
4	250	35	16-17
5	250	35	19-20

AE pattern is obtained during welding, irrespective of the number of passes and weld quality, while the registered events follow the welding process. AE parameters and pattern during five pass welding (restrained butt joint) are given in Table 1 and Figure 4. Results of radiographic testing performed after weld cooling, show that welding quality was satisfactory (Figure 5).

Figure 4 presents the fragments of location screens of EMA-3 program, where the lower part shows the location scheme with transducer numbers, and given under it are the coordinates of registered AE events (vertical lines, the height of which corresponds to event amplitude of 0–500 mV). Above the location scheme the clusters based on AE events are shown by bars with flags (bar colour corresponds to a certain amplitude of AE events, the flag shows the number of AE events in the respective cluster). This description also applies to Figures 7, 21 and 23.

AE pattern during the first and fifth welding passes (Figure 4) differs only slightly both by the number of AE events, and by their location (the pattern was largely identical during the other three passes). The nature of location of the formed clusters is stochastic, in keeping with the stochastic nature of AE signal generation during welding, and as such they do not carry any essential information on welded joint quality. However, the standards of sound welding process can be in principle created on their base.

The next important result is the fact that as the sample cools after welding; the number of registered AE events gradually decreases and reaches zero mark even before the complete cooling of the weld. The time for disappearance of AE data after completion

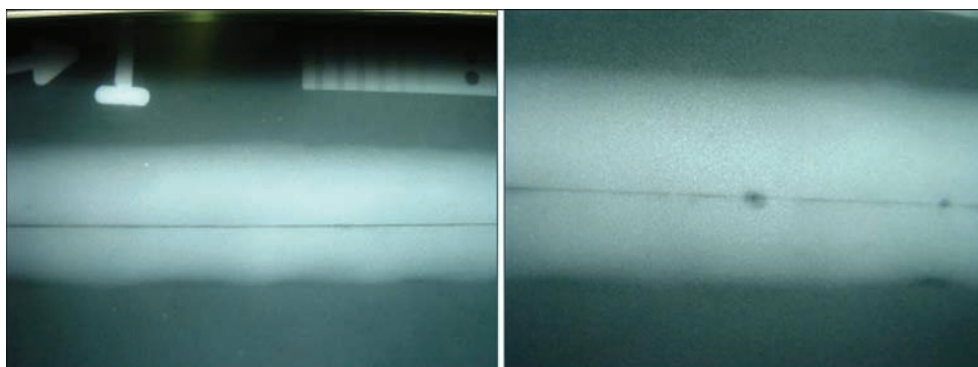
**Figure 4.** Photos of EMA system location screen. First (top) and last (below) stages of welding plates acc. to Table 1

of the welding process can be used as a criterion of its quality. For instance, in the above-described experiment where weld quality is rather high, a rapid reduction of the number of AE events was observed with cooling, and at lowering of weld temperature to 48 °C — their complete absence further on.

Behaviour of 13KhGMRB material can be characterized in a quite different way. During welding with ANP-2 electrode ( $d = 4.0$  mm) AE activity similar to that found in 09G2S steel was observed, but a crack approximately 100 mm long initiated in the material (Figure 6). This resulted in recording AE events in the crack vicinity on the second day after welding (Figure 7). Transducers 1 and 2 here were located close to the crack edges.

Despite the slight acoustic activity, its very presence after the complete cooling of the sample shows that the AE method is highly sensitive to defects, the development of which was not completely inhibited after completion of the welding process and subsequent complete cooling of the sample to room temperature.

Thus, one of the features of welded joint quality is AE absence after complete cooling of the weld, and the time for AE disappearance can serve as a quantitative characteristic of welding quality (material sound-

**Figure 5.** Radiography of individual weld areas after five welding passes

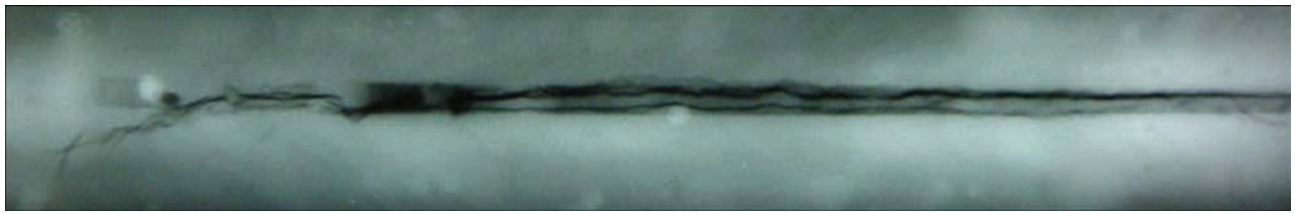


**Figure 6.** Radiography of a crack in as-welded 13KhGMRB material

ing can continue also after cooling, sounding time depends on the material).

As the scope of this series of experiments on AE testing of the welding process was quite limited, continuation of such studies should be recommended, as in case of obtaining results which could be used in production, it would allow a significant improvement of welded product control directly during its manufacture. Note also that such research has been more actively pursued abroad lately [4–6, 12–13].

Let us consider the possibility of AE testing of large-sized structures by a small number of AE transducers. As a rule, such structures contain a large number of welds. A feature of local structures is the fact that many of them have exhausted their planned service life, but for economic reasons they cannot be replaced completely, or even partially. The only method to continue their safe operation is periodic inspection or continuous monitoring. Here, there is no other nondestructive method, besides AE, which would allow performing 100 % control of such structures with a small number of samples. At the same time, testing results obtained by AE method can be effectively verified by other methods due to the fact that AE application allows localizing the dangerous areas with rather high accuracy, and checking of the obtained data by other methods should be performed in them. This essentially accelerates the process of evaluation of the state of the structure being controlled, and, at the same time, allows verifying the reliability of AE testing results.

One of such demonstration trials was testing by AE method a coil of P-101 furnace of total length of about 1200 m that consists of four flows, which have the respective radiation and convection sections each. The coil is a pipe of 219 mm diameter and 10 mm thickness and is an increased danger facility, as the pipe wall temperature can be up to 523 °C, working

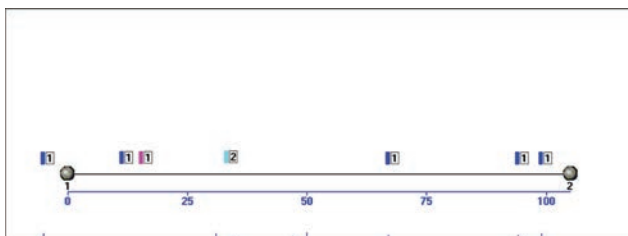


**Figure 7.** Photo of EMA system location screen (data on the next day after welding (13KhGMRB))

pressure is 60 atm, and the working medium is explosive vacuum distillate. The total number of welds is close to 500. Note that complete control of the entire surface of the coil by other nondestructive testing methods would have required hundreds of times longer period and complex preparatory operations. Now in this case, in order to perform the testing, it was necessary to scrape and degrease four areas of 13 mm diameter to mount transducers on them (Figure 8) and fasten them by a special acoustically transparent couplant. Previous check showed a slight attenuation of AE signals in the material (12Kh18N10T steel); so that it was possible to conduct complete testing of the coil in just 2 stages of 600 m each. This is indicative of an essential advantage of the AE method in terms of time and effort consumption, compared to other nondestructive methods, as well as of the possibility in principle of performing 100 % testing of the object state with a small number of transducers without the need to move them to other locations during testing.

Loading was applied by a procedure standard for AE testing — pressure increase up to 20 atm with subsequent soaking for 10 min, then again pressure increase and soaking, repeating it several times up to maximum test pressure of 60 atm. Testing procedure here took about 100 min.

As the results of the conducted coil testing have already been published [7], let us focus on the derived conclusions. They are important, as after AE testing the critical locations indicated by AE method, were checked by independent experts, using two nondestructive methods — dye penetrant flaw detection and radiography, which can be efficiently used to check

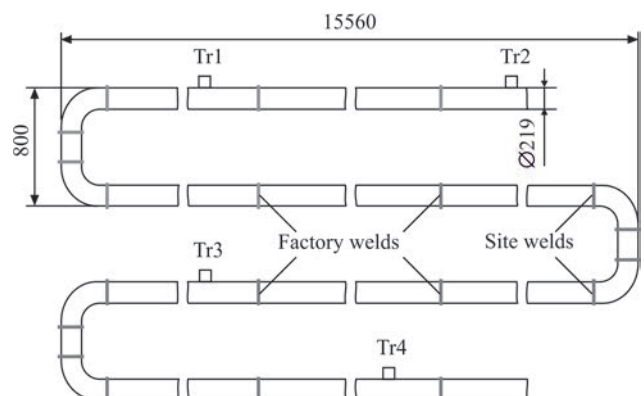


**Figure 8.** Scheme of location of welds and AE transducers (D1–D4) during coil testing

**Table 2.** Results of AE testing of the first flow confirmed by dye penetrant and radiographic flaw detection

Area	Crack		Pore		Undercut	
	Quantity	Max. length/depth, mm	Quantity	Max. dia, mm	Quantity	Max. length, mm
Radiation	2	4/2	2	2	1	300
	1	60/3	2	2	3	200
	3	8/3	3	3	2	200
	2	5/2	–	–	1	100
	2	6/3	–	–	–	–
	2	8/3	–	–	–	–
Convection	2	6/2	3	2	–	–
	4	8/2	–	–	–	–
Transition	–	–	2	3	1	60

the AE data [8]. It allowed confirming the high reliability of AE data, as well as determining the defects which were exactly the cause for AE event generation. For greater clarity, let us give in Table 2 just the data obtained for the first flow.

As we can see most of the defects found in welds are cracks, followed by pores, and the number of found undercuts is the smallest. This statistics typical for all the four flows, suggests that the AE method can be used with success to control the service properties of large-sized welded structures, which are also potentially dangerous for the environment. This is the most important conclusion, but the derived data further allow assessing how useful could be the continuous AE monitoring of this facility. Table 2 shows that the pipe continued to operate with a crack in the weld, which was 60 mm long and 3 mm deep, i.e. almost one third of the pipe thickness. A probable cause for the pipe not breaking can be the static indeterminateness in the location close to this weld. Structures with such a feature can go on operating for years in the presence of rather large cracks (for instance, bridge, truss and crane structures). Results of metallographic examination of typical weld defects are given in Figure 9.

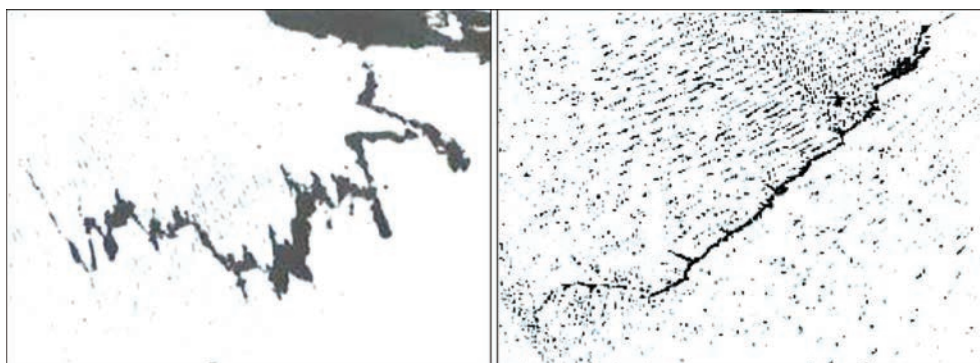
Then the following question arises: how can we determine that the crack poses a threat for the structure at this stage of operation? There are a large number of calculation methods, including those based on fracture mechanics. In the case of correct definition of the prob-

lem and its solution by a competent specialist rather reliable result can be obtained. However, calculations take time, which may be lacking during the real operation of the structure, as destruction may take place earlier. An alternative to calculations is continuous AE monitoring, using standardized and certified methods of danger assessment and prediction of breaking load. At continuous monitoring, any development of a defect dangerous for the structure, will be recorded in advance, which will be followed by the system giving a colour and sound hazard signal about in real time, and the screen will display the quantitative indices of breaking load prediction (Figure 14 [1]). This is a fast and safe method of accident prevention.

In this case the respective dangerous crack was detected by AE method as a propagating defect. The rapidity of crack development showed the need for repair of this dangerous section. Here, the overall dimensions of the dangerous defect and its location are not important for AE method. Only its acoustic activity matters. Now, application of additional control methods showed that the defect is indeed present, and allowed establishing its dimensions.

Repair of a certain number of welds was recommended, proceeding from the results of AE testing of P-101 furnace coil (Table 3).

The total number of rejected welds was 102. Considering that the total number of welds is equal to close to 500, let us approximately assess the integral

**Figure 9.** Typical cracks in P-101 furnace coil,  $\times 120$

**Table 3.** Recommended number of repaired areas of P-101 furnace coil by the results of AE testing

Area	1 <sup>st</sup> flow	2 <sup>nd</sup> flow	3 <sup>rd</sup> flow	4 <sup>th</sup> flow
Radiation	12	19	8	12
Convection	9	-	-	9
Transition	5	13	15	-
Total	26	32	23	21

damage of the object of control as a whole, using the ratio of the number of defective welds to their total number as the damage parameter [9, 10], in keeping with the following formula:

$$\Delta W_{av} = (1 - N_{dam}/N_{tot}) \cdot 100 \%, \quad (1)$$

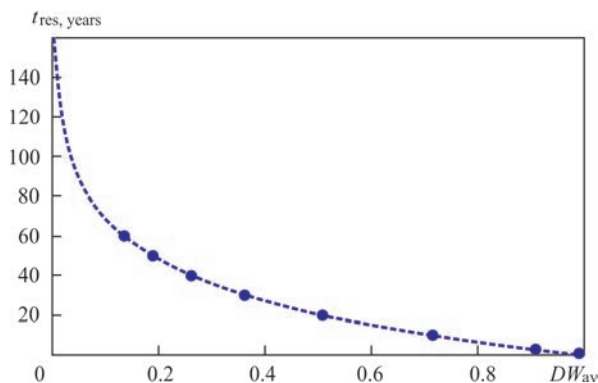
where  $\Delta W_{av}$  is the integral damage of the object of control;  $N_{tot}$  is the total number of welds;  $N_{dam}$  is the number of damaged welds, and we will obtain  $\Delta W_{av} \approx 20 \%$ .

It is interesting to check the dependence of damage on operating life, considering that at the moment of testing the coil has operated for 15 years. The authors have obtained a generalized formula for arithmetic mean value of damage  $\Delta W_{av}$  on a large number of pipes of the main gas pipelines, using five independent methods. It can be described [9] as:

$$\Delta W_{av} = ae^{bt} \cdot 100 \%, \quad (2)$$

where  $t$  is the operating life;  $a = 0.1352$ ;  $b = 0.0333$  [9].

Thus, for this object of control  $\Delta W_{av} = 0.1352 \exp(0.0333 \cdot 15) \cdot 100 \% \approx 22 \%$ . As we can see, the error at comparison of 20 % damage data calculated by testing results and their verification by formula (2) is negligible. The formula is used only for materials, which have been in service. It means that the generalized damage formula (1) is valid not only for pipes of the main pipelines, which operate under quite different loading and environmental conditions, but also for the tested furnace coil. Calculation of the residual life of the object at the moment of testing based on formula (2) will also be valid. This can be done using a nomogram (Figure 10), which correlates the residual life with damage [9–11]. The difference consists in that in the diagram the damage is expressed not in

**Figure 10.** Nomogram for determination of residual life by known damage level

percent, but in fractions of a unity, and  $\Delta W_{av} = 1$  corresponds to maximum damage.

It can be determined that at 20 % damage (or 0.2 in the nomogram) the integral residual life of the coil was  $\approx 47$  years at the moment of testing.

Thus, the results of AE testing of such facilities allow determination of dangerous sections, requiring repair, which include cracks, pores and undercuts of different dimensions and in different locations. Assessment of the obtained data allows evaluation of the integral damage of the objects of control and their residual life.

Note that despite the intensification of such research abroad [4–6, 12–16], their main disadvantage is absence of clearly normalized quantitative assessment of damage, prediction of destruction and probability. Here, it is dangerous to proceed from table data at evaluation of the state of both the base material and welded joint material, as even the adjacent sections of one and the same structure can have different physico-mechanical characteristics, different damage and different danger level, respectively. A rather promising local approach, which is also based on AE testing data, should be noted [17].

Large-scale testing of samples of pipeline materials from different regions of Ukraine with different operating time, conducted by PWI Department of Technical Diagnostics of Welded Structures, demonstrated an essential AE diversity, including differences in AE parameters:

- time of emergence of the first AE event (from 1 s to 2 min since the moment of testing start);
- loading, at which discrete AE appears (2–55 % relative to breaking load);
- level of continuous discrete AE (10–500 mV);
- oscillation of the level of continuous AE (2–1000 %);
- total number of AE events (7–12000);
- AE amplitude at the same deformation stages (1–500 mV);
- AE activity at the same deformation stages ( $1-100 \text{ s}^{-1}$ );
- change of the number of AE events in materials with accumulated damage (from 2–10 times reduction to similar increase).

The above allows stating that no common AE pattern is found for the studied materials. However, the results of the conducted testing can be conditionally divided into 2 main groups [9]. The first group, which occurs more seldom, is characterized by reduction of the number of AE events in the material after many years of operation. The second, most characteristic group, differs by a significant increase of the number of events. Materials of the second group are characterized by a lower total level of AE amplitudes. Additional metallographic studies confirmed the assump-

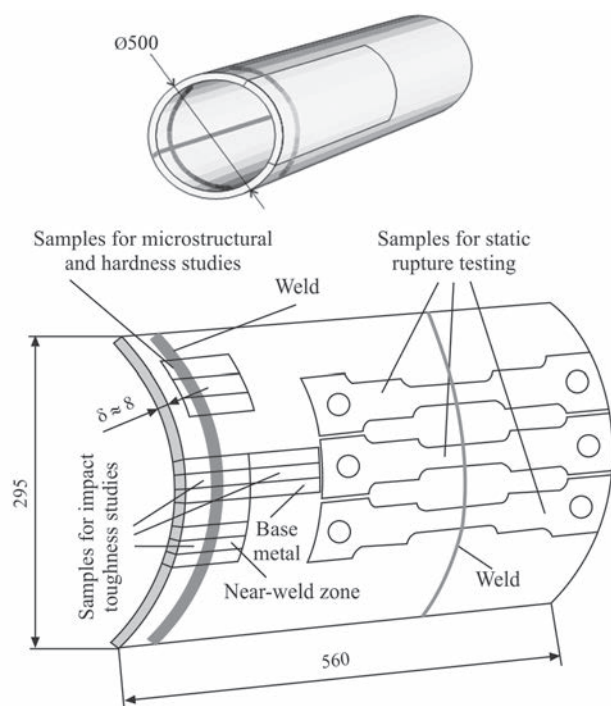


**Figure 11.** Scheme of cutting out samples from a test pipe fragment

tion that for the first group the main change, associated with the operating time, is embrittlement, which leads to lowering of the number of AE events. For the second group, contrarily, increase in the number of AE events is indicative of accumulation of a large amount of scattered damage, that is confirmed by additional experiments conducted by four different methods and is the base at construction of AE model in ductile materials, where destruction develops by the mechanism of initiation, propagation and coalescence of a large number of pores. Such diversity leads to incorporating different parameters into the criterion (1), depending on the obtained AE data, in order to calculate the damage and residual life. Now, if the number of AE events almost does not change after a long operating period, it can be assumed that a mixed mode of damage accumulation is realized, namely embrittlement with simultaneous development of pores. At the same time, it should be noted that the algorithms of breaking load

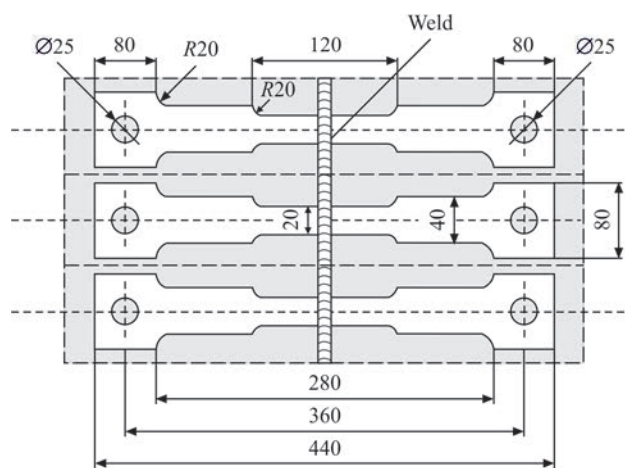


**Figure 12.** Scheme of cutting out AE-01R samples for AE studies at static tension

prediction, incorporated in SW of EMA type systems, perform with the same reliability, irrespective of the above-mentioned diversity of fracture modes.

We will demonstrate the effectiveness of evaluation of the state of material using the destruction prediction in the case of a pipe from the main pipeline, where an accident occurred earlier, and will compare the results with the data obtained by other methods. The material for investigations was taken from an area near the destruction location (pipe fragment with the weld closest to the destruction area). In keeping with the certificate, the pipe is made from steel 20 with 500 mm diameter and 8 mm wall thickness. Figures 11–13 show the schemes of manufacturing samples of different type for an integrated study of the properties of the obtained pipe fragment. Note that in Figure 11 the weld and samples in the right-hand part are shown conditionally for greater clarity. In reality, samples of AE-01R type were cut out of the same part of the pipe, as the others, from an area located to the left, so that the weld was in the middle of the sample (Figure 12). Samples of MI-50 type were used for determination of impact toughness of the material. Samples in the form of a rectangular parallelepiped were also prepared, which were used to study the material microhardness and to conduct AE scanning by

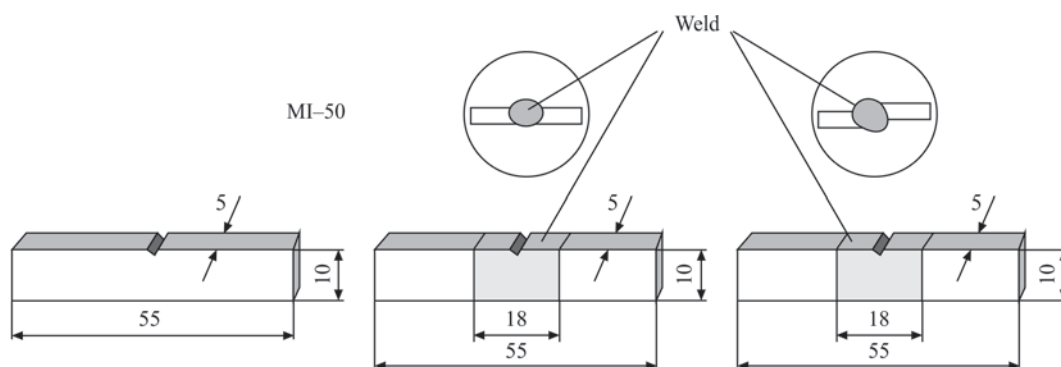


**Figure 13.** Scheme of preparation of MI-50 samples for impact toughness testing

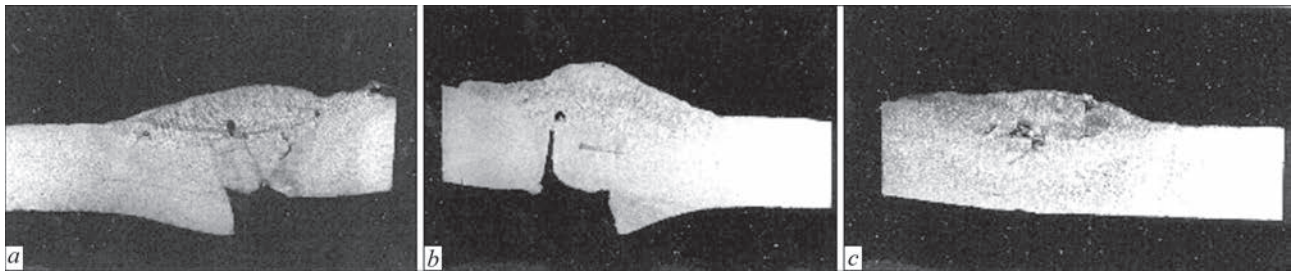


**Figure 14.** Weld macrostructure ( $\times 2.5$ ). Samples I (a), II (b), III (c)

**Table 4.** Chemical composition of base metal and weld metal of the studied samples, wt.%

Analyzed object	C	Si	Mn	Cr	Ni	Mo	V	S	P	[O]	[N]
Base metal	00.137	00.138	00.40	00.05	<0.05	<0.03	<0.02	00.013	00.009	00.02	00.073
Weld	0.129	0.430	0.90	0.06	0.05	<0.03	0.03	0.020	0.017	0.043	0.011

one AE transducer emitting an acoustic signal from one end face of the parallelepiped and subsequent receiving of the modified signal by another transducer at the other end face [2, 9–11].

Macrostructural analysis was conducted after etching the samples in 20 % aqueous solution of ammonium sulphate. The microstructure was examined after etching in nital (4 % solution of nitric acid in ethyl alcohol). Investigations and filming of the microstructure were conducted in Polivar-met microscope. Hardness was measured by M-400 hardness meter of KOMPAS Company with the load of 25 gf (micro-hardness) and 1 kgf (integral hardness).

Chemical composition of base metal and weld metal is given in Table 4.

Chemical composition studies showed that the pipe material does not correspond to the specification and it is not steel 20. Proceeding from the results of chemical analysis of the studied samples and norms of chemical composition of steels, specified by GOST 1050-88, we can come to the conclusion that the pipe is made from steel 15 ps (semi-killed). Manufacturing pipes from such steels is allowed only under the condition that the gas pressure in them will not exceed 4 at. Visual examination of the welded template submitted for investigations, showed that the weld surface structure is coarse-layered with traces of repair welds

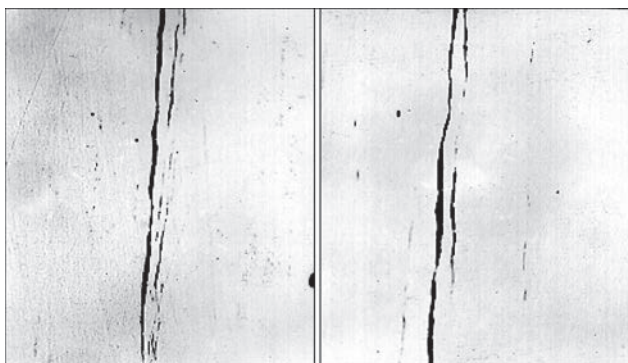


**Figure 15.** Nonmetallic inclusions in base metal (ductile silicates)

over the entire weld length. Dents from the root side, lacks-of-penetration, and individual metal leakage are found in the weld root part practically along its entire length. Welds are porous, with individual slag inclusions and slag interlayers between the welds (Figure 14, a). The depth of the root lacks-of-penetration in individual cases reaches 50–60 % of thickness of the metal being welded (Figure 14, b, c). Welding was conducted with great edge misalignment (Figure 14, c) and a gap between them. Overlaps are present on the surface of the product being welded.

Contamination by nonmetallic inclusions was controlled in keeping with GOST 1778–70. Quantitative microscope of Omnimet model was used for their determination. It is found that the base metal is contaminated, mainly, by inclusions of the type of ductile silicates located mostly in the sample center (by the sheet thickness). Respective photos are given in Figure 15. The level of contamination by the above inclusions corresponds to 4.5 points to GOST 1778–70 (Sh1 method, SP scale). Calculation of the contamination showed that in the most contaminated locations the ductile silicate content was equal to 2.366 vol.%. Other inclusions (sulphides, oxysulphides) are contained in the base metal in very small amounts (less than point 1 to GOST 1778–70).

Oxides of globular-shaped inclusions of the size from several micrometers to submicrons were detected in weld metal (Figure 16). Quantitative analysis showed that the content of nonmetallic inclusions in the upper beads of samples I, II and III is equal to 0.156, 0.122 and 0.105 vol.%, respectively.

Defects and microstructure of various areas of the welded joint were studied in detail on microsections. Analysis showed that the base metal microstructure is the same on all the three samples. It consists of ferrite and pearlite with striation, corresponding to point 2 (GOST 5640–68) and ferrite grain size corresponding

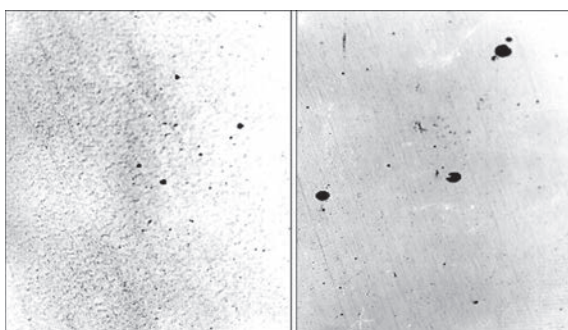


**Figure 16.** Nonmetallic inclusions (oxides) in weld metal

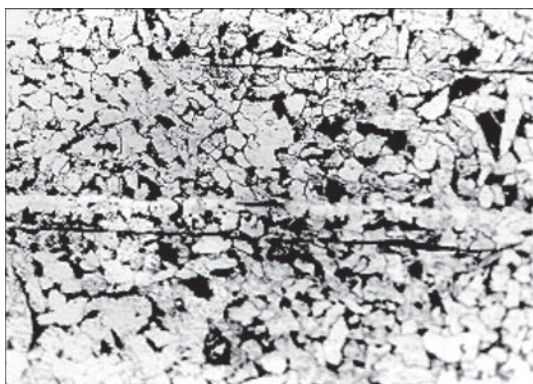


**Figure 17.** Base metal microstructure ( $\times 400$ )

to No.8 (GOST 5639–82). Figure 17 shows the photographs of base metal microstructure.

A characteristic feature of base metal structure is presence of a white band of heterogeneity in the sample center (in the direction of sheet thickness). It is known that segregation bands of this type are often saturated by carbon in quantities sufficient for martensite precipitation.

In the studied steel, however, the mentioned band consists of ferrite. This is confirmed, in particular, by measurements of microhardness, which, similar to respective microhardness of ferrite grains, is equal to Vickers  $HV$ –1180–1300 MPa. Integral hardness of base metal is here equal to  $HV$ –1450–1500 MPa. In sample 1 defects were studied at magnification greater than at macroexamination. Discontinuities were detected which can be characterized as pores (Figure 18). The microstructure of upper weld is a mixture of po-

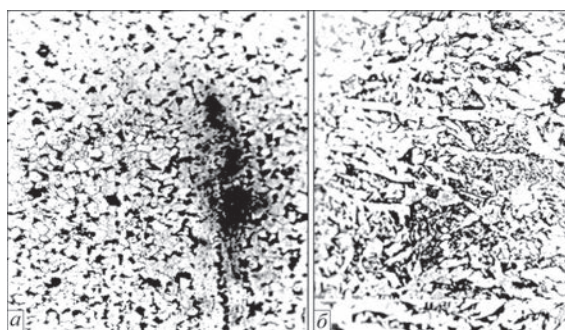


**Figure 19.** Microstructure ( $\times 400$ ) of upper weld (*a*) and fusion zone of base metal with another weld (*b*)

lygonal ferrite, pearlite and lamellar ferrite with disordered second phase (Figure 19, *a*).  $HV$  microhardness of these components is equal to 1100–1300, 2200 and 1700–1800 MPa, respectively. Integral hardness of the upper weld is equal to 1500–1600 MPa. At  $\times 40$  magnification a slag-filled root channel, macropores and micropores are visible (Figure 18).

The microstructure of the lower weld, subjected to heating at superposition of the upper weld, consists of mixed ferrite and pearlite (Figure 19, *b*). The same photo shows the zone of fusion with the base metal. One can clearly see that ductile silicates in the fusion zone have changed under the impact of the weld pool heat. No grain growth was detected in the overheated zone.

Analysis of the microstructure of sample III also showed presence of multiple defects in the welded joint metal. So, lacks-of-penetration in the form of a comma are observed near the pores, as well as extended lacks-of-penetration located mainly between the beads. Figure 20 gives the photos of the metal of a sample with lacks-of-penetration which pose a serious danger for the operated pipeline, as they significantly lower the strength of welded joints in the pipes. The microstructure and hardness of various areas of the welded joint in this sample does not differ from the microstructure and hardness of the previous samples in the respective areas.

It should be noted that no increase of the grain size in the overheated zones was observed in the HAZ of all the studied samples. In other areas of the HAZ,

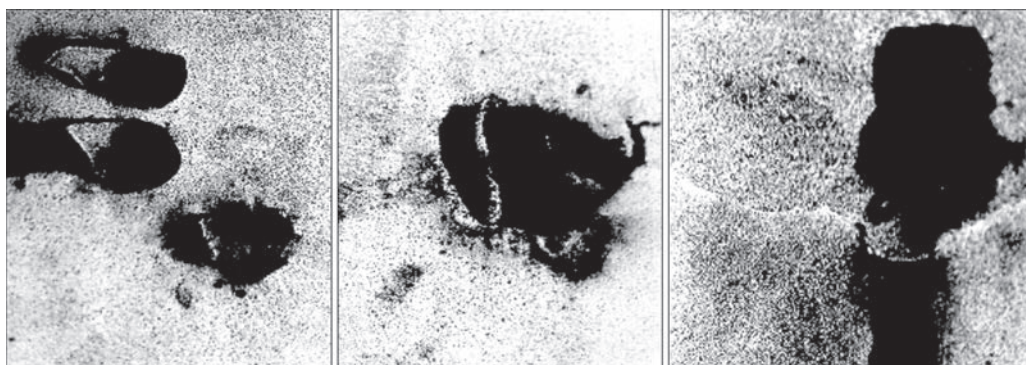


**Figure 18.** Pores in the weld of the sample ( $\times 40$ )

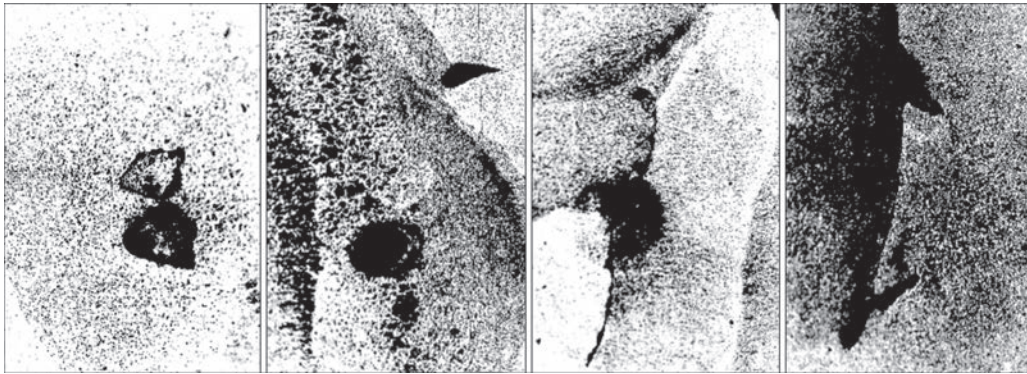


**Figure 20.** Defects in sample III ( $\times 40$ )

the metal structure consists of fine-grained ferrite and pearlite. Hardness of all the HAZ areas is not higher than 2000 MPa.

The general conclusion from chemical and metallographic analyses of the welds showed that multiple welding defects, as well as application of another steel grade instead of the design one led to destruction of the pipeline neighbouring section, but they could also cause destruction of the pipe fragment which was studied.

Material damage also demonstrates an essential lowering of impact toughness. For material in as-delivered condition it is equal to 218 J/cm<sup>2</sup>. For MI-50 samples the data (Table 5) give a clear idea of both the state of the pipe base metal and of the welds.

As one can see, in the worst case the impact toughness decreased 2.5 times, while damage will be equal to 60 %, in keeping with formula (1).

AE scanning [2, 8–10] of three samples in the form of a parallelepiped showed that the maximum damage of the metal is observed in the direction normal to the pipe surface, and it is equal to 68 %. We will determine the strength of the material of the pipe, assuming that it is made from steel 20, to obtain the reference characteristics for comparison with the real material, from which the pipe is made. The initial parameters of the material are as follows: ultimate strength  $\sigma_t = 440$  MPa, yield limit  $\sigma_y = 288$  MPa, relative elongation  $\psi = 28\text{--}34$  %, reduction in area  $\psi = 28\text{--}34$  %, base metal impact toughness [ $\alpha_n$ ] = 218 J/cm<sup>2</sup>. Further on in the calcula-

tion we will denote the pipe wall thickness by value  $\sigma$ , regarding it as a thin shell ( $r/\delta \gg 10$ ).

Pipe calculation can be performed, taking into account ratio  $r/\delta = 41.34 \gg 10$  by the Laplace formula for a thin shell. According to the above formula, the stresses acting in the pipe, will be defined as  $\sigma = pr/(2\delta_{ef})$ , where  $\sigma_{ef}$  is the real thickness of the shell wall. At selection of value  $\sigma_{ef}$  it should be taken into account that only the thickness of lacks-of-penetration and other imperfections, changing the real wall thickness, should be subtracted from it, not forgetting also the fact that they are the stress raisers. The stress concentration factor  $K$  for concentrators of such a shape is equal to 4.5.

Thus, with the specified pipe dimensions  $\sigma = 113.7$  MPa, that is lower than  $\sigma_y = 288$  MPa. That is, when the material is in a nonembrittled state, the impact of stress concentration will lead to its redistribution in the raiser zone.

At material embrittlement, plastic deformations will be absent and  $\sigma_{ef} = 113.7 \cdot 4.5 = 511.6$  MPa  $> \sigma_t$ . Thus, in the concentration zone the stresses will be higher than the ultimate strength and material destruction will take place. A recommended measure for preventing destruction is lowering the working pressure to 20–25 atm. As the material corresponds to steel 15 ps by its chemical composition and other characteristics, even lower performance is anticipated for it.

To complete analysis of service properties for this pipe, including the welds, we should analyze the results of AE studies of AE-01R sample for static tension. We will give typical screen images of EMA-3.92 program with the results of breaking load prediction and the respective graphs of testing samples from steel 20 first for material without any hours worked, taken from emergency stock (Figures 21–22), and then for the pipe material to be analyzed (Figures 23–24). All the elements of the location screen correspond to those described above for Figure 4 and in work [1]. Given above the location scheme are the results of breaking load prediction and their automatic conversion by EMA program to ultimate strength, according to the known

**Table 5.** Impact toughness of pipe metal ( $t_{test} = 20$  °C)

No	Pipe area	Impact toughness, J/cm <sup>2</sup>
1	Base metal	187
2		170
3		165
4	Weld	155
5		130
6		88
7	Weld with edge misalignment	182
8		155
9		140

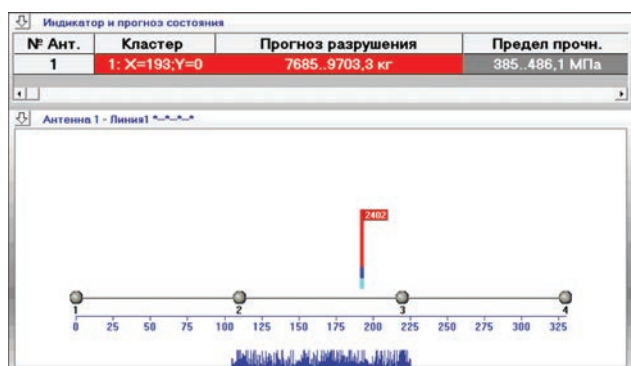


**Figure 21.** Screen of EMA-3.92 program after testing a typical sample of steel 20 from emergency stock

geometrical characteristics of the sample. In the graphs (Figures 22, 24) the bars show the amplitudes of discrete AE events (mV), loading  $P$  (kg) and total curve  $N$  of AE event accumulation, depending on testing time.

As we can see from Figure 21, the predicted ultimate strength fully corresponds to the specifications of steel 20. It should be also noted that the predicted breaking load, which in reality was equal to 9068 kg (Figure 22), corresponds to the requirements to its accuracy, according to the certificate for EMA type systems and falls within  $\pm 15\%$ .

The graph (Figure 22) is characterized by the presence of a large number of events with maximum amplitudes. The curve of damage accumulation (total curve  $N$  of AE amplitudes) has a bend directed upwards, and it to a great extent follows the loading curve. As was reported in [1], this is an indication of absence of a welded joint in the sample.

For the tested sample from the damaged pipe, which, in addition had a weld, the predicted ultimate strength is significantly lower than the specifications of steel 20. It confirms, first, that another material was tested (as was already mentioned, this is steel 5ps), and secondly, that the material was damaged by the mechanism of pore initiation, development and coalescence with further cracking. Note that in this test also the predicted

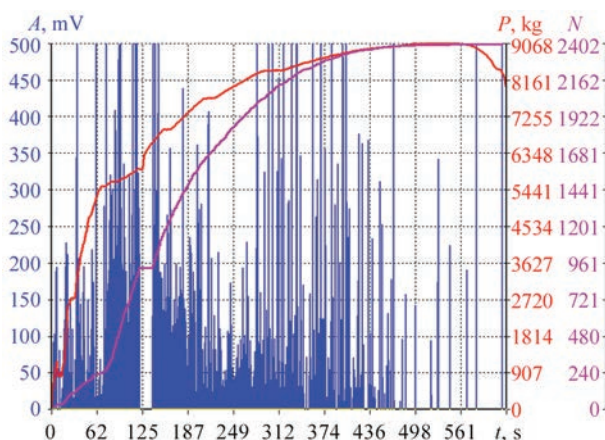


**Figure 22.** Graph of testing a typical sample of steel 20 from emergency stock

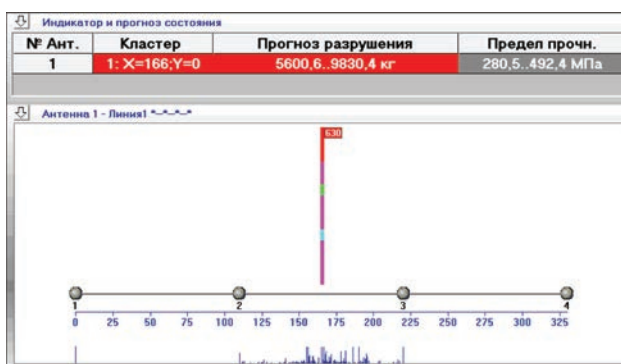


**Figure 23.** Screen of EMA-3.92 program after testing a typical sample of steel 20 with pipe damage

breaking load, which in reality was equal to 6576 kg (Figure 24), corresponds to the requirements to its accuracy and falls within the limits of  $\pm 15\%$ .

Compared to the results of testing a sample from the emergency stock, the graph (Figure 24), is characterized by a small number of events, and they mostly have low amplitudes. The curve of damage accumulation (total curve  $N$  of AE amplitudes) has a bend, directed downwards, and does not follow the load curve that is indicative of the presence of a welded joint in the sample.

In keeping with formula (1) we will calculate the damage of a sample with the welded joint, compared to a reference sample from emergency stock. We will use the sum of events,  $N$ , as the damage parameter. After calculations, we will obtain the damage value of 73%. The validity of such a damage level is indicated also by all the previous results, confirmed by metallurgical examinations.

As this damage value is the largest of those obtained for this pipe, we will use it for residual life assessment. In keeping with the nomogram (Figure 10), it is equal to  $\approx 10$  years for damage level of 0.73. Considering the large number of detected defects, the difference of the steel grade from the specification and probable destruction at overloading, it was recommended replacing the damaged pipe section with such values.

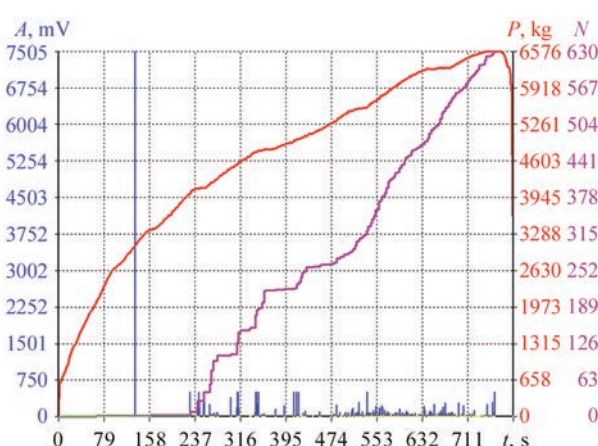


**Figure 24.** Graph of testing a welded sample from damaged pipe

Thus, integrated study of the material from an accident-prone pipe allows stating that AE method is sensitive to a change of service properties of welds, and at timely application it can help prevent emergency situations.

## Conclusions

1. The high sensitivity of AE method to initiation and propagation of defects of different types in welds, both during welding and during their further operation is demonstrated.

2. A characteristic, which could be used for quality control during welding, could be the time, during which acoustic activity disappears after welding is completed.

3. In the case of a coil of P-101 furnace it is shown that AE method is efficient during testing of large-sized potentially dangerous structures with a large number of welds. Here testing of large surfaces can be performed with a minimum number of transducers (four in this case). Additional testing methods are used to show exactly which defects are characteristic for different sections of the coil of P-101 furnace.

4. A method of integral assessment of damage of this type of facilities is proposed. Reverse check showed that the procedure of residual life calculation proposed by the authors is right for such facilities.

5. In the case of an emergency pipe section of the main gas pipeline, it is shown how an integrated assessment of damage level in base metal and welded joints can be performed with application of different methods. AE method was used to confirm the conclusion reached in Part 1 as to the possibility to determine the presence of a welded joint in the material by the angle of inclination of the total curve of AE events.

6. It is confirmed that breaking load prediction, performed by EMA type systems can be used for welded joints. It is shown that alongside the breaking load proper, its correct automatic conversion to ultimate strength is possible. Obtained results of conversion coincide with mechanical properties of the studied materials, determined by other methods.

7. Industrial application of AE technique is an efficient method to evaluate the service properties of welded joints that is highly important as they are one of the main causes for damage of structures in operation. Continuous AE monitoring provides the most reliable guarantee of prevention of emergency situations, as AE method immediately reacts to the smallest changes in the material state.

1. Nedoseka, S.A., Nedoseka, A.Ya., Yaremenko, M.A. et al. (2021) Acoustic emission method at evaluation of the state of welds and their service properties. Pt 1. Effect of welded joint

type on acoustic emission. *The Paton Welding J.*, **2**, 46–52. <https://doi.org/10.37434/as2021.02.09>.

2. Nedoseka, A. Ya., Nedoseka, S.A. (2020) *Fundamentals of design and diagnostics of welded structures: Manual*. 5<sup>th</sup> Ed. Ed. by B.E. Paton. Kiev, Indprom [in Russian].
3. Nedoseka, A. Ya., Nedoseka, S.A., Yaremenko, M.A. et al. (2013) Software of AE diagnostic systems EMA-3.9. *Tekh. Diagnost. i Nerazrush. Kontrol*, **3**, 16–22 [in Russian].
4. Huang, W., Yang, S., Lin, D., Kovacevic, R. (2009) Real-time monitoring of the weld penetration state in laser welding of high-strength steels by airborne acoustic signal. ASME. Turbo expo: Power for land, sea, and air: cycle innovations; industrial and cogeneration; manufacturing materials and metallurgy. *Marine*, **4**, 799–805.
5. ASTM E749/E749M-17 (2017) *Standard practice for acoustic emission monitoring during continuous welding*. ASTM International, West Conshohocken.
6. Zhang, L., Basantes-Defaz, A.C., Ozevin, D. et al. (2019) Real-time monitoring of welding process using air-coupled ultrasonics and acoustic emission. *Int. J. Adv. Manuf. Technol.*, **101**, 1623–1634. <https://doi.org/10.1007/s00170-018-3042-2>.
7. Nedoseka, A. Ya., Nedoseka, S.A., Yaremenko, M.A. et al. (2003) About application of acoustic emission method for control of industrial structures. *Tekh. Diagnost. i Nerazrush. Kontrol*, **3**, 3–6 [in Russian].
8. Shcherbinsky, V.G., Feoktistov, V.A., Polevik, V.A. et al. (1987) *Methods of flaw detection of welded joints*. Moscow, Mashinostroenie [in Russian].
9. Nedoseka, S.A. (2010) *Diagnostics and prediction of service life of welded structures by acoustic emission method: Syn. of Thesis for Dr. of Tech. Sci. Degree*. Kyiv [in Ukrainian].
10. Nedoseka, S.A., Nedoseka, A. Ya., Boichuk, O.I. et al. (2020) Features of acoustic emission at evaluation of the state of materials. *Tekh. Diagnost. i Nerazrush. Kontrol*, **2**, 3–12 [in Ukrainian]. <https://doi.org/10.37434/dnk2020.02.01>.
11. Nedoseka, S.A., Nedoseka, A. Ya. (2010) Integrated assessment of damage level and residual life of metals with certain operating life. *Ibid.*, **1**, 9–16 [in Russian].
12. Karlov, S.A., Sulzhenko, V.A., Yakovlev, A.V. (2019) Acoustic emission control of weld quality in marine engineering: *Transact. of Krylov State scientific center: Special Issue* [in Russian].
13. Ivanov, A.B., Ievlev, V.A., Neustupov, A.S. et al. (2019) Implementation of a new method for quality control of field welded joints of pipelines: *Transact. of Krylov State scientific center: Special Issue 2* [in Russian].
14. Droubi, Mohamad & Faisal, Nadimul & Orr, Fraser & Steel, John & El-Shaib, Mohamed (2017) Acoustic emission method for defect detection and identification in carbon steel welded joints. *J. of Constructional Steel Research*, **134**. 10.1016/j.jcsr.2017.03.012.
15. Aboali, Abdalla et al. (2014) Screening for welding defects using acoustic emission technique. *Advanced Materials Research*, **1025–1026**, Trans. Tech. Publ., Ltd., Sept. 2014, 7–12. Crossref. doi:10.4028/www.scientific.net/amr.1025-1026.7.
16. Savchenko, S.V., Timchik, G.S. (2017) Method of control of welded joints on ballistic steels using acoustic emission. *Visnyk NTU KhPI. Series: Mechanical-technological systems and complexes*, Vol. 20 [in Ukrainian].
17. Skalsky, V.R. (2003) Evaluation of accumulation of bulk damage in solid, based on acoustic emission signals. *Tekh. Diagnost. i Nerazrush. Kontrol*, **4**, 29–36 [in Ukrainian].

Received 22.03.2021

## PORTABLE MODULE FOR HEAT TREATMENT OF WELDED JOINTS OF RAILWAY RAILS

**E.O. Panteleimonov**

E.O. Paton Electric Welding Institute of the NAS of Ukraine  
11 Kazymyr Malevych Str., 03150, Kyiv, Ukraine. E-mail: [office@paton.kiev.ua](mailto:office@paton.kiev.ua)

The design features of the portable module for heat treatment of welded joints of railway rails produced by the method of flash butt welding are considered. The process of heat treatment includes an induction heating of welded joints with the currents of 2.4 kHz frequency and a subsequent hardening of the rolling surface of the head by a compressed air. The design of the portable module includes inductors connected directly to matching transformers. The inducing wires repeat the shape of the rail surface bend with increased air gaps above the web and flanges and contain magnetic conductors located above the rolling surface, side surfaces of the head, web and flange of a rail. It was shown that in the welded joints of R65 type rails made of K76F steel after heat treatment in a portable module in the zone of hardening cooling of the head, a uniform fine-grained structure with hardness is formed, reaching the level of hardness of the base metal. The hardness of the metal in the deep layers of the rail head increases also relative to the hardness of the base metal at the appropriate depth. 10 Ref., 2 Tables, 5 Figures.

*Keywords:* rails, welded joints, heat treatment, portable module, metal hardness

The problem areas of welded joints of railway rails made by the method of flash butt welding are local zones with the change in the structure and hardness of the metal in the area of the heat-affected-zone (HAZ). To achieve structural homogeneity of the metal and increase the mechanical properties of welded joints, heat treatment (HT) is used. The technology of HT of welded joints with high frequency currents provides a uniform heating of rail elements in the butt zone, required rate of phase transformations in the HAZ metal structure, low temperature difference between the surface and deep layers of a rail [1, 2]. As a result of using new types of high-strength rails on the world's railways, it became necessary to improve the technology and equipment for HT of welded joints. In the studies conducted in China, the effect of HT on the structure and hardness of welded joints metal was studied. It was found that mechanical properties of welded joints are improved after heating to the normalization temperature [3]. During the construction of railways in China, in the equipment for HT of welded joints detachable single-turn inductors without magnetic conductors with parallel inducing wires were used [4]. In the Russian Federation the complexes for HT of welded joints with the currents of 8–15 kHz frequency were created, in which multi-turn inductors without magnetic conductors are applied [5].

At the PWI the works are carried out to improve the technology and equipment for HT of welded joints of railway rails. A portable module for HT of joints

of rails of type R50, R65 and R75 with the currents of 2.4 kHz was created. The process of HT includes heating of welded joints of the rails to a temperature of 850–950 °C and a subsequent hardening of the rolling surface of the head by a compressed air. The portable module is designed for application in track conditions as a part of mobile rail welding machines and in workshop conditions of rail welding enterprises.

In this paper, the design features of the portable module are considered and the results of its testing at HT of welded joints of R65 type rails made of K76F steel are presented. As a power source for high-frequency currents, thyristor frequency converter TPChT-160/2.4 was used.

In the design of the portable module, the inductors 1 are directly connected to the matching transformers, forming the heating units 2 (Figure 1). The heating units are located on the frame 3. To move the heating units to the side surfaces of the rail 4, the actuators are used. The frame is also equipped with the sprayer 5 with the unit 7 for compressed air supply, the control panel 6, the units 8 and 9 are used for supply and drain of cooling liquid, the clamps 10 are used for mounting the portable module on a rail, the laser pointer is used to guide inductors to a welded butt, limit switches, connectors for connecting a high frequency power source. The pyrometer for measuring the temperature of heating joints is mounted on one of the heating units. The electrical circuit of the portable module provides a sequence of operations for heating welded joints and hardening of the rolling surface of rails. The weight of the portable module is 65 kg [6, 7].

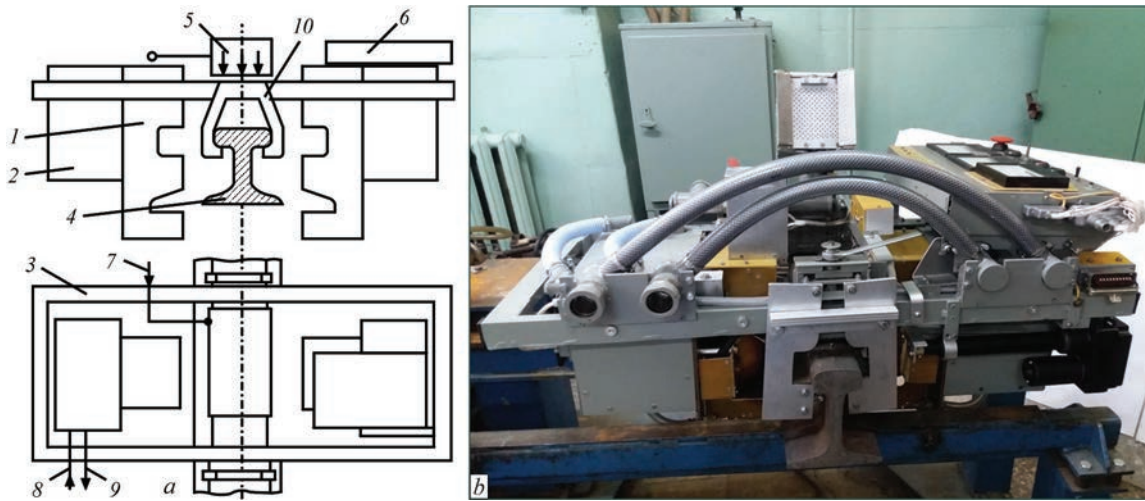


**Figure 1.** Portable module for heat treatment of welded joints of railway rails: design scheme (a) and general view (b) (description 1–10 see in the text)

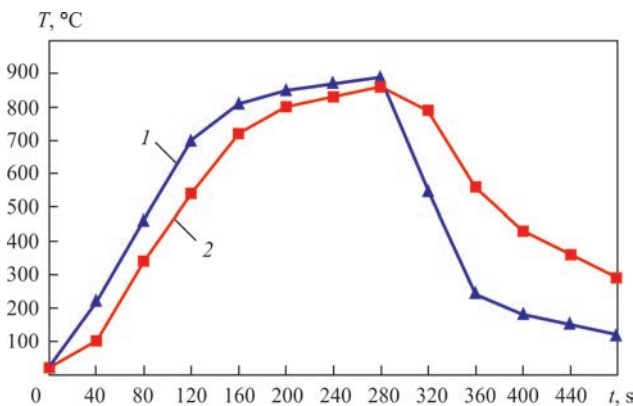


**Figure 2.** Time dependences of temperature of heating rolling surface (RS) of rail and layer at a depth of 25 mm from the rolling surface (25 mm from RS) while performing HT in the portable module: 1 — RS; 2 — 25 mm from RS

The required power distribution on rail elements is achieved by the fact that the inducing wires of the inductors repeat the shape of the rail bend surface with increased air gaps above the web and flanges and contain magnetic conductors above the rolling surface, side surfaces of the head, web and flange of the rail. After heating the welded joints for 140 s, the temperature difference between the rolling surface of the rail and the layer at a depth of 25 mm did not exceed 60 °C [8, 9]. To reduce the temperature drop to 40 °C, the heating time of the joints on the portable module was increased to 260–280 s. The heating rate of the rolling surface of the rail R65 to the temperature of magnetic transformations was 5.4 °C/s and at a depth of 25 mm from the rolling surface it was 4.6 °C/s (Figure 2). After the loss of the magnetic properties by the

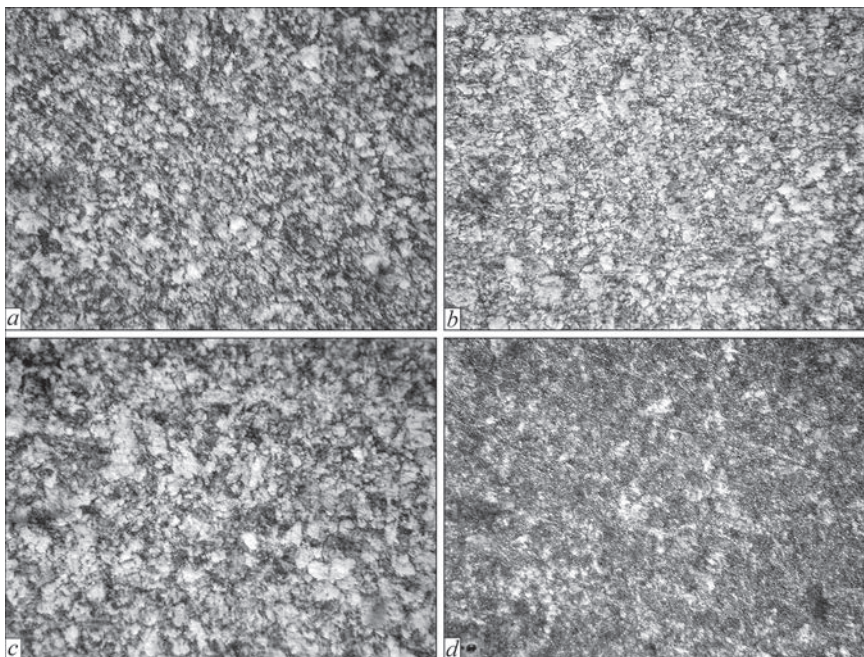


**Figure 3.** Microstructure (×500) of metal of welded joints of R65 type rails made of K76F steel at a depth of 5 mm from the rolling surface: a — base metal; b — joint line; c — 10 mm from the joint line; d — zone of partial recrystallization

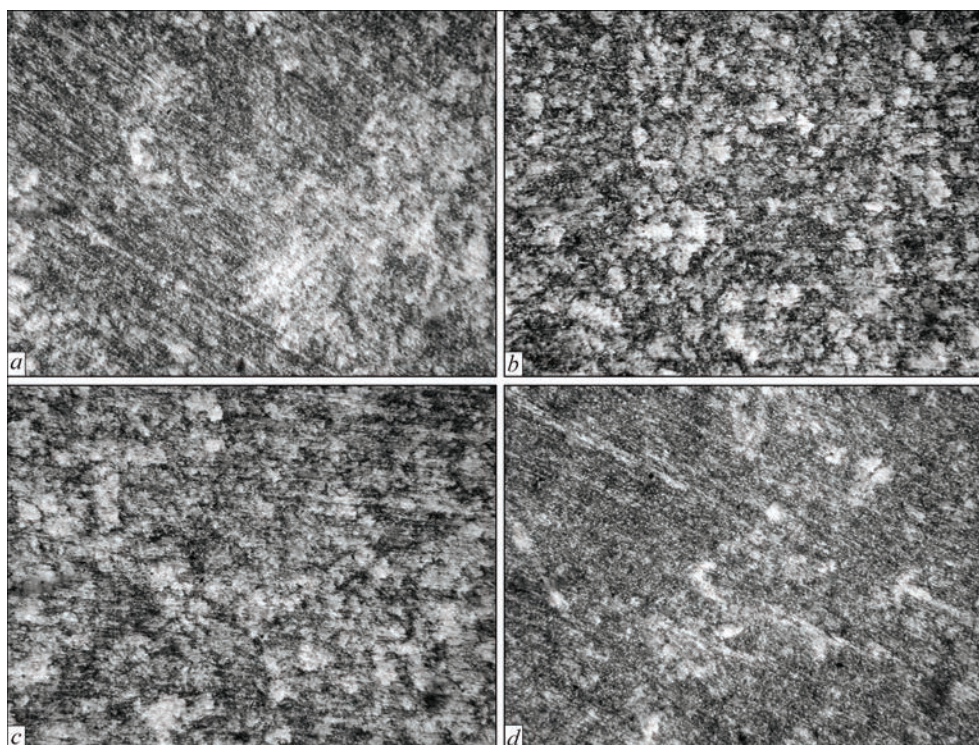


**Figure 4.** Microstructure ( $\times 500$ ) of metal of welded joints of R65 type rails made of K76F steel at a depth of 25 mm from the rolling surface: *a* — base metal; *b* — joint line; *c* — 10 mm from the joint line; *d* — zone of partial recrystallization

metal, the heating rate of the rolling surface decreased to 1.06–1.08 °C/s. The width of HAZ of welded joints after HT reached 52–58 mm, which is greater than the width of HAZ of joints of high-strength and high-alloy rails after welding [10].

In the study of welded joint metal, longitudinal specimens were used. The surface of the specimens coincided with the axis of symmetry of the rail. To reveal the microstructure of the metal, the method of chemical etching of polished specimen surfaces in a 4 % alcohol nitric acid solution was used. The grain size of the metal was determined according to GOST 5639-82.1. The integral hardness of metal *HRC* was measured in a hardness tester TK-2M at a load of 150 kg.

The studies showed that in the zone of hardening of the base metal, at a depth of 5 mm from the rolling surface, the areas of sorbite and troostite were present (Figure 3). The structure is fine-grained, grain size number is 8 (Table 1). After HT of welded joints, the metal at a depth of 5 mm from the rolling surface along the joint line had a uniform grain of the sorbite type with a grain size number 10. At a distance of 10 mm from the joint line a medium and heterogeneous structure of the sorbite type with areas of troostite are present. Grain size number is 7–8. In the zone of partial recrystallization at a distance of 22–24 mm from the joint line, the grain is fine dispersed, uniform, of the sorbite type with the areas of troostite. Grain size number is 10. At a depth of 25 mm from the rolling surface in the structure of the base metal

the areas of ferrite and sorbite were present (Figure 4). The base metal had a clear heterogeneity. Grain size number is 7 (Table 2). The structure of the metal in the HAZ width has the type of sorbite and a uniform grain. As compared to the hardening zone metal, the grain number decreased to 7–8.

At a depth of 5 mm from the rolling surface of rails, the hardness of the base metal was *HRC* 37–38 (Figure 5). After HT of welded joints, the metal at a depth of 5 mm from the rolling surface along the joint line had a hardness of *HRC* 33, which is lower than the hardness of the base metal. At a distance of 10 mm from the joint line, the hardness of the metal approached the level of the base metal; in the zone of a partial recrystallization at a distance of 22–24 mm from the joint line it decreased to *HRC* 29–30. At a depth of 25 mm from the rolling surface of the rail,

**Table 1.** Grain size number of metal of welded joints of R65 rails from K76F steel at a depth of 5 mm from the rolling surface

Joint line	10 mm from the joint line	Partial recrystallization zone	Base metal
10	7–8	10	8

**Table 2.** Grain size number of metal of welded joints of R65 rails from K76F steel at a depth of 25 mm from the rolling surface

Joint line	10 mm from the joint line	Partial recrystallization zone	Base metal
7–8	7	7–8	7

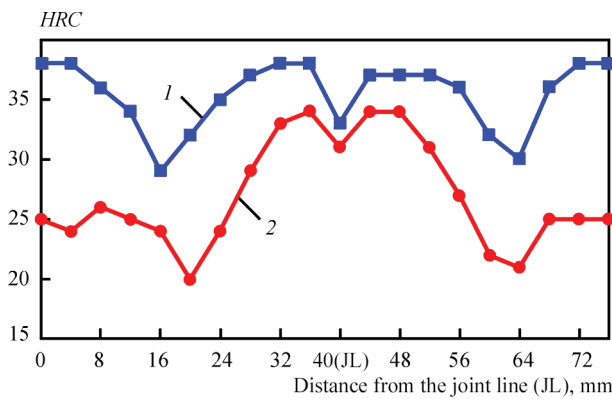


**Figure 5.** Distribution of metal hardness along the HAZ width at a depth of 5 mm and 25 mm from the rolling surface (RS) of welded joints of R65 rails made of steel K76F: 1 — 5 mm from RS after HT; 2 — 25 mm from RS after HT

the hardness of the base metal of the rail was *HRC* 24–25. The hardness of the metal between the zones of a partial recrystallization increased to *HRC* 31–34, which is higher than the hardness of the base metal at such a depth (*HRC* 24–25). In the zones of a partial recrystallization the hardness decreased to *HRC* 20–22.

### Conclusions

1. The portable module for HT of welded joints of railway rails produced by the method of flash butt welding was created. The technology of HT of welded joints includes induction heating with the currents of 2.4 kHz and a subsequent hardening of the rolling surface of the head by a compressed air.

2. The portable module is designed for application in track and workshop conditions.

3. The heating equipment of the portable module provides a uniform heating of rail elements in the zone of welded joints.

4. Investigations of welded joints of R65 type rails made of K76F steel after HT in a portable module

showed that a uniform fine-grained structure with a hardness reaching the level of hardness of the base metal is formed in the zone of hardening cooling of a rail head. Also the hardness of the metal in the deep layers of the rail head increases relative to the hardness of the base metal at the appropriate depth.

1. Golovin, G.F., Zimin, N.V. (1979) *Technology of heat treatment of metals using induction heating*. Leningrad, Mashinostroyeniye [in Russian].
2. Nesterov, D.K., Sapozhkov, V.E., Levchenko, N.F. et al. (1990) Heat treatment of rail steel using induction heating. *Metallovedenie i Termich. Obrab. Metallov*, **8**, 30–34 [in Russian].
3. Gong, L., Zhu, L., Zhou, H. X. (2017) Effect on hardness and microstructures of rail joint with ultra-narrow gap arc welding by post weld heat treatment. *Engineering Materials*, **737**, 90–94.
4. Ding Wei, Song Hongtu, Li Li, et al (2012) *Heat treatment device of welding joint of steel rail*. China Pat. CN 201120285569.
5. Feshchukov, A.N., Zeman, S.K., Murkin, M.K. (2016) *System for heat treatment of welded joints of railway rails in track conditions*. RF Pat. 57752, Int. Cl. E01B31/18 [in Russian].
6. Panteleimonov, E.O. *System for heat treatment of welded joints of railway rails in track conditions*. Ukraine Pat. on utility model 114593, Int. Cl. E01B31/18 [in Ukrainian].
7. Panteleimonov, E.O. *Portable module for heat treatment of welded joints of railway rails*. Ukraine Pat. on utility model 143908, Int. Cl. E01B 31/18 (2006.01), C21D 1/10 (2006.01) [in Ukrainian].
8. Panteleimonov, E.O. *Induction device for heat treatment of welded joints of railway rails*. Ukraine Pat. on utility model 109123, Int. Cl. C21D 1/10 (2006.01) [in Ukrainian].
9. Panteleimonov, E.A., Gubatyuk, R.S. (2016) Induction device for heat treatment of welded joints of railway rails. *The Paton Welding J.*, **10**, 41–43.
10. Kuchuk-Yatsenko, S.I., Antipin, E.V., Didkovskiy, O.V. et al. (2020) Evaluation of quality of welded joints of high-strength railway rails of modern production taking into account the requirements of Ukrainian and European standards. *Ibid.*, **7**, 2–10. DOI: <https://doi.org/10.37434/as2020.07.01>.

Received 03.02.2021

# XX INTERNATIONAL INDUSTRIAL FORUM - 2021

INTERNATIONAL TRADE FAIRS

# November 16-19

METAL-WORKING

WELDING

HYDRAULIC PNEUMATICS

BEARINGS

UKRUSEE TECH

UKFOUNDRY

UKRPROP AUTOMATIZATION

FITTINGS, STANDARDS AND INSTRUMENTS

HOISTING AND TRANSPORTING STOREHOUSE EQUIPMENT

INDUSTRIAL SAFETY

**ORGANIZER:**  
International Exhibition Centre

General Information Partner:  
**ОБСЛУЖУВАННЯ ІНЖЕНЕРІВ**

Exclusive Media Partner:  
**ЖУРНАЛ ГОЛОВНОГО ІНЖЕНЕРА**

Technical Partner:  
**РентMedia**

[www.iec-expo.com.ua](http://www.iec-expo.com.ua)  
[www.tech-expo.com.ua](http://www.tech-expo.com.ua)

## «PATON» INDUSTRIAL PARK

At the current stage of development of Ukrainian economy there are urgent tasks to improve the efficiency of Ukrainian manufacturing plants, as well as attracting investments to provide the conditions for sustainable growth. One of the tools for solving these problems is establishing and developing industry parks — special territories with the required transport-engineering infrastructure, as well as buildings (production, storage, administrative and other premises), which are designed for accommodating and servicing various manufacturing and other plants. Use of a common infrastructure, services of managing company and possibilities for cooperation with other park participants allow reducing the administrative and infrastructure costs, thus increasing the effectiveness of their operation and competitiveness of the manufactured products.

Creation of industry parks in Ukraine opens up new prospects for regional development, has a positive impact of financial activity of local manufacturing plants, that allows establishing business contacts in the «investor – local government organs – business» chain.

This is exactly why both in the developed countries of the world, and in the post-Soviet space one can see increase in the number of industry parks that is attributable both to the growing demand for high-technology products, and activation of investment processes in the market.

In Ukraine the process of creation of industry parks is regulated by the Law of Ukraine «On Indus-



Central building of PWI PPWE

trial Parks» of June 21, 2012, No.5018-VI. This Law specifies the legal and organizational fundamentals of creation and functioning of industry parks in the territory of Ukraine, with the purpose of ensuring the economic development and improving the competitiveness of the territories, activation of investment activity, creating new jobs, development of modern manufacturing and market infrastructure.

Guided by the abovementioned advantages, at the end of 2020 the PWI Pilot Plant of Welding Equipment initiated creation of «PATON» Industrial Park, which was included into the Register of Industrial Parks. The new Industrial Park will be located in the



Kyiv District, Fastiv region, near urban-type settlement Glevakha.

*«The main purpose of creation of the industry park is development of manufacturing of welding equipment and consumables, attracting investments, required for development of the region, creating new jobs, introduction of advanced technologies into industrial production and enhancing economic development of the territory»* — noted Anatolii Stepakhno, Head of PWI PPWE Management.

The objectives set by the initiators of establishing the «PATON» Industrial Park are quite ambitious, in particular, creating favourable conditions for initiating and further development of industrial production; new approaches to manufacturing, and production process control, introduction of advanced technologies; development of communal infrastructure; increasing the power capacity of the region; attracting foreign and local investments into the regional economy; filling the state and local budgets; creating new jobs, including highly-qualified ones; promoting medium-business development; international activity; filling the market with national high-quality products and increasing export outside the country.

The functional purpose of «PATON» Industrial Park is establishing industrial production of modern high-quality welding equipment for various purposes and welding consumables; manufacturing various-purpose packing for leading Ukrainian and foreign plants; complex services on warehouse storage of goods, logistics, etc.

The Park will take up an area of more than 17 ha, 43 km from the capital, near international highway E95 in the direction of Odessa. The convenient location of «PATON» Industry Park is due to its closeness to the capital of Ukraine (20 min by car) and to the main transport arteries (international highway and railway), customs terminal (2.5 km) and international airports (Kyiv — 27 km, Boryspil — 59 km).

The project of «PATON» Industrial Park envisages creating up to 2000 new jobs, building its own sys-

tems of power and water supply, and heating systems, construction of modern production, office and warehouse premises and other facilities.

Successful realization of the project will have a positive impact on the economic and social development of the adjacent towns and Fastiv region of the Kyiv district as a whole: it will promote investment activity of both the local and foreign plants, that will allow faster realization of the strategy of import substitution, will have a positive impact on development of infrastructural objects of the region, will improve the effectiveness and coordination of contacts with local authorities, will promote strengthening of economic potential of territorial communities, will ensure development of small and medium business that, in its turn, will increase the number of newly created jobs with competitive salary and high standards of social guarantees.

*«An indubitable advantage of the local legislation is the fact that the State, while funding the development of infrastructure of such industry parks, can be an additional source of investments for them, lowering the actual business expenses, and can favour creation of attractive investment climate both for local and foreign investors. Owing industry parks to functioning in Ukraine, the State can influence not only restoration of the competitiveness of local manufacturing plants, but also introduction of national high-technology products into the global investment market»* — Anatolii Stepakhno comments on the project capabilities.

In keeping with the data of the Ministry of Economy, as of 28.12.2020, 45 industry parks were included into the Register of Industrial Parks, 23 of which already have managing companies, and 10 parks have already involved their first participants. Such data are indicative of the still early phase of development of such a tool of economic advancement as industry parks as a whole, and of great prospects for new projects in this field.

Pilot Plant of Welding Equipment of the E.O. Paton Electric Welding Institute is a leading manufacturer of welding equipment in Ukraine, and also one of the leaders in the market of welding equipment and consumables in the territory of CIS countries. The plant was established in 1959 as a unit of the E.O. Paton Electric Welding Institute. As of 2021, the Plant serially produces a wide range of welding equipment and consumables under PATON™ trade mark, which are supplied to more than 30 countries all over the world, besides Ukraine.





*Continuous path to improvement for more than 60 years*

## A NEW STAGE IN DEVELOPMENT OF PATON TRADE MARK

Development of welding equipment manufacture in Ukraine has almost a century of history, of which 62 years are closely connected with the activity of PWI Pilot Plant of Welding Equipment, which was founded at PWI in January of 1959 to implement new developments of PWI and PWI EDTB specialists. During the entire period from its establishment and up to now the Plant has manufactured hundred thousands of welding equipment units for enterprises of different profile almost on all the continents of the world. At present PWI PPWE is a major manufacturer of welding equipment in Ukraine and one of the market leaders in the post-Soviet space. Owing to proprietary developments, high production standards and considerable experience of the Plant specialists, the welding units and electrodes under PATON™ trade mark are highly evaluated by welding experts both in Ukraine and far beyond its borders.

Expansion of export markets for sale of its products is one the highest priorities of the Plant development strategy. At present PATON™ products are supplied to more than 50 countries all over the world: from Latin America to the Far East. And the list of these countries is constantly growing! Just from the beginning of 2021 it was complemented by a number of European (Denmark, Great Britain), African (Kenya) and Middle East countries (Saudi Arabia, Bahrain).

The Plant management took a decision on updating the Company name and changing it to PATON INTERNATIONAL, exactly to enhance the export



vector. It is anticipated that such a step will allow emphasizing for the users and partners of the Plant the international focus of the business, which has long overgrown the limits of Ukrainian market, and will facilitate promotion of the PATON™ brand in the world. As it often happens, the need for such changes was dictated by the market itself, as in modern realities even the company name should meet certain user requirements: simplicity, conciseness, comprehensibility and clarity.

Some time ago the Plant, together with its partners, initiated the process of establishing representative offices in those countries, where the largest quantity of products are exported. The main purpose of creating



such offices is to ensure effective operation of the Plant in the local market and to provide high-quality support to local users. Later on it is planned to unify the names of the offices, using a common trade mark — PATON Poland, PATON Great Britain, Paton Denmark, PATON Egypt, PATON Georgia, PATON South Korea, and more than 20 other offices. And just the current name of the main company with experimental-design base and production facilities located in Ukraine, enables logically uniting all the offices within a single business — PATON INTERNATIONAL. This is exactly the name that will be equally understandable for users and partners of the Plant in any country and will promote formation of trust in the Ukrainian brand.

The Plant has an impeccable reputation of a reliable manufacturer and supplier of high-quality welding equipment and consumables and it is committed to maintaining its reputation at such a high level. Owing to the Plant cooperation with the leading Ukrainian and international certification bodies, PATON™ products meets all the necessary requirements and is certified on a regular basis. In order to strengthen its positions in the international market, as well as minimize the risks of export activity, the

Plant has signed a cooperation agreement with an export-credit agency. Such cooperation opens up possibilities of extended insurance of international shipments of the Plant products, additionally guaranteeing fulfillment of shipment conditions by all the parties in this process. During the short period of this agreement existence, the Plant has already used it during recent deliveries to Burkina Faso, Nigeria, South Africa and Kenya. Use of this additional insurance mechanism has the purpose of further improvement of the image of PATON INTERNATIONAL Company as a reliable international trade partner and strengthening the position of PATON™ products in the global market.

Owing to the above measures, the Plant continues to move towards the posed goals: ensuring stable development of its research and production potential, increasing its production of high-quality welding equipment and consumables and advancing PATON™ products among the greatest possible number of welding specialists from different countries, thus enhancing its own contribution to development of the Ukrainian manufacturing industry and popularization of «MADE IN UKRAINE» brand among consumers around the world.



E.O. Paton Electric Welding Institute of the NAS of Ukraine  
National Technical University of Ukraine  
«Ihor Sikorsky Kyiv Polytechnic Institute»  
International Association «Welding»

The Tenth International Conference  
**BEAM TECHNOLOGIES in WELDING  
and MATERIALS PROCESSING**

6 – 11 September 2021

Ukraine, Odesa

**Conference Chairmen**

Prof. I. Krivtsun

**Conference topics**

- *Laser and electron-beam welding, cutting, surfacing, heat treatment, coating deposition*
- *Electron-beam melting and refining*
- *Hybrid processes*
- *3D-technologies*
- *Modelling and materials science of laser and electron-beam technologies*

**EQUIPMENT ♦ TECHNOLOGIES ♦ MODELLING**



**LTWMP 2021 Organizing Committee**  
03150, 11, Kazymyr Malevych str., Kyiv, Ukraine  
E.O. Paton Electric Welding Institute of the NAS of Ukraine  
Tel./fax: (38044) 200-82-77  
E-mail: [journal@paton.kiev.ua](mailto:journal@paton.kiev.ua)  
[www.pwi-scientists.com/eng/ltwmp2021](http://www.pwi-scientists.com/eng/ltwmp2021)



## IN MEMORY OF S.I. KUCHUK-YATSENKO



Serhiy Ivanovych Kuchuk-Yatsenko, the first Deputy Director of the E.O. Paton Electric Welding Institute of the NAS of Ukraine, Academician of the National Academy of Sciences of Ukraine passed away **on March 22, 2021**.

After graduating from the Kyiv Polytechnic Institute, Serhiy Ivanovych was assigned to work at the E.O. Paton Electric Welding Institute, where he passed a glorious working path from a young expert engineer to professor, doctor of technical sciences, chief of one of the leading departments, first Deputy Director of the Institute on research work, Academician of the National Academy of Sciences of Ukraine. In 1960, S.I. Kuchuk-Yatsenko defended a candidate and in 1972 a doctoral thesis. In 1978 he was elected a corresponding member and in 1987 a full member of the National Academy of Sciences of Ukraine.

The research activity of S.I. Kuchuk-Yatsenko is associated with studies of physical and metallurgical processes in welding of different materials in a solid phase. In particular, he obtained new data on the peculiarities of producing joints with the formation of a thin layer of melt on the contact surfaces of parts to be welded, its behaviour under the action of electrodynamic forces and features of its interaction with the gaseous medium in the contact zone. It was for the first time shown that the state of the melt during deformation of parts to be welded has a dominant effect on the formation of metal bonds between the contact surfaces and the formation of chemical heterogeneity in the joint area. The influence of oxide structures in the melt on the quality of joints was studied in detail and the ways of minimizing oxidation processes in the specified welding period were determined. Along with the mentioned studies, S.I. Kuchuk-Yatsenko for many years had been carrying out specifically-targeted studies of transient processes of heating and damage of single contacts at high energy concentrations. A number of new regularities, characterizing the energy indices of the process of contact fusion of metals, determined the ways of automatic control of the basic parameters of the process in order to obtain the most favourable conditions for heating and deformation of parts to be welded.

As a result of the mentioned fundamental studies, S.I. Kuchuk-Yatsenko developed new methods

of flash butt welding by continuous, pulsed, pulsating melting, patented in the leading countries of the world. Based on them, S.I. Kuchuk-Yatsenko together with the staff colleagues developed the technologies of welding for different products, control systems and new models of welding equipment that have no analogues in the world practice. The equipment is featured by a high efficiency, the minimum consumed power and weight, provides a stable and high quality of joints. These advantages are the most significant during welding of parts of a complex configuration with large cross-sections. Research and engineering activity of S.I. Kuchuk-Yatsenko was characterized by a comprehensive approach to solving the set problems. His basic investigations were accompanied by the development of original welding technologies, automatic and recently computerized control of the welding process and the creation of modern welding equipment.

With his direct participation, industrial production of new welding equipment and its mass implementation into production was organized. Here are some of the most significant stages of activity of S.I. Kuchuk-Yatsenko.

For more than fifty years, S.I. Kuchuk-Yatsenko dealt with works on welding rails. Due to the technologies and equipment for rail welding, developed with his active participation and supervision, for the first time in the world practice it was possible to use a highly efficient flash butt welding in field conditions, which greatly contributed to the transition of railways to seamless tracks. With an active participation of S.I. Kuchuk-Yatsenko, on the terms of the PWI documentation, the serial production of such equipment was organized at the Kakhovka Plant of Electric Welding Equipment, which in the 1970s became a world exporter of such equipment. Over the past years, more than ten generations of rail welding machines were created and are still used in many countries around the world. S.I. Kuchuk-Yatsenko took an active part in the improvement of this equipment and welding technology, which allows maintaining its high competitiveness. In recent years, new generations of welding machines were created that allow welding rails of infinite length during the repair of seamless tracks with the simultaneous stabilization of their stress state. In 1966, for the development and implementation of a machine for flash butt welding of rails in the repair and construction of seamless railway tracks, as a member of the author's team S.I. Kuchuk-Yatsenko

was awarded the Lenin Prize. He was awarded the title of «Honorary Railwayman of the USSR».

The developments of S.I. Kuchuk-Yatsenko and his colleagues were also successfully used in machine-building plants in the manufacture of circumferential billets, shafts and billets from dissimilar materials. The use of multiposition flash butt welding was especially effective, which allowed welding large-sized parts simultaneously in several places (engine bodies, radiators of powerful transformers). The introduction of one installation in the production line of crankcases of powerful diesel units at one of the locomotive plants allowed increasing the labour efficiency by 70 times and releasing 380 welders. A significant effect was also obtained as a result of multiposition welding at the Zaporizhzhya Transformer Plant in the manufacture of transformer radiators. In 1976, as a member of the author's team S.I. Kuchuk-Yatsenko was awarded the State Prize of the Ukr.SSR for creation and industrial implementation of the new technology and highly-efficient assembly and welding complexes for mass production of large-sized structures from unified elements. For the first time in the world practice, S.I. Kuchuk-Yatsenko with a group of staff colleagues developed an original technology of flash butt welding of products of a complex shape and a large cross-section of high-strength alloys based on aluminium, which provided producing joints with the strength almost equal to the strength of the base metal. Based on it, the production of unique equipment was developed and mastered, which is used in the manufacturing of space technique at Ukrainian plants. In 1986, as a member of the author's team S.I. Kuchuk-Yatsenko was awarded the USSR State Prize for the creation of the technology and equipment for flash butt welding of structures made of high-strength aluminium alloys. S.I. Kuchuk-Yatsenko made a significant contribution to the technology and equipment for flash butt welding of pipelines of different purpose. With his active participation, the technologies, control systems and equipment for flash butt welding of pipes with a diameter from 60 to 1400 mm were developed and its large-scale implementation at the construction of pipelines on the territory of the former USSR was performed. With the use of FBW, more than 70000 km of different pipelines were welded, including 4000 km of the most powerful pipelines in the Far North. The use of FBW allowed increasing labour efficiency and providing the reliability of pipelines. This work was also awarded the Lenin Prize in 1989.

Under the supervision of S.I. Kuchuk-Yatsenko and with his direct participation, the works on the creation of pressure welding technologies for stationary joints of pipes for different purposes continued. For the first time in the world practice, the technologies and equipment for press welding with the use of magnetically impelled arc heating were developed to join pipes with a diameter of up to 300 mm and a wall thickness of 5–15 mm, which were characterized by a high efficiency with a minimal energy consumption of the process.

S.I. Kuchuk-Yatsenko took an active part in all stages of implementation of the mentioned works. In 1998 he was awarded the title of «Honoured Worker of Science and Technology of Ukraine» and in 2000 he received the E.O. Paton Prize for the research work «Welding in solid phase». S.I. Kuchuk-Yatsenko is the author of more than 700 scientific publications, including 10 monographs, 350 author's certificates, as well as more than 300 Ukrainian and foreign patents, many of which were purchased by foreign companies under license agreements.

Academician S.I. Kuchuk-Yatsenko dealt with current problems in the field of welding, creation of advanced technologies for joining hard-to-weld materials. He headed one of the leading scientific departments of the E.O. Paton Electric Welding Institute. For a long time S.I. Kuchuk-Yatsenko fruitfully cooperated with the Kakhovka Plant of Electric Welding Equipment, one of the leading manufacturers of welding equipment in Ukraine. He took an active part in the organization of serial production of machines for flash butt welding of railway rails and pipes.

S.I. Kuchuk-Yatsenko was the Deputy Chairman of the Academic Council of the PWI, a member of the Editorial Board and the editor-in-chief of the «Paton Welding Journal». He trained more than ten candidates and doctors of technical sciences. He was elected the first President of the Society of Welders of Ukraine, was a member of its Board, a member of the Society of Welders of the USA and Great Britain.

For his merits the scientist was awarded two Orders of the Red Banner of Labour, the Order of the Badge of Honour, the Order of Prince Yaroslav the Wise and different medals.

The talent of the scientist and the chief, warm-heartedness and kindness gained S.I. Kuchuk-Yatsenko the authority and respect of the welding community. Friends, colleagues and students are deeply saddened by this loss, and the memory of Serhiy Ivanovych will remain forever in their hearts.

*Team of the E.O. Paton Electric Welding Institute,  
Editorial Board and editorial staff of «The Paton Welding Journal»*